National Library of Canada
Acquisitions and Bibliographic Services Branch
395 Wellington Street
Ottawa, Ontario
K1A 0N4

Bibliothèque nationale du Canada
Direction des acquisitions et des services bibliographiques
395, rue Wellington
Ottawa (Ontario)
K1A 0N4

Your file Votre référence

Our file Notre référence

NOTICE

The quality of this microform is heavily dependent upon the quality of the original thesis submitted for microfilming. Every effort has been made to ensure the highest quality of reproduction possible.

If pages are missing, contact the university which granted the degree.

Some pages may have indistinct print especially if the original pages were typed with a poor typewriter ribbon or if the university sent us an inferior photocopy.

AVIS

La qualité de cette microforme dépend grandement de la qualité de la thèse soumise au microfilmage. Nous avons tout fait pour assurer une qualité supérieure de reproduction.

S'il manque des pages, veuillez communiquer avec l'université qui a conféré le grade.

La qualité d'impression de certaines pages peut laisser à désirer, surtout si les pages originales ont été dactylographiées à l'aide d'un ruban usé ou si l'université nous a fait parvenir une photocopie de qualité inférieure.

Canada

NORMALIZED ENERGY-BASED METHODS TO PREDICT THE SEISMIC DUCTILE ENERGY RESPONSE OF SINGLE-DEGREE-OF-FREEDOM STRUCTURES

by

Niandi Wang

Thesis submitted to the School of Graduate Studies
in partial fulfillment of the requirements
for the Master of Applied Science Degree in Civil Engineering
under the auspices of the Ottawa-Carleton Institute for Civil Engineering

Feburary 1993

ISBN 0-315-83846-9

UNIVERSITÉ D'OTTAWA
UNIVERSITY OF OTTAWA

To My Family

Abstract

As energy-based methods could provide more insight into the ultimate cyclic seismic performance than traditional design methods, this research essentially focuses on the study of energy demands for single-degree-of-freedom systems. Starting from the basic idea that a typical dynamic earthquake excitation can be conceptually described as a complex sequence of pulses and sine-waves of various durations, frequencies and intensities, energy response spectra for simple pulses or sine-wave excitations are first constructed, the behaviour of each energy contribution is studied and two new energy normalization methods are proposed. Assuming that earthquake ground motion excitation can be simulated by pulses and sine-waves, by utilizing the simple-pattern-excitation energy spectral results, the structural energy demand under real seismic excitation can be predicted.

Acknowledgements

My special thanks go to my supervisor, Dr. Michel Bruneau for his support, advice and patience, without his directions, this thesis could not have been done. I would like to express my gratitude to the professors, especially Dr. H. Tanaka, Dr. S. Ng and Dr. M. Saatcioglu, for their excellent teaching and pedagogy. Also thank all the supporting staffs in Civil Engineering Department for their kindness and help all the time.

My deep thanks go to my family members, for their support and encouragement throughout my life and studies.

Table of Contents

List of Tables

List of Figures

Notations

C	viscous damping coefficient, kg/s
C_{cr}	critical damping coefficient, $C_{cr} = 2\omega M$, kg/s
D	dynamic magnification factor, dimensionless
E	absolute energy, J
E	relative energy, J
E^{NG}	normalized energy using normalization method 1, dimensionless
E^{NR}	normalized energy using normalization method 2, dimensionless
$E^{NR\prime}$	predicted normalized energy from an actual earthquake, dimensionless
E_a	absorbed energy, J
E_d	damping energy, J
E_h	irrecoverable hysteretic energy, J
E_h'	predicted hysteretic energy, J
E_i	absolute input energy, J
E_i'	relative input energy, J
E_k	absolute kinetic energy, J
E_k'	relative kinetic energy, J
E_p	plastic energy, J
E_s	recoverable elastic strain energy, J
K	stiffness of system, N/m
k_1	integration constant, dimensionless
M	mass of system, kg
N	number of sine-wave cycles, dimensionless
R	(NBCC 1990) force modification factor, dimensionless
R	system's restoring force that can be expressed as $K \cdot u$ for a linear elastic system, N
R_y	yield strength of the system, N
t	time, s
t_d	duration of the ground excitation, s
T	structural period, $T = 2\pi/\omega$, s
$\bar{T}$	period of the applied sine-wave load, s
u	relative displacement of system, m

u_g	ground displacement relative to a fixed reference axis, m
u_t	absolute displacement of system, m
$\dot{u}$	relative velocity of system, m/s
$\dot{u}_g$	ground velocity, m/s
$\dot{u}_t$	absolute velocity of system, m/s
$\ddot{u}$	relative acceleration of system, m/s^2
$\ddot{u}_t$	absolute acceleration of system, m/s^2
$\ddot{u}_g$	ground acceleration, m/s^2
U	calibration factor, U=0.6
V	seismic design force (base shear), N
Ve	equivalent lateral seismic force, N
V_i	absolute equivalent velocity, m/s
V_i'	relative equivalent velocity, m/s
β	ratio of applied load frequency to natural frequency of system, $\beta = \bar{\omega}/\omega$, dimensionless
Δ_y	yield displacement of the structure, m
η	strength ratio expressed as $R_y/M\ddot{u}_{gmax}$, dimensionless
θ	phase angle, rad
ξ	viscous damping ratio of the system, $\xi = C/C_{cr}$, dimensionless
μ	displacement ductility factor, dimensionless
ϕ	amplitude of the steady state response, m
ω	natural circular frequency of the system, $\omega^2 = K/M$, 1/s
$\bar{\omega}$	circular frequency of the applied load, 1/s

Abbreviations

Eq.	equation
IDRS	inelastic design response spectra
MDOF	multiple-degree-of-freedom
MF	magnification factor
NBCC	national building code of Canada
SDOF	single-degree-of-freedom

CHAPTER 1

INTRODUCTION

1.1 General

A number of design methods are currently available to assist structural engineers in providing earthquake resistant structures. The dynamic elastic modal analysis and static-equivalent lateral seismic force procedure typically recommended by most building codes are undeniably the most popular, although in some unusual circumstances, linear elastic and/or non-linear inelastic time-history analyses can also be used. All these methods essentially concentrate on establishing a peak demand for a particular design parameter, such as maximum displacement, ductility, and member forces. Other important aspects of seismic performance, such as cumulative cyclic ductility, number of yielding reversals, incremental collapse, low-cycle fatigue, energy dissipation capacity, etc., are only indirectly considered in design by semi-arbitrary restrictions on the magnitude of the permissible strength reductions from the elastic-response level. For example, the 1990 edition of the National Building Code

of Canada (NBCC 1990) uses a static-equivalent lateral seismic force specified as:

$$V=\frac{VeU}{R} \tag{1.1}$$

where Ve is the equivalent lateral seismic force representing elastic response, R is the force modification factor, and U=0.6 is a calibration factor. This design basis is essentially equivalent to an inelastic design response spectra (IDRS) where the permissible strength reduction R corresponds to a tolerated peak displacement ductility demand for a given type of structural system. However, the code-specified R values for various types of structural systems are set such that they indirectly consider the particular cyclic ultimate performance germane to each system.

While safe and conservative, these current seismic-resistant design methods are implicitly addressing the needs of new construction. Therefore, when investigating the adequacy of existing structures against earthquakes, particularly in regions of low and moderate seismicity, traditional design and analysis methods may lead to overly-conservative assessments of the demand as they fail to provide a comprehensive description of the required ultimate cyclic resistance. Unfortunately, no simple method currently exists which could be directly used by designers to this end.

Recently, energy-based methods have gained a renewed attention, and they could offer one possible solution to this problem (as well as to many others). These methods are based on the premise that the energy demand during an earthquake (or an ensemble of earthquakes) can be predicted and that the energy supply of a structural element (or a structural system) can be established. For a satisfactory design, the energy supply should be larger than the energy demand (Housner and Jennings 1977, Kuwamura and Galambos 1989). Therefore, requiring less efforts than complex non-linear inelastic analyses, energy-based methods could provide more insight into the ultimate cyclic seismic performance than traditional design methods. However, much

remains to be learned on seismic-related energy demands before these could be used in practice.

This research will essentially focus on the study of energy demands for single-degree-of-freedom (SDOF) systems. Starting from the basic idea that a typical dynamic earthquake excitation can be conceptually described as a complex sequence of pulses or sine-waves of various durations, frequencies and intensities, energy response spectra for simple pulses or sine-wave excitations will be first constructed and the behaviour of each energy contribution will be studied. Assuming that earthquake ground motion excitation can be simulated into such pulses and sine-waves, hopefully, by utilizing the simple-pattern-excitation energy spectral results, the structural energy demand under real seismic excitation could be predicted.

1.2 Objectives

The objectives of this thesis are threefold:

(i) To study the behaviour of various components of the non-linear inelastic seismic energy equation when single-degree-of-freedom (SDOF) systems are subjected to simple pulse and sine-wave excitations, and to provide additional insight into the significance and parametric dependency of each component.

(ii) To propose simple normalization methods for these energy parameters to facilitate the analysis and future comparisons between various researchers' results.

(iii) To investigate whether hysteretic energy demand could be predicted for given ground excitations simply from known normalized energy spectra for pulses and sine excitations.

1.3 Outline of Thesis

The research is carried out in four major steps as described in the following specific chapters.

(i) In Chapter 2, the existing literature on this topic is reviewed and dynamic non-linear energy equations are presented.

(ii) In Chapter 3, the energy analysis of SDOF systems subjected to rectangular pulse excitations is investigated.

(iii) In Chapter 4, a similar study is conducted for SDOF systems subjected to sine-wave excitations.

(iv) In Chapter 5, it is shown how the previously constructed simple normalized energy spectra can be used to determine seismic structural hysteretic energy demand.

Finally, conclusions and suggestions for further research are presented in Chapter 6.

CHAPTER 2

DEVELOPMENT OF THE EQUATIONS OF MOTION AND ENERGY FOR NON-LINEAR SDOF SYSTEM

2.1 Equation of Motion for a SDOF System

The SDOF system is not only the simplest model of structural dynamics, but also the most fundamental model used in seismic response investigations. Its usefulness is foremost in the modal analysis of multiple-degree-of-freedom (MDOF) systems where complex structures can be decomposed into and analyzed as a number of equivalent SDOFs. More importantly, however, concepts first formulated based on the study of SDOF systems have become the building blocks on which earthquake engineering is founded. Thus, the following review of the equations of motion and energy for a SDOF system is worthwhile.

For a lumped-mass SDOF system, as shown in Figure 2.1, subjected to a ground excitation, the equation of motion can be written as:

$$M\ddot{u}+C\dot{u}+R=-M\ddot{u}_g \tag{2.1}$$

where M is the mass of the system, C is the damping coefficient, R is the restoring force that can be expressed as $K \cdot u$ for a linear elastic system, u, $\dot{u}$ and $\ddot{u}$ respectively denote the displacement, velocity and acceleration of the system relative to its base, and $\ddot{u}_g$ stands for the ground acceleration relative to a fixed reference axis (Biggs 1964, Clough and Penzien 1975).

Although structural responses can be directly obtained by solving Eq. 2.1, it is more desirable to express the equation in a normalized form in order to facilitate the design procedure where a family of related systems can share the same result. In this manner, Eq. 2.1 can be rewritten as:

$$\ddot{u}+2\omega\xi\dot{u}+\omega^2u=-\ddot{u}_g \tag{2.2}$$

where ω is the natural circular frequency of the system (ω^2 = K/M) and ξ is the viscous damping ratio (expressed as a fraction of the critical damping ratio) which is equal to $C/2M\omega$.

Consequently, from Eq. 2.2 only simple analysis is needed to determine the responses of all elastic SDOF systems having the same frequency and damping ratio subjected to the same excitation. These responses can be conveniently summarized by response spectra which plot, as an example, the maximum relative displacement against frequency for constant amount of damping on given dynamic excitation (Naeim et al. 1989, Mahin and Lin 1983).

However, since an earthquake of only moderate intensity can cause significant damage

in a building designed for code forces, the structural stiffness (and sometimes strength) can vary during the seismic excitation. In such cases, nonlinear inelastic analysis is better suited to predict the magnitude of the parameters needed for structural aseismic design.

As the true non-linear analysis, which involves the step-by-step integration of the equation of motion can require a prohibitively expensive computing effort, the ductility-factor method has been developed as following.

The method is based on the observation that inelastic behaviour can be interpreted from linear elastic analysis (Clough and Penzien, 1975). For instance, when the nonlinear member's deformation is identical to the elastic response deformation, i.e. when the maximum displacement, u, for the SDOF system shown in Figure 2.1 is constant regardless of the system's structural strength, then directly from the member force-displacement relationship shown in Figure 2.2, the ratio of u to the elastic-limit deformation, Δ_y, is equal to the ratio of the force elastically developed, R, to the yield force, R_y. This can be written as:

$$\frac{u}{\Delta_y} = \frac{R}{R_y} \tag{2.3}$$

And the ductility ratio, μ, is thereafter defined as:

$$\mu = \frac{u}{\Delta_y} \tag{2.4}$$

Because it implicitly reflects the deterioration of the strength of inelastic systems, this normalized factor has been extensively used in non-linear aseismic design and structural evaluation.

Furthermore, by substituting Eq. 2.4 into Eq. 2.2, the equation of motion can be derived for non-linear inelastic systems as:

$$\ddot{\mu}+2\omega\xi\dot{\mu}+\omega^2\mu=-\omega^2\Delta_y\ddot{u}_g=-\omega^2(\frac{M}{R_y})\ddot{u}_g \tag{2.5}$$

Introducing a non-dimensional parameter

$$\eta=\frac{R_y}{M\ddot{u}_{gmax}} \tag{2.6}$$

which is the ratio of a system's yield strength to the maximum inertia force of an infinitely rigid structure, Eq. 2.5 becomes:

$$\ddot{\mu}+2\omega\xi\dot{\mu}+\omega^2\mu=-\frac{\omega^2}{\eta}\frac{\ddot{u}_g}{\ddot{u}_{gmax}} \tag{2.7}$$

from which ductility responses of non-linear systems having the same natural frequency and strength ratio, η, subjected to the same ground excitation can be determined through simple analysis, and ductility spectra (Mahin and Lin 1983) can be subsequently constructed.

2.2 Energy Methods

2.2.1 Literature Review

Although the above-mentioned ductility factor has been traditionally used as a criterion to establish inelastic design response spectra (IDRS) for earthquake-resistant

design of buildings, it lacks consideration of seismic cyclic response because only the resultant maximum response is taken into account. As an alternative, the energy-based design method by its definition is likely to remedy the defect of the ductility factor method.

The energy method was first proposed by G. W. Housner (1956). He pointed out that the effect of the ground motion is to feed energy into the structure, some of this energy being dissipated through damping and the remainder stored in the structure in the forms of kinetic energy (i.e. motion of the mass) and strain energy (i.e. deformation of the structural members). Based on the idea (in 1956) that a safe and economical aseismic design should proceed through plastic analysis or limit-design, while allowing permanent deformations to occur without failure of a member, it was suggested that the design be tied to the concept of plastic energy, E_p, dissipated by structure and related to the inelastic deformation by:

$$E_p = E_t - E_e \tag{2.8}$$

where E_t is the maximum kinetic energy which would be obtained if the structure behaved completely elastically, and E_e is the elastic energy of the structure when it reaches yield point. Although this energy equation was rudimentary, the fundamental concept of energy method promoted by him that at any instant the sum of the kinetic energy, strain energy, energy dissipated through normal damping and energy dissipated through permanent deformation, will be equal to the total energy input was first formulated in this paper and provided the initial sparks to the later developments of the energy method.

Since the 1960s, the seismic nonlinear inelastic behaviour of structures gained considerable attention, e.g. Akiyama 1985, Anderson and Bertero 1969, Bertero and Popov 1965, Bruneau and Mahin 1990a, 1990b, 1992, Goel and Berg 1968, Hadjian 1982, Housner and Jennings 1977, Jennings 1965, Iwan 1980, Kuwamura and

Galambos 1989, Mahin and Lin 1983, Newmark and Hall 1973, Niekell 1976, Pecknold and Riddle 1978, Sedarat and Bertero 1990, Trifunac and Brady 1975, Uang 1991, Uang and Bertero 1986, Veletsos and Newmark et al 1965, among many which addressed various aspects of the earthquake-resistant design problem, but few even considered the energy concepts proposed by Housner other than indirectly.

In the 1980s, the energy approach was brought anew to researchers' attention. In particular, Mckevitt et al (1979) proposed a simple energy method for seismic structural design, Kato and Akiyama (1982) used energy method based on Housner's equation (1956) for design of steel buildings, Zahrah and Hall (1984) studied seismic energy absorption in SDOF systems, and Tembulkar and Nau (1987) investigated seismic energy dissipation capacity for inelastic modelling. However, the most explicit definition of the energy method was formulated by Uang and Bertero (1988a). They emphasized the physical meaning of each energy term and investigated the reliability of the energy method to predict the energy dissipation capacity of a given structural member or system, their proposed equations will be presented in next section. Subsequently, the subject attracted attention from many researchers as expressed in the many papers on energy-based earthquake-resistant design methods recently published (Conte and Mahin et al. 1990, Fajfar and Fischinger 1990, Fajfar et al. 1990 and 1991, Leger and Dussault 1991, McCabe and Hall 1989, Uang and Bertero 1988b, 1990, Wu and Hanson 1989).

Among the recent publications, papers written by Leger and Dussault (1991) and Fajfar et al. (1991) are noteworthy. In both of these studies where the hysteretic energy is found contributing to structural damage, although the ratio of hysteretic energy to input energy is proposed as a normalization measure, the definition of input energy is totally different. Although, in both cases, findings are very meaningful and valuable, the ambiguous definition of the seismic input energy, i.e. whether it should be defined based on earthquake record characteristics as suggested by Fajfar, by Bertero's equation as used by Leger, or by any other strategy still needs to be

clarified.

2.2.2 Uang and Bertero's Method

Since the energy method proposed by Uang and Bertero (1988) is clearly defined and has already received some acceptance, this research will essentially use the same energy terms and definitions.

Basically two types of energy methods have been proposed: the absolute energy method and the relative energy method. Each approach, although derived from the same equation of dynamic equilibrium for the SDOF system of Figure 2.1, leads to a specific and consistent set of energy terms and physical interpretations, as demonstrated below.

2.2.2.1 Equations for Absolute Energy Method

When the system in Figure 2.1 is subjected to a horizontal ground motion, the total displacement of the structure, u_t, can be expressed as:

$$u_t = u + u_g \tag{2.9}$$

where u is the relative displacement between the reactive mass of the structure and its base, and u_g is the ground displacement. Directly,

$$\ddot{u}_t = \ddot{u} + \ddot{u}_g \tag{2.10}$$

where the double-dotted terms are the acceleration corresponding to the respective

displacement terms. Therefore, Eq. 2.1 can be rewritten as:

$$M\ddot{u}_t+C\dot{u}+R=0 \tag{2.11}$$

By integrating Eq. 2.11 with respect to u,

$$\int M\ddot{u}_t du+\int C\dot{u}du+\int Rdu=0 \tag{2.12}$$

By replacing u by $(u_t - u_g)$ in Eq. 2.12, the first term becomes

$$\begin{aligned}\int M\ddot{u}_t du&=\int M\ddot{u}_t(du_t-du_g)=\int M\frac{d\dot{u}_t}{dt}du_t\\ -\int M\ddot{u}_t du_g&=\frac{M\dot{u}_t^2}{2}-\int M\ddot{u}_t du_g\end{aligned} \tag{2.13}$$

Then substituting Eq. 2.13 into Eq. 2.12:

$$\frac{M\dot{u}_t^2}{2}+\int C\dot{u}du+\int Rdu=\int M\ddot{u}_t du_g \tag{2.14}$$

The first term of the above equation is referred to as the "absolute" kinetic energy, E_k, since the absolute velocity is used to calculate it. Thus,

$$E_k=\frac{M\dot{u}_t^2}{2} \tag{2.15}$$

The second term in Eq. 2.14 relates to the damping energy, E_d, which is,

$$E_d=\int C\dot{u}du=\int C\dot{u}^2dt \tag{2.16}$$

and the third term in Eq. 2.14 is defined as the absorbed energy, E_a, which is

composed of recoverable elastic strain energy, E_s, and irrecoverable hysteretic energy, E_h. Thus,

$$E_a=\int Rdu=E_s+E_h \tag{2.17}$$

where E_s is equal to $R^2/2K$, and E_h is computed as the sum of the areas delimited by each loop traced by the force-displacement relationship of a system as it undergoes non-linear inelastic response.

The right-hand side term in Eq. 2.14 is defined as the absolute input energy, E_i,

$$E_i=\int M\ddot{u}_t du_g \tag{2.18}$$

since the inertia force, $M\ddot{u}_t$, applied to the structure is expressed in terms of the total acceleration relative to a fixed reference axis. It can be seen from Eq. 2.11 and Figure 2.1 that this force is equal to the restoring force plus damping force, and is also the total force applied to the structure's foundation. Therefore E_i represents the work done by the total base shear, $M\ddot{u}_t$, on the foundation's displacement, u_g.

Thus Eq. 2.14, the absolute energy equation, can be summarized as:

$$E_i=E_k+E_d+E_a=E_k+E_d+E_s+E_h \tag{2.19}$$

2.2.2.2 Equations for Relative Energy Method

By directly integrating Eq. 2.1 with respect to u, it becomes,

$$\int M\ddot{u}du+\int C\dot{u}du+\int Rdu=-\int M\ddot{u}_g du \tag{2.20}$$

The first term in Eq. 2.20 is,

$$\int M\ddot{u}du=\int M\frac{d\dot{u}}{dt}du=\int M\dot{u}d\dot{u}=\frac{M\dot{u}^2}{2} \tag{2.21}$$

and the "relative" kinetic energy, E_k', can be defined as:

$$E_k'=\frac{M\dot{u}^2}{2} \tag{2.22}$$

Note that, as the relative structural velocity is used to calculate the relative kinetic energy, and formulas for E_d and E_s remain unchanged.

The right hand term of Eq. 2.20 is the relative input energy, E_i', but now it represents the work done by the equivalent static lateral force, $-M\ddot{u}_g$, on the relative displacement, u. Therefore, the relative energy equation can be expressed as:

$$E_i'=-\int M\ddot{u}_g du=E_k'+E_d+E_s+E_h \tag{2.23}$$

2.2.2.3 Additional Comments

From the above presentation of energy equations, it can be seen that, in both methods, the input energy should be always equal to the sum of the kinetic, damping and absorbed energies, that is, energy balance always exists. This phenomenon, at the essence of all energy methods, has been used throughout this research programme to assess the accuracy of calculations and validate computer results: checking this balance ensures that an energy method is correctly used, and this is viewed as an important consideration throughout the conduct of this research.

2.2.3 Example

In order to demonstrate how the above various energies are calculated and how the energy balance works when a system is subjected to a specific ground excitation, an example is given in this section.

Assuming an undamped linear elastic SDOF system with mass of M and stiffness of K subjected to a simple rectangular pulse ground acceleration, as shown in Figure 2.3a. Over the interval $0 \le t \le t_d$, the ground velocity can be expressed as

$$\dot{u}_g = \int \ddot{u}_g dt = \ddot{u}_g t \tag{2.24}$$

as shown in Figure 2.3b, and the ground displacement is

$$u_g = \int \dot{u}_g dt = \frac{1}{2}\ddot{u}_g t^2 \tag{2.25}$$

as shown in Figure 2.3c. The system's relative displacement during the excitation is (Clough and Penzien 1975):

$$u = \frac{-M\ddot{u}_g}{K}(1-\cos\omega t) = \frac{-\ddot{u}_g}{\omega^2}(1-\cos\omega t) \tag{2.26}$$

and the corresponding relative structural velocity and acceleration can be obtained,

directly from Eq. 2.26, by

$$\dot{u}=\frac{-\ddot{u}_g}{\omega}\sin\omega t \tag{2.27}$$

$$\ddot{u}=-\ddot{u}_g\cos\omega t \tag{2.28}$$

Thus by substituting Eqs. 2.24 and 2.27 into Eq. 2.15, the absolute kinetic energy is:

$$E_k=\frac{M\dot{u}_t^2}{2}=\frac{M}{2}(\dot{u}+\dot{u}_g)^2=\frac{M\ddot{u}_g^2}{2}(\frac{1}{\omega}\sin\omega t-t)^2 \tag{2.29}$$

The damping energy is zero for an undamped system.

$$E_d=0 \tag{2.30}$$

The recoverable strain energy is:

$$E_s=\frac{1}{2}Ku^2=\frac{M\ddot{u}_g^2}{2\omega^2}(1-\cos\omega t)^2 \tag{2.31}$$

The hysteretic energy is null here since the system is linear elastic.

$$E_h=0 \tag{2.32}$$

The absolute input energy, by substitution of ü and $ü_g$ into Eq. 2.18, is

$$\begin{aligned} E_i &= \int M(ü+ü_g)du_g = Mü_g\int(1-\cos\omega t)\ d(\frac{1}{2}ü_g t^2) \\ &= Mü_g^2\int(1-\cos\omega t)t\ dt \\ &= Mü_g^2\ (\frac{t^2}{2}-\frac{t}{\omega}\sin\omega t-\frac{1}{\omega^2}\cos\omega t+k_1) \end{aligned} \tag{2.33}$$

Here, taking the condition that E_i is zero at the beginning when t is zero, the integration constant, k_1, is found to be $1/\omega^2$. If all right-hand side terms in Eqs. 2.29, 2.30, 2.31 and 2.32 are added up, the sum is equal to the above E_i, and therefore the energy balance is analytically verified. Alternatively, instead of using a closed-form solution, a step-by-step numerical procedure could be adopted, and this balance would be verified computationally provided the integration step would be chosen to be sufficiently small. Any resulting unbalance would reflect inaccuracy of calculation which can be remedied by further refinements in the size of integration step.

Similarly, by the absolute energy method, the relative kinetic energy is

$$E_k' = \frac{M}{2}\dot{u}^2 = \frac{Mü_g^2}{2\omega^2}\sin^2\omega t \tag{2.34}$$

The damping, strain and hysteretic energies are the same as in the above absolute energy method, and the relative input energy is

$$E_i' = -\int M ü_g du = \frac{Mü_g^2}{\omega^2}(1-\cos\omega t) \tag{2.35}$$

Note that energy balance still analytically exists here since the sum of E_k', E_d, E_s, and E_h is equal to E_i'.

Thus from this simple example, it can be seen that (i) for an undamped elastic SDOF system E_d and E_h are always zero, and (ii) according to Eqs. 2.31 and 2.34 the maximum E_k' is equal to the maximum E_s during the excitation.

CHAPTER 3

SDOF SYSTEM SUBJECTED TO RECTANGULAR PULSE EXCITATION

3.1 Introduction

Since a typical earthquake excitation could be interpreted as a complex sequence of pulses or sine-waves of various durations, frequencies and intensities, structural responses to such simple patterns of dynamic excitations need be studied first. This will allow the construction of energy spectra which could facilitate the prediction of structural energy demand under real seismic excitations, and also the identification of some valuable fundamental principles which could not be easily extracted and understood from the study of more complex excitations. Responses to simple impulse are investigated in this chapter, while responses to sine-wave loading will be studied in Chapter 4.

By comparing the maximum displacement responses of elasto-plastic SDOF system

subjected to pulses of different shapes in Figure 3.1 a to d (Biggs 1964), it can be seen that the rectangular pulse excitation leads to the largest displacement response. Based on this, and for simplicity, the rectangular pulse loading has been selected for the research presented in this section. It is noteworthy that the spectra in Figure 3.1 also provide a convenient source of ductility results for the consideration of the same problem in an energy approach.

The content of this chapter is divided into four main parts. In Section 3.2, the linear elastic response to rectangular pulse excitation is reviewed. Then in Section 3.3, four sample cases are studied for comparison and better understanding of the various energy responses to a fixed rectangular pulse excitation and different structural parameters. Later, in Section 3.4, energy spectra are presented for large numbers of structural parameters under the same loading. Finally, in Section 3.5, normalization methods are proposed to construct non-dimensional energy spectra so that various energy responses can be easily obtained for arbitrary rectangular pulse excitations.

3.2 Review of Linear Elastic Response of SDOF System Subjected to Rectangular Pulse Loading

The linear elastic solution of the equation of motion for a SDOF subjected to rectangular impulsive load is well-known (Clough and Penzien, 1975). For an undamped system, the displacement response is given as following.

When the system is being excited by ground motion ($0 \leq t \leq t_d$), it is under the loading

phase, which is also called Phase 1. During that time,

$$u=\frac{M\ddot{u}_g}{K}(1-\cos\omega t) \tag{3.1}$$

When the impulse is over ($t>t_d$), the system then begins free-vibration, also referred to as Phase 2. From that point,

$$u=\frac{\dot{u}_{td}}{\omega}\sin\omega(t-t_d)+u_{td}\cos\omega(t-t_d) \tag{3.2}$$

where u_{td} and $\dot{u}_{td}$ are the displacement and velocity of the system at the end of the excitation respectively.

Considering a damped system instead, it is known that, for short duration pulses, damping has little effect when the system is under excitation, and Phase 1 remains essentially unchanged. But the effect of damping must be considered in Phase 2 for $t>t_d$, and the response becomes

$$u=e^{-\xi\omega t}\left(\frac{\dot{u}_{td}+\xi\omega u_{td}}{\omega}\sin\omega t+u_{td}\cos\omega t\right) \tag{3.3}$$

From Eq. 3.1, it is obvious that the maximum possible displacement is $2M\ddot{u}_g/K$, that is to say, if a constant force is suddenly applied to a linear elastic system and sustained a sufficiently long time, the maximum resulting displacement is exactly twice that which would be obtained for the same force applied statically. Using the notation previously presented, this implies that systems with $\eta = 2$ are ensured linear-elastic response when subjected to rectangular impulse. This well known result is reported in all structural dynamics text books (Clough and Penzien 1975, Biggs 1964).

3.3 Case Studies on Displacement and Energy Response Time Histories

In this as well as the next section, an arbitrarily selected rectangular pulse as shown in Figure 3.2 is used in the analyses. Its peak ground acceleration, $\ddot{u}_{gmax}$ of 1 m/s^2, and the duration, t_d of 0.5 s, are sufficient to define it. Normalization considerations not constraining the size of rectangular pulse are introduced in a later section.

It is also noteworthy that ground velocity and displacement corresponding to a rectangular pulse, as illustrated in Figure 2.3, are not base-corrected, contrary to most earthquake records. In theory, if base correction was performed to the rectangular pulse, it would not launch the supporting foundation into a constant velocity and an increasing displacement subsequently to the end of the pulse excitation, as shown in Figure 2.3b and c, instead, ground velocity and displacement at the end of the pulse would return to zero. Simple attempts to base-correct a constant amplitude rectangular pulse would rapidly demonstrate that it cannot logically be done. Only more complex forms of excitation, notably not producing a constant velocity throughout when integrated (like an earthquake excitation), can be base-corrected. However, at this point, to keep things simple, and because, as will be demonstrated later, only some less meaningful energy terms are somewhat affected by the absence of a base-corrected input time history, base-correction will be ignored in this chapter.

To illustrate important conceptual differences in the energy response obtained when considering the relative or absolute energy criteria, four different SDOF systems having an arbitrarily selected mass of 1 kg are subjected to the aforementioned pulse base-excitation. These four SDOF systems, to be studied in the following examples,

are:

Example 1) T = 0.5 s, ξ = 0%, η = 1.0

Example 2) T = 0.5 s, ξ = 0%, η = 2.0

Example 3) T = 0.5 s, ξ = 2%, η = 1.0

Example 4) T = 1.0 s, ξ = 2%, η = 1.0

The effect of damping (ξ = 0% and 2%) will be illustrated by comparing the results of Example 1 and 3. The differences between typical inelastic and elastic responses will be expressed in comparing Example 1 and 2 (η = 1.0 and 2.0) respectively. The influence of the fundamental period of vibration will be illustrated by comparing Example 3 and 4 (T = 0.5 and 1.0 s). In each case, relative and total displacement time histories as well as absolute and relative energy time histories are presented for comparison. The individual input energy, kinetic energy, hysteretic energy and damping energy time history responses (when exist) are also displayed on the same plot to provide perspective.

3.3.1 Example 1

For this SDOF system having T = 0.5 s, ξ = 0%, η = 1.0, the resulting displacement ductility ratio μ is 6.3. The structure responds elastically only when its displacement does not exceed the yield displacement. From the relative displacement history shown in Figure 3.3, it can be seen that the SDOF system starts to behave inelastically at t $\approx$ 0.1 s, and eventually oscillates elastically about a "plastic residual offset" subsequently to the end of the excitation. It is obvious that, in this case, the maximum displacement ductility demand μ is a relatively good damage index as when the structure exceeds the yield displacement, it must be damaged.

Figure 3.4 is the absolute displacement time history. Gross differences in magnitudes make the relative displacement contribution to the total displacement imperceptible. This is a consequence of base correction not being done. Since the support excitation

is the same throughout all four examples, the dominance of absolute displacement time history over relative displacement will consistently recur. Hence, the equivalent of Figure 3.4 will not be presented for the subsequent examples.

Similarly to the relative displacement response history, both relative kinetic and recoverable strain energies (Figure 3.5) will first rapidly increase to reach at the onset of yielding, a maximum value which will be sustained for the remaining duration of the pulse loading. After termination of the pulse load, they will start to fluctuate in a reciprocating exchange of energy, in accordance to the classic free-vibration response of an undamped spring. In this phase of oscillation, when the structure reaches its maximum displacement, the strain energy is the maximum, while the kinetic energy is zero; alternatively, when the structure crosses the new static equilibrium point, the strain energy is zero, while the kinetic energy is the maximum. In the absence of damping, the maximum values of the kinetic and strain energies remain equal and constant when the structure oscillates.

As the structure retains a plastic residual deformation at the end of the pulse excitation, the hysteretic energy reaches and remains a maximum constant value (Figure 3.5), which can be related to the relative displacement response. Note that the hysteretic energy is only due to the structural inelastic deformation, the fluctuation of displacement within system's elastic range after the pulse loading is reflected by the recoverable strain and kinetic energies.

As also shown in Figure 3.5, the relative input energy is the sum of the relative kinetic, hysteretic and strain energies; damping energy is not applicable here. Once the pulse excitation is over, it can be seen that the input energy does not change anymore.

In Figure 3.6, results for the same SDOF system, but expressed in terms of absolute energies, are presented. For clarity a different vertical scale is used. There, the

strain and hysteretic energies are identical to those in Figure 3.5, but the kinetic and input energies are considerably different. Such differences between the absolute and relative kinetic and input energies are expected. For example, the equation of absolute kinetic energy is based on the absolute velocity, itself the sum of the relative velocity and the ground velocity (Eq. 2.15). Therefore the relative kinetic energy could be considered as just a subset of the absolute one. However, it is disconcerting to observe that the absolute input energy includes a free vibration phase which persists to fluctuate long after termination of the pulse ground excitation, i.e. the input excitation. Moreover, although the maximum value of kinetic energy is not equal to that of strain energy anymore, energy balance still exists.

3.3.2 Example 2

In this example (Figures 3.7, 3.8, 3.9), the SDOF's period and the damping ratio remain equal to those of the first example; only η changes to 2.0, which implies a stronger structure. Here, as expected (Figure 3.7), the structure behaves elastically over the entire displacement response time history.

As the structure remains elastic through out the response, it is able to return to a near zero displacement after it reaches a maximum displacement in spite of the pulse excitation being still applied. For similar reasons, after the excitation, the structure oscillates in free vibration about the initial zero axis as shown in Figure 3.7.

Figures 3.8 and 3.9 are the relative and absolute energy time histories. Here, the input energy (E_i or E_i') is equal to the sum of the kinetic energy (E_k or E_k') and strain energy only, since both the hysteretic and damping energies are zero. In the linear elastic range, the same observation as in Example 1 can be made regarding the different behaviour of those absolute and relative quantities. Besides, from the relative energy time histories (Figure 3.8), it can be seen obviously that over the

duration of the pulse loading, the maximum values of E_k' and E_s are not necessarily equal since external work due to the ground motion is continuously being applied.

3.3.3 Example 3

In this third example, T and η are again the same as in the first example, but in this case, the damping ratio ξ is 2%. The maximum displacement ductility ratio μ calculated is 5.5, slightly less than 6.3 obtained in the first example. Not surprisingly, as shown in Figures 3.10, 3.11, 3.12, the displacement response, as well as kinetic energy and strain energy will progressively attenuate as a function of the damping ratio.

From the relative energy time histories (Figure 3.11), it can be found that:

- All the non-damping energy values, including the relative input energy, are reduced by the presence of damping.
- The damped out relative kinetic and strain energies are converted directly to the dissipated damping energy.
- The relative input energy still keeps constant after the excitation.
- Also, as before, in order to follow the interconversion of kinetic and potential energy in the post-loading range, when E_k' is the maximum, E_s must be zero.

The fact that the gradually damped out kinetic and strain energies are converted into damping energy, as observed in Figure 3.11, can be easily explained mathematically by substituting Eq. 2.22 into Eq. 2.16. This gives

$$E_d = \int_0^t C \frac{2E_k'}{M} dt = 4\omega\xi \int_0^t E_k' dt \tag{3.4}$$

which states that the damping energy at time t equals the integral of the kinetic energy

over the interval from 0 to t, multiplied by a constant. Thus, when the kinetic and strain energies are completely attenuated, the damping energy will have reached its maximum.

In light of the important effect of damping on the overall energy distribution, a close scrutiny of the energy results is warranted, particularly when comparing Figures 3.11 and 3.5. This influence of damping is illustrated in Table 3.1 by comparing each energy value at 0.5 s, 1.0 s and 10.0 s with those in Example 1. These three time comparison points are selected as indicative of the structural response at three distinct stages: at the end of the pulse loading (0.5 s), a short and long period of time after termination of the pulse excitation (1.0 s and 10.0 s respectively).

From Table 3.1, it can be observed that in the presence of 2% damping, there is approximately a 14% drop of the maximum sustained hysteretic energy dissipated by the system. This is because, for a damped system, the damping energy can dissipate part of the input energy, and therefore reduces the amount of the hysteretic energy which needs to be dissipated by the structure.

Table 3.1 Comparison of relative energies in Example 1 and 3

Energy (Nm)	Time (s)					
	0.5		1.0		10.0	
	Ex. 1	Ex. 3	Ex. 1	Ex. 3	Ex.1	Ex.3
E_i'	0.0361	0.0325	0.0366	0.0329	0.0366	0.0329
E_k'	0.0032	0.0020	0.0025	0.0015	0.0030	0.0000
E_s	0.0032	0.0032	0.0007	0.0010	0.0002	0.0000
E_h	0.0298	0.0261	0.0334	0.0285	0.0326	0.0285
E_d	0.0000	0.0011	0.0000	0.0018	0.0000	0.0043

The absolute energy time histories are also constructed in Figure 3.12. Some observations can be summarized below:

- The strain, hysteretic and damping energies still remain the same as in Figure 3.11.
- All the non-damping absolute energies (Figure 3.6) are also greater than the ones when damping exists.
- As the non-base-corrected ground velocity (Figure 2.3) is used to calculate the absolute kinetic energy, E_k does not damp out as quickly as E_k' in the free vibration phase. Instead, it fluctuates and finally converges to a constant value of 0.125 N.m which is equal to $M\dot{u}_g^2/2$ when the relative velocity reduces to 0.
- The absolute input energy behaves like the absolute kinetic energy. After reaching a peak at the end of the excitation, it begins oscillating with decreasing amplitude and eventually levels off to a constant.

3.3.4 Example 4

In this example, a damping ratio ξ of 2% and η value of 1.0 are still being used, but the period of structure, T, is changed to 1.0 s. This makes the structure more flexible than in Example 1 to 3. Although the resulting displacement (Figure 3.13) and energy values (Figure 3.14 and 3.15) are greater (notice the different scales used in these figures), all plots are similar in shape to those in Example 3. As implied herein, a relationship exists between the period of the structure and pulse excitation duration. The mechanisms of this dependency with respect to structural energy considerations, will be investigated in the following attempts at normalization.

3.4 Energy Spectra

3.4.1 Introduction

To facilitate the design of structures subjected to severe seismic dynamic excitations, it would be desirable to develop energy spectra which would indicate how the peak energy responses of SDOF systems vary with the characteristics of the structure for a particular excitation. If various peak energy responses are plotted as a function of structural period, strength (η value) and damping ratio, the resulting spectra then could be used to determine the response of a particular system to a specific type of excitation. In addition, various spectra could potentially be combined to derive a set of design energy spectra which would incorporate the uncertainties related to the nature of the excitation. However, one of the necessary condition for the existence of such spectra is an accepted normalization procedure. Hence, in order to reveal trends in energy spectra and possible meaningful and stable normalization procedures, the study of energy spectra under simple dynamic excitation is essential before tackling

the more complex seismic problem.

In Section 3.4.2, input, kinetic, hysteretic and damping energy spectra are constructed, using the NONSPEC computer program (Mahin and Lin 1983), for SDOF systems with period ranging from 0.025 to 5.0 s, damping ratios of 0% and 2%, strength ratios, η, equal to 0.2, 0.4, 0.6, 0.8, 1.0, 1.02, 1.05, 1.1, 1.2, 1.3, 1.4, 1.6, 1.8, and 2.0, a 1 kg mass and the same rectangular pulse excitation used previously. It is noteworthy that the selected strength ratios are identical to those used by Biggs (1964) to construct his maximum displacement ductility spectra. This enables the verification of maximum ductility demands with Biggs' results in the early parts of this research program.

3.4.2 Energy Spectra

In this section, eleven sets of energy spectra (as shown from Figure 3.16 to 3.26) are constructed. Figures 3.16 to 3.20 consist of absolute and relative kinetic energy, strain energy, hysteretic energy and absolute input energy spectra derived for undamped SDOF systems, whereas Figures 3.21 to 3.26 are for systems with 2% damping and include an additional damping energy spectra.

All these energy spectra are constructed for SDOF systems subjected to the same rectangular pulse load defined in Section 3.3 (Figure 3.2). The horizontal axis is normalized as a function of t_d/T and responses are calculated over the range from 0.1 to 20. This is identical to the horizontal axis in Biggs' spectra (Biggs 1964), as shown in Figure 3.1. The dimensionless t_d/T ratio captures the relative relationship between the duration of rectangular pulse and the structural period. For example, when t_d/T is as small as 0.1, i.e. when the period of structure is 10 times greater than the pulse duration, the structure is mostly driven by the initial impulse magnitude as the system has hardly any time to deflect before the end of the pulse. On the other

hand, when t_d/T is as big as 10, i.e. when the structural period is 10 times less than the pulse duration, the structure has sufficient time to reach very large deformation prior to the end of pulse. Pulses embedded with earthquake ground motion records are generally contained between these limits. Using a t_d value of 0.5 s, structural period ranging between 0.025 and 5 s have been used to derive Figure 3.16 to 3.26, and within this range a large number of structural periods were considered to make each spectrum sufficiently smooth and continuous.

In these Figures, the various energy quantities are expressed in Joule unit (J) along the vertical axes. As the absolute kinetic and input energies typically have larger values as explained in Section 3.3.1, they share a different scale, with the y-coordinate varying from 0.1 to 0.5 J, and log-log scales are used for better readability. The strain, hysteretic, damping and relative kinetic energy spectra because of their smaller magnitude, share a y-axis varying from 0 to 0.12 J; in this case, a linear-log plot was found most suitable.

In this section, the magnitude of the pulse acceleration is still assumed as 1 m/s^2. For the different η values considered, structural yield strength can be derived based on Eq. 2.6. Note that for a given earthquake peak ground acceleration, the bigger the dimensionless η value is, the more strength the system has.

In these spectra, each point represents the maximum energy response obtained for that given structure (i.e. for a selected η, ξ and T), and the specific rectangular pulse excitation (i.e. t_d/T and $\ddot{u}_g$). In other words, each individual value read from these spectra represents the maximum energy reached during the corresponding extended energy time history. For instance, from Figure 3.16, the E_k of 0.17 J corresponding to t_d/T of 1.0 and η of 1.0 in the absolute kinetic energy spectra is obtained from the absolute kinetic energy time history of Section 3.3.1, Example 1, for which the peak energy value can be read from Figure 3.6.

By comparing the energy spectra of the same type for the damped and undamped cases and studying as well as each individual spectra from Figure 3.16 to 3.26, it can be found that:

- Figure 3.16 and 3.21, together with Figure 3.17 and 3.22, 3.18 and 3.23, 3.19 and 3.25, 3.20 and 3.26, in pairs, for undamped and damped systems respectively, are very similar in shape, the undamped systems always having the higher energy demand. This effect of damping has already been described in the sample case studies of Section 3.3.3.
- The energy balance cannot be checked directly using only spectra. The sum of the maximum E_k, E_s, E_h, and E_d will always be greater than the maximum E_i for a given structure since these maximum values generally occur at different times through out the time histories. However, the energy balance has been checked to exist for every single case throughout these histories.
- The individual kinetic, strain, hysteretic and damping energies are found to be more significant and meaningful than the input energy spectra. The relative input energy spectra were felt not worth constructing.
- The absolute kinetic energy spectra (Figure 3.16 for 0% damping, Figure 3.21 for 2% damping), strain energy spectra (Figure 3.17 and 3.22) and relative kinetic energy spectra (Figure 3.20 and 3.26) have similar shape, although the absolute energy spectra always have greater values as expected. In these spectra, the lower energies are observed to occur for the larger t_d/T and lower η values, except in the relative kinetic energy spectra where E_k' is sometimes larger for low η values, such as 0.2, 0.4, 0.6 and 0.8. This can be explained as following: for a given η, a larger t_d/T results in a stiffer system. Hence, the slope in the system's force-displacement relationship diagram (Figure 2.2) is greater, and for the same structural force within the elastic range, the resulting displacement is then less; based on the definitions of the strain and kinetic energies, a smaller displacement would also cause a smaller velocity, which in turns leads to smaller strain and kinetic energies. Alternatively, from a different perspective, for a given t_d/T, a larger η value corresponds to a

stronger system. Hence, in the force-displacement relationship diagram (Figure 2.2), for the same slope, R_y is larger, with potential to lead to higher strain or kinetic energy demands. As for the exceptions in the relative kinetic energy spectra, which occur for structures with η of 0.2 to 0.8, in the long t_d/T range, the corresponding SDOF systems subjected to rectangular pulse excitation are so substantially under-strength, that throughout the excitation, their velocity keeps increasing much more rapidly than if the system remained elastic due to the low (or zero) post yield stiffness. Consequently, so does the maximum relative kinetic energy. However, the recoverable strain energy will not change since the yield displacement remains the same. All the energy due to displacement beyond the yield point becomes irrecoverable hysteretic energy.

- The hysteretic energy spectra for the simple case of a system subjected to rectangular pulse excitation can be easily related to the maximum displacement ductility ratio spectra, largely because the nonlinear component of the response is not cyclic: displacement will reach a maximum value in one direction and then fluctuate within the elastic range around the new plastic offset. Consequently, the hysteretic energy equation can be written, according to the structural bilinear force-displacement relationship model (Figure 2.2), as:

$$E_h = R_y(u_{max} - \Delta_y) = R_y(\mu - 1)\Delta_y = (\mu - 1)(\eta M\ddot{u}_{gmax})^2/K \tag{3.5}$$

where $u_{max} = \mu\Delta_y$, and $R_y = \eta M\ddot{u}_{gmax}$. Using Eq. 3.5, values in the hysteretic energy spectra can be checked against those in Biggs' displacement ductility ratio spectra (Figure 3.1a). For example, if the period of an undamped system with η value of 1.0 and mass of 1 kg is 0.5 s, its stiffness is then

$$K = (2\pi/T)^2 M = 157.91\,(N/m) \tag{3.6}$$

From Figure 3.1a the maximum displacement ductility ratio for such a system is 6.0. Based on Eq. 3.5,

$$E_h = (6.0-1)(1.0\times1.0\times1.0)^2/157.91 = 0.0317 \; Joule \tag{3.7}$$

which is indeed the value read from the hysteretic energy spectra (Figure 3.18). In other words, Biggs' ductility ratio spectra can easily be converted into an hysteretic energy spectra for rectangular pulse loading. Hence, this implies that for rectangular pulse excitation, the hysteretic energy and displacement ductility ratio are equivalent structural damage index.

- The damping and relative energies are closely related as shown in Eq. 3.4. Therefore the total loss of relative kinetic energy due to damping effect is converted to be the maximum damping energy. Moreover, the peculiar shape of the damping energy spectra (Figure 3.24) in the low η and large t_d/T range can be explained much like being done above for the relative kinetic energy spectra (Figure 3.26)(i.e. under-strength systems yielding at progressively larger velocities). It is debatable, however, whether damping energy should be accounted as dissipating simultaneously to hysteretic energy, which would occur in this case as long as the relative energy is non-zero. This is currently a pecularity of the way energy methods equations are set-up. Whether to correspond realistically to the proper physical behaviour of such structures remains to be investigated in future research.

3.5 Normalization

3.5.1 Preliminary Concepts

In the previous sections, the parameters t_d, $\ddot{u}_g$ and M were arbitrarily given the values

of 0.5 s, 1 m/s^2, and 1 kg. Actually, those parameters can hold any values and need not be constrained as done before. To generalize the previous findings, in this section, normalization procedures are sought.

Uang and Bertero (1988a) proposed a first normalization method based on the idea that the input energy can be converted to an equivalent velocity by the following relationships:

$$V_i=\sqrt{\frac{2E_i}{M}} \quad or \quad V_i'=\sqrt{\frac{2E_i'}{M}} \tag{3.8}$$

for absolute and relative energy methods respectively. Yet, V_i and V_i' are not dimensionless and are not generalized in terms of structural strength or ground excitation parameters.

In order to have a general dimensionless energy measure recognizing the latter, the maximum ground velocity, which is $\int_0^{t_d}\ddot{u}_g dt$ for the rectangular pulse excitation, is integrated into a first new proposed normalization equation, expressed as:

$$E^{NG}=\frac{2E}{M(\int_0^{t_d}\ddot{u}_g dt)^2} \tag{3.9}$$

where E can be any absolute or relative energy, i.e. E_i, E_i', E_k, E_k', E_s, E_h or E_d, and E^{NG} is that energy normalized by ground motion parameters corresponding to the input energy, or more exactly the kinetic energy produced by an infinitely stiff and strong structure subjected to the same ground excitation.

A second new proposed normalization method is formulated to integrate structural

strength of an idealized structural force-displacement model, such as the bilinear model as shown in Figure 2.2, by the following expression:

$$E^{NR}=\frac{E}{R_y\Delta_y} \tag{3.10}$$

where E is any energy (as before), and E^{NR} is that energy normalized by the work needed to yield this SDOF system under monotonically increasing loading. However, since E_i, E_i', E_k, E_k', E_s and E_d do not have a known direct relationship with the aforementioned structural force-displacement relationship, also called hysteresis models, and $R_y\Delta_y$, it does not appear logical to use this second method to normalize energies other than E_h.

Since the denominators in Eq. 3.9 and 3.10 are always constant with the energy unit of Joule (J) for any given rectangular pulse and structure, both of the normalization methods would result in non-dimensional energy quantities, i.e. the normalized energies would be unique and easily established values.

In order to illustrate the reliability of the above two normalization methods, a numerical example is provided following. Another set of input parameters, different from the ones used up to now in this chapter, is arbitrarily selected as displayed in Table 3.2. Nonlinear step-by-step dynamic time-history analyses are conducted, resulting maximum energies are recorded and normalized values are calculated. By applying the two proposed normalization methods, it can be seen that, for the same values of normalized excitation duration, t_d/T, strength ratio, η, and damping ratio, ξ, each energy term for which the normalization method is deemed applicable has a unique normalized value as expected. The small numerical inaccuracies as exhibited in Table 3.2 and quantified in Table 3.3 are negligible. They are mostly attributable to the different time steps chosen for the step-by-step analyses of structures having different periods, and minor round-off errors also. Hence, the proposed

normalization methods are promising in use, and normalized energy spectra will be constructed in next section.

Table 3.2 Normalized energies calculated for an example with $\xi = 0\%$, $t_d/T = 1.0$, $\eta = 1.0$

Energy Term	Maximum Energy		
	Non-Normalized (J)	Normalized	
		E^{NG}	E^{NR}
(a) For M = 1 kg, $\ddot{u}_g$ = 1 m/s^2, t_d = 0.5 s			
E_i	0.2054	1.643	-
E_k	0.1720	1.376	-
E_s	0.003229	0.02583	-
E_h	0.03343	0.2674	5.279
E_i'	0.03661	0.2929	-
E_k'	0.003223	0.02578	-
(b) For M = 100 kg, $\ddot{u}_g$ = 4 m/s^2, t_d = 1.5 s			
E_i	2915	1.619	-
E_k	2438	1.354	-
E_s	46.06	0.02559	-
E_h	477.0	0.2650	5.230
E_i'	523.1	0.2906	-
E_k'	45.81	0.02545	-

Table 3.3 Comparison of results from Table 3.2

Energy Term	Normalized Energy					
	E^{NG}			E^{NR}		
	From (a)	From (b)	Error (%)	From (a)	From (b)	Error (%)
E_i	1.643	1.619	1.5	-	-	-
E_k	1.376	1.354	1.6	-	-	-
E_s	0.02583	0.02559	0.93	-	-	-
E_h	0.2674	0.2650	0.90	5.279	5.230	0.93
E_i'	0.2929	0.2906	0.79	-	-	-
E_k'	0.02578	0.02545	1.3	-		

3.5.2 Normalized Energy Spectra

Figures 3.27 to 3.37 are normalized energy spectra corresponding to non-normalized ones (Figures 3.16 to 3.26) constructed in Section 3.4.2, including spectra for input (absolute), kinetic (absolute or relative), strain, hysteretic and damping energies obtained using the first normalization method. The advantages of this normalization method are: (i) the shapes of normalized and non-normalized spectra are similar, as can be seen by comparing Figures 3.16 to 3.26 with Figures 3.27 to 3.37; (ii) The normalization factors, consisting of the structural mass and maximum ground velocity square, can be interpreted physically as the input energy corresponding to an infinitely rigid mass resting on the ground. For that infinitely rigid mass, assuming the frictional resistance between that mass and the ground is not exceeded, the only energy that can possibly exist to balance the input energy is the kinetic energy, regardless of relative or absolute as relative and total velocities are identical; this energy somewhat provides a measure of the raw energy potential of a given ground

excitation as felt at one geographic location. Hence, the normalized maximum strain, hysteretic, damping or relative kinetic energy amount demanded by SDOF systems using the first method should not exceed 1.0, since these energies are normalized by a maximum input energy. Figures 3.28, 3.29, 3.31, 3.32, 3.33, 3.34, 3.35 and 3.37 confirm this result. On the other hand, the absolute input and kinetic energies which more sensitively reflect the presence of non-base-corrected ground motion, it can still be observed and rationalized that for increasingly stiff SDOF systems (i.e. with decreasing periods T, and correspondingly increasing t_d/T), the E_k^{NC} and E_i^{NC} should converge toward a value of 1, as can be seen in Figures 3.27, 3.30, 3.32, and 3.36.

Figures 3.38 and 3.39 are the normalized hysteretic energy spectra for Figure 3.18 and 3.23 using the second normalization method. Recall that it is felt this method only logically works for the hysteretic energy. As different structures have different R_y and Δ_y values, the resultant normalized energy spectra from this method are not in the same shapes as the non-normalized ones. Systems with smaller η and larger t_d/T have smaller R_y and Δ_y, resulting in relatively big normalized values. It can be also seen that the trends expressed in Figures 3.38 and 3.39 can easily be understood: (i) the structural hysteretic energy demand will increase for systems having progressively lower η value (i.e. lower normalized strength ratio) for a given value of normalized period; (ii) for a given η, systems with shorter periods will have higher normalized hysteretic energy demand because of their correspondingly smaller yield displacements, and; (iii) when η equals to 2.0, E_h^{NR} will always be 0, as expected.

3.5.3 Additional Comments

Till now only rectangular pulse ground excitation has been considered. Of all the energies studied, it is clear that the hysteretic energy is the parameter of major significance for seismic structural survival, and from this point onwards in this research project, more attention will be paid to the hysteretic energy.

CHAPTER 4

SDOF SYSTEM SUBJECTED TO SINE-WAVE EXCITATION

4.1 Introduction

Consistent with the observation that earthquakes are complex sequences of pulses and sine-waves of various frequencies, periods and intensities, and having already studied SDOF systems subjected to rectangular pulse excitations in Chapter 3, in this chapter, the energy-related behaviour of SDOF systems subjected to sine-wave excitation will be investigated.

By following the same approach as in Chapter 3, a further review of the well known solution for the linear elastic response of SDOF system subjected to harmonic loading (Clough and Penzien 1975) is first made. Then simple case studies will be examined to determine trends in energy response, and finally spectral normalization will be conducted.

4.2 Review of Linear Elastic Response of SDOF System Subjected to Harmonic Loading

For a SDOF system subjected to a harmonically varying ground-motion acceleration of amplitude $\ddot{u}_g$ and circular frequency $\bar{\omega}$, the differential equation of motion is (Clough and Penzien 1975)

$$M\ddot{u}+C\dot{u}+Ku=-M\ddot{u}_g Sin\bar{\omega}t \tag{4.1}$$

When the system is undamped, the above equation reduces to

$$M\ddot{u}+Ku=-M\ddot{u}_g Sin\bar{\omega}t \tag{4.2}$$

for which the relative displacement response of the structure is

$$u=\frac{M\ddot{u}_g}{k}\frac{1}{1-\beta^2}(Sin\bar{\omega}t-\beta Sin\omega t) \tag{4.3}$$

where

- $M\ddot{u}_g/k$ is the maximum displacement which would be produced if the load $M\ddot{u}_g$ was applied statically;
- $1/(1-\beta^2)$ is called dynamic magnification factor (MF), representing dynamic amplification effect of harmonically applied load;
- $Sin\bar{\omega}t$ represents response component at frequency of the applied load, i.e. the steady state response directly related to the load;
- ($\beta Sin\omega t$) stands for response component at natural vibration frequency, which is the free vibration effect induced by initial conditions. Since in practice

damping will cause this term to eventually vanish, it is called the transient response component;

- β is the ratio of frequencies of applied load to natural vibration frequency, $\bar{\omega}/\omega$.

When the system is damped, assuming the structural frequency remains the same, the general solution of Eq. 4.1 is

$$u = e^{-\xi\omega t}(A Sin\omega t + B Cos\omega t) + \frac{M\ddot{u}_g}{k}\frac{1}{(1-\beta^2)^2+(2\xi\beta)^2}[(1-\beta^2)Sin\bar{\omega}t - 2\xi\beta Cos\bar{\omega}t] \tag{4.4}$$

The first term representing the transient response to the applied loading, damps out quickly, and generally is of little interest. The second term is the steady state response at the frequency of the applied loading, but out of phase with it. It is well known (Clough and Penzium, 1975) that, the steady state response can also be written as

$$u=\phi Sin(\bar{\omega}t-\theta) \tag{4.5}$$

where the amplitude, ϕ, of the steady state response is expressed as:

$$\phi=\frac{M\ddot{u}_g}{k}[(1-\beta^2)^2+(2\xi\beta)^2]^{-\frac{1}{2}} \tag{4.6}$$

and the phase angle, θ, by which the steady state response lags behind the applied load is

$$\theta=\tan^{-1}\left(\frac{2\xi\beta}{1-\beta^2}\right) \tag{4.7}$$

The ratio of the resultant response amplitude to the static displacement which would be produced by the force $M\ddot{u}_g$ is called the dynamic magnification factor D and is given by

$$D=\frac{\phi}{\frac{M\ddot{u}_g}{k}}=[(1-\beta^2)^2+(2\beta\xi)^2]^{-\frac{1}{2}} \tag{4.8}$$

Clearly, from Eq. 4.8, the dynamic magnification factor, D, varies with the frequency ratio, β, and the damping ratio, ξ. The classic plot of this relationship is reproduced in Figure 4.1.

It may be noted from Figure 4.1 that the peak steady state response occurs at a frequency ratio near unity for slightly damped systems. This is the condition where the frequency of the applied load equals the natural vibration frequency, and it is called resonance. From Figure 4.1, it is apparent that the steady state response of an undamped system tends toward infinity at resonance. Moreover, it can be easily derived from Eq. 4.8 that at resonance, i.e. $\beta = 1$, the dynamic magnification factor is inversely proportional to the damping ratio.

$$D_{\beta=1}=\frac{1}{2\xi} \tag{4.9}$$

Figure 4.2 illustrates how the dynamic resonant response builds up in cases with and without damping. For the undamped system, it will eventually produce unbounded response and significant distress in the structure unless its frequency is changed. On the other hand, damping limits the resonant response amplitude as illustrated in the lower sketch of Figure 4.2.

4.3 Case Studies of Displacement and Energy Response Time Histories

In this section, an arbitrarily selected sine-wave excitation, as shown in Figure 4.3, is used in analysis, with the peak value of ± 1 m/s^2, period of 2.0 s. Later, normalization considerations will be addressed as those done earlier for rectangular pulses to produce the spectra dependent only on non-dimensional values of these parameters.

It is noteworthy that the sine-wave ground motion selected is not base corrected either, and that, consequently the ground displacement will again increase along the time history. Although this has some influence on absolute input and kinetic energies as mentioned in Section 3.3, the other energy terms as well as the displacement ductility ratio are not affected by this. Since hysteretic energy is the term of major interest in earthquake-resistant design, base-correction would not produce additional valuable knowledge and has been omitted.

Two examples are presented below to illustrate the typical response of SDOF systems subjected to the sine-wave excitation of Figure 4.3. It should be noted that in this section, only undamped response is considered. The effect of damping is expected to be identical to what has been observed in Chapter 3. Besides, only relative displacement and relative energy response time histories are constructed for these examples since they can more vividly reflect structural response.

In first example, β is 1 (i.e. the period of structure is 2.0 s), and η values of 9999 and 2.0 are considered to compare the elastic and inelastic resonant responses. In second example, β is 0.75 (i.e. the period of structure is now 1.5 s), and η values of

9999 and 2.0 are again used to obtain elastic and inelastic behaviour respectively. Structural mass is arbitrarily taken as 1 kg for both examples.

4.3.1 Example 1

Figure 4.4 compares the undamped relative displacement time histories of SDOF systems having the same period of 2.0 s, and η values of 9999 and 2.0 respectively. The elastic system with η of 9999, vibrates with an unbounded amplitude as predicted for resonance, as described in Section 4.2. However, for the inelastic system with η of 2.0, as soon as the yielding threshold of magnitude 0.203 m is exceeded, though β is still equal to 1, the response is bounded, i.e. the amplitude of vibration stops increasing after the first few cycles. Note that, for inelastic system, the magnitude of the maximum value of displacement is asymmetric about the zero axis, as a consequence of plastic offsets of the at-rest position introduced by the presence of nonlinear inelastic excursions. This is well illustrated in Figure 4.15 for simple structural hysteresis loops using bilinear force-displacement relationship; there, it can be observed that for loading, unloading and load reversal cycles, the value of yield displacement is re-defined either by deducting $2\Delta_y$ when unloading from the maximum positive inelastic displacement reached, or reciprocally by adding $2\Delta_y$ to the minimum negative inelastic displacement reached when reloading. Here, in Example 1, for the assumed bilinear force-displacement relationship, Δ_y is 0.203 m. Moreover, in this case of constant-amplitude-sine-wave loading, the two re-defined yield displacements do not change from their values of -0.0815 m and 0.1568 m, whereas the maximum and minimum displacements are also constant and equal to 0.3245 m and -0.2492 m after a few cycles.

Figures 4.5 and 4.6 are the relative energy time histories for η of 9999 and 2.0 respectively. By comparing these two figures, the following can be observed.

- The elastic system has generally greater energy demands except for the

hysteretic energy which exists only in the inelastic system. Note that Figure 4.5 and 4.6 are plotted in different scales.

- For the elastic system, during the ground motion, the relative kinetic energy, E_k', and the strain energy, E_s, reciprocally fluctuate within the unbounded envelope of the input energy, E_i' (Figure 4.5).
- For the inelastic system, in the presence of the hysteretic energy, E_h, during the excitation, the maximum values of E_k' and E_s reached at each cycle remain stable, in agreement with what is expected by observation of the displacement time history in Figure 4.4, whereas E_h keeps increasing by a constant value for every half cycle of the sine-wave loading (Figure 4.6). This behaviour of hysteretic energy is substantially different than what was obtained previously for rectangular pulse excitation. The harmonic sine-wave ground acceleration excitation causes structural cyclic inelastic response and stabilizes it into a fixed pattern past the first few cycles of excitation.
- It can be easily verified that the sum of two consecutive steps in the hysteretic energy time history is equal to the area under one hysteresis loop.
- Energy balance still exists for both structures.

4.3.2 Example 2

In this example, β is equal to 0.75, and therefore, the period of the structure is 1.5 s. Figure 4.7 shows the relative displacement time history for η of 9999. The system behaves elastically with the resulting response being the same as that predicted by Eq. 4.3. Also, the system vibrates in a repeated pattern whose period is the least common multiple of the periods of the system and the sine-wave ground excitation.

When η is 2.0, the yield displacements in reversed direction of hysteresis loops are permanently offset to -0.0075 m and 0.0843 m, for the same reasons described in Example 1. The system rapidly becomes inelastic and the response pattern observed

for the elastic system does not exist (Figure 4.8). The magnitude of maximum displacement is close to that of Figure 4.7 when η is 9999 for the elastic system: β of 0.75 does not produce resonance and, in fact, the amplitude of vibration in this case is much less.

Figure 4.9 shows the relative energy time histories for η values of 9999. The energy histories are bounded and exhibit a particular repetitive pattern. Since energies are related to the displacement response, the period of each pattern is also the least common multiple of the periods for the system and the load.

For η is 2.0 as displayed in Figure 4.10, the maximum kinetic and strain energies are not so different from those obtained for the elastic system, while the resultant maximum input energy constantly grows as hysteretic energy accumulates. By comparing Figure 4.10 with Figure 4.6 of Example 1, they are found to be of similar shape, although the growth of hysteretic energy per cycle is less, i.e. the area under each hysteretic loop is smaller than before.

4.4 Normalized Energy Spectra

4.4.1 Preliminary Concept

As per the same logic described in Chapter 3 for rectangular pulse excitations, normalized spectra are also needed for sine-wave ground excitations. The two normalization methods previously proposed and used are retained here. But before constructing the normalized spectra, it must be ensured that these normalization procedures still work well for the case at hand, i.e. the normalized spectra are generally applicable irrespectively of which parameter(s) change(s).

For the first normalization method (Eq. 3.9), the consideration of structural mass in the method is not affected by the sine-wave nature of ground motion, but the maximum ground velocity, which was defined as $\int_0^{t_d} \ddot{u}_g dt$ for rectangular pulse excitation, is inadequate for sine-wave loading and need to be improved. By substituting the appropriate maximum sine-wave velocity of $\ddot{u}_{gmax}\bar{T}/2\pi$ into Eq. 3.9, a first normalization method for harmonic sine-wave excitation could be proposed as:

$$E^{NG} = \frac{2E}{M\left(\frac{\ddot{u}_{gmax}\bar{T}}{2\pi}\right)^2} \tag{4.10}$$

but the input and the hysteretic energies being cumulative and increasing at each yield excursion,. Eq. 4.10 is not adequate either, except for kinetic and strain energies. To normalize cumulative unbounded and periodic energies here, the number of cycles of the sine-wave loading must be taken into account, as in the proposed form below of a normalized energy per input cycle.

$$E^{NG} = \frac{2E}{NM\left(\frac{\ddot{u}_{gmax}\bar{T}}{2\pi}\right)^2} \tag{4.11}$$

where N stands for the number of cycles of a sine-wave.

By the same logic, the form of the second proposed normalization method becomes

$$E_h^{NR} = \frac{E_h}{NR_y\Delta_y} \tag{4.12}$$

Beyond this periodicity consideration, the normalization parameters defined in the previous chapter are unchanged and their rationalization need not be repeated here.

As for the construction of the normalized energy spectra, the dimensionless quantity, β, (i.e. $T/\bar{T}$) is a more meaningful representation of normalized period for x-axis, and is used here.

In order to illustrate the reliability of the above new proposed normalization formulas, a numerical example is provided following. Another set of input parameters different from the ones used in Example 2 of this chapter are arbitrarily selected and displayed in Table 4.1. Resultant maximum energies and normalized values are calculated and tabulated there. By comparing E^{NG} or E^{NR} of the two cases, it can be seen that, for the same normalized excitation period, β, strength ratio, η, and damping ratio, ξ, each energy term for which the normalization method is deemed applicable has a unique normalized value as expected. Small numerical errors as exhibited in Table 4.2 are negligible for the same reason exposed in Chapter 3. Hence the proposed normalization procedures are effective, and the corresponding normalized energy spectra will be constructed in next section.

Table 4.1 Normalized energies calculated as an example with $\xi = 0\%$, $\beta = 0.75$, $\eta = 2.0$

Energy Term	Maximum Energy		
	Non-Normalized (J)	Normalized	
		E^{NO}	E^{NR}
(a) For M = 1 kg, $\ddot{u}_{gmax}$ = 1 m/s^2, T = 1.5 s, $\bar{T}$ = 2.0 s, t_d = 20 s			
E_i	5.304	10.47	-
E_k	0.6061	11.96	-
E_s	0.1162	2.294	-
E_h	4.958	9.787	2.175
E_i'	5.086	10.04	-
E_k'	0.1836	3.624	-
(b) For M = 100 kg, $\ddot{u}_{gmax}$ = 5 m/s^2, T = 0.45 s, $\bar{T}$ = 0.6 s, t_d = 9 s			
E_i	1811	10.59	-
E_k	136.5	11.98	-
E_s	26.12	2.292	-
E_h	1731	10.12	2.250
E_i'	1762	10.31	-
E_k'	41.58	3.648	-

Note: E_i, E_i' and E_h must consider the number of cycles of the sine-wave loading in their normalization as proposed by Eq. 4.11.

Table 4.2 Comparison of results from Table 4.1

Energy Term	Normalized Energy					
	E^{NG}			E^{NR}		
	From (a)	From (b)	Error (%)	From (a)	From (b)	Error (%)
E_i	10.59	10.47	1.1	-	-	-
E_k	11.98	11.96	0.17	-	-	-
E_s	2.292	2.294	0.087	-	-	-
E_h	10.21	9.787	3.2	2.175	2.250	3.4
E_i'	10.31	10.04	2.6	-	-	-
E_k'	3.624	3.648	0.66	-		

Although it is possible to construct all the energy spectra, as done in Chapter 3, it is neither desirable nor practical to do so. The meaning and significance of each energy term has already been established in previous chapters, and it is elected to concentrate, from now on, on the hysteretic energy. This is in line with the stated objectives of this research project. It is noteworthy that kinetic and strain energies are not dissipative and could not be useful for damage predictions. As for damping energy, although it is dissipative, the hysteretic energy spectra do, indirectly, take into account the presence of damping ratio factor. Hence, the damage predictions for systems with different damping coefficients would simply need refer to hysteretic energy spectra derived for the appropriate damping percentage.

4.4.2 Normalized Hysteretic Energy Spectra

In this section, general hysteretic energy spectra are constructed for sine-wave excitations using the two proposed normalization methods. It is hoped these spectra, together with the normalized hysteretic energy spectra for rectangular pulse excitation, would find use to predict the hysteretic energy demand of simple systems subjected to real earthquake excitations.

4.4.2.1 Normalization Method 1

Figures 4.11 and 4.12 are the resulting normalized hysteretic energy spectra produced using

$$E_h^{NG} = \frac{2E_h}{NM\left(\frac{\ddot{u}_{gmax}\bar{T}}{2\pi}\right)^2} \tag{4.13}$$

for damping ratio of 0% and 2% respectively. Again, using this method, the shape of the figures closely corresponds to the hysteretic energy spectra without normalization (not presented here), as the denominator of Eq. 4.13 is constant for a given input. It is observed that the undamped normalized hysteretic energies are slightly bigger than those for systems with a 2% damping ratio.

Again, any point on spectra corresponds to the maximum value obtained throughout an hysteretic energy time history which itself is related to a particular physical displacement time history. This perspective helps explain why in both Figures 4.11 and 4.12, for big η values E_h^{NG} varies much as a function of β, while for small η, it does not. For structures nearing resonant response, if the potential to develop a strong elastic response exists prior to yielding, the structure can be visualized as

entering the inelastic range with a larger velocity (i.e. a larger impact or kinetic energy) at each cycle, which in turn requires more hysteretic energy to be stopped. Stronger structures (with larger η) possess more of such an elastic displacement response, whereas for weak systems (with smaller η), such elastic response can hardly develop.

4.4.2.2 Normalization Method 2

Figures 4.13 and 4.14 are the normalized hysteretic energy spectra produced using

$$E_h^{NR} = \frac{E_h}{NR_y\Delta_y} \tag{4.14}$$

for damping ratio of 0% and 2% respectively. Since this normalization method is related to the yield strength and displacement of the system, it is felt these normalized spectra can reflect the structural energy demand in a more straightforward and rational manner. As revealed by both figures, systems with higher η value have lower hysteretic energy demands, i.e. stronger structures yield less and consequently have a higher ability to resist cyclic dynamic excitations.

When $\beta < 0.8$, systems start to respond as if subjected to pulse excitations, since the period of sine-wave is becoming relatively bigger than the structural period and each cycle of loading could be considered as a pulse impacting the system. Thus for one cycle of excitation and one η value, smaller β results in greater energy demand.

4.4.3 Additional Comment

In this and the previous Chapters, normalized hysteretic energy spectra for SDOF

structures subjected to rectangular pulse and constant amplitude sine-wave ground excitations have been constructed according to two proposed normalization methods respectively. In both cases, the hysteretic energy is found to be a good indicator of the structural nonlinear cyclic cumulative behaviour. It remains to investigate how these spectra could be used to predict hysteretic energy demand under real earthquake excitation.

CHAPTER 5

SDOF SYSTEM SUBJECTED TO REAL EARTHQUAKES

5.1 Introduction

It is hoped, as already mentioned, that the normalized hysteretic energy spectra for individual rectangular pulses and sine-wave excitations derived in Chapter 3 and 4, can be used to predict the energy demand of SDOF systems subjected to real earthquakes. In this chapter, the feasibility of the two normalization methods will be first studied for systems subjected to real earthquakes. Then prediction of hysteretic energy using the previously derived pulse spectra will be attempted statistically by considering earthquakes as a sequence of equivalent rectangular pulses. Finally, similar prediction will be also attempted by modelling real earthquakes as multiple sine-wave patterns and series of separate half sine-waves.

Five major earthquakes will be considered to obtain the statistical information needed

to have reliable prediction spectra. They are the Imperial Valley El Centro Earthquake of May 18, 1940 (S00E component), San Fernando Pacoima Dam Earthquake of Feb. 9, 1971 (S16E component), Helena Montana Earthquake of Oct. 31, 1935 (S00W component), Western Washington Olympia Earthquake of Apr. 13, 1949 (N04W component), and Parkfield California Earthquake of Jun. 27, 1966 (N65E component).

5.2 Extension of Proposed Normalization Methods to Real Earthquakes

Of the two normalization methods proposed in Chapter 3 and 4, the first one uses the maximum ground velocity and structural mass in its normalization equation, whereas the second one considers structural yield strength and displacement. Both performed very well for the simple rectangular pulse and sine-wave excitations. Whether these methods can be realistically applicable to real earthquakes, and how they could be used to predict the corresponding energy demands remains to be determined.

For a real earthquake, it is difficult to directly normalize the hysteretic energy against a unique value of maximum ground velocity as per the first method in spite of the ground information being always base-corrected. Obviously, the highly random nature of any given earthquake excitation does not land itself well to such a rigid frame work. A number of different normalization approaches have been considered but none proved to be dominantly superior to the ones adopted in the remaining of this work.

On the contrary, the second proposed normalization method is easily applicable for real earthquake excitations, as the yield strength, R_y, and yield displacement, Δy of

any structure can always be determined. However, it is limited to the hysteretic energy spectra for reasons previously mentioned. Hence, only the second normalization method is proposed in this chapter.

5.3 Prediction of Seismic Hysteretic Energy by Equivalent Rectangular Pulses Method

In order to predict seismic hysteretic energy from spectra derived for rectangular pulse excitations, any earthquake must first be modelled as a sequence of rectangular pulses. Toward this goal, the following procedure is introduced:

For a given earthquake's ground acceleration time history record, each of the numerous crossing of the zero axis, such as points i, j, k in Figure 5.6, delimitates the boundaries of a positive or negative area. Any such single positive or negative area can be considered as a pulse with a maximum acceleration value and a corresponding area. In order to change such an irregularly shaped pulse to an equivalent rectangular pulse of same maximum acceleration and area, an equivalent time duration, t_d, must be defined as illustrated in Figure 5.6. By repeating the same procedure to every area thus defined by two consecutive crossings of the time axis of the earthquake acceleration time history diagram, an actual earthquake record can be replaced by a sequence of discontinuous rectangular pulses. The resulting distribution of such equivalent pulses for a particular earthquake is shown in Figure 5.1.

Computer programs were written to make the above procedure simple, fast and more accurate (list of these programs is provided in Appendix A). One program converts the raw earthquake acceleration data into a sequence of equivalent rectangular pulses defined by their amplitudes and equivalent durations, and a second program calculates

the cumulative normalized hysteretic energy at the end of the excitation. For the later program, information on the previously constructed normalized hysteretic energy spectra for rectangular pulse excitation is contained in a matrix, and the corresponding hysteretic energy for a given equivalent pulse can be directly obtained by double interpolation. The resulting sum of these portions of normalized hysteretic energies calculated by the computer program is actually a raw predicted normalized hysteretic energy for a given earthquake, and noted as $E_h^{NR\prime}$. This $E_h^{NR\prime}$ is then compared with the true normalized hysteretic energy noted as E_h^{NR} directly and separately calculated for the earthquake itself using NONSPEC. Finally, the ratio of predicted to actual hysteretic energy can be determined for an ensemble of earthquakes.

As mentioned in Section 5.1, five earthquakes are selected to generate statistical results. For each earthquake, the true normalized hysteretic energies, E_h^{NR}, and corresponding predicted values, $E_h^{NR\prime}$, are calculated and compared for various undamped SDOF systems over ten structural periods (0.1 s, 0.2 s, 0.3 s, 0.4 s, 0.6 s, 0.8 s, 1.0 s, 1.25 s, 1.5 s and 2.0 s) and six structural strength ratios (0.4, 0.6, 0.8, 1.0, 1.2 and 1.4). Here, only the 0% damping ratio case is considered; the principle would be the same for damped systems.

After many comparisons, it was found that the predicted results are not often close to the actual earthquake ones. This discrepancy is understandable because the equivalent rectangular pulse method assumes a zero initial velocity and displacement at the beginning of every pulse, which is actually not true in reality. Nonetheless, a certain trend was discovered to exist for the ratio of $E_h^{NR\prime}$ to E_h^{NR} as a function of different structural periods and strength ratios.

The simplest way to establish the relationship between the predicted and actual normalized hysteretic energy results is to construct their ratio-spectra. To immediately establish the general trend for an average of many earthquakes, instead of building one set of spectra for each earthquake, the mean curves for five

earthquakes are constructed as a function of various structural periods and strength ratios, as shown in Figure 5.2. For completeness, the mean plus one standard deviation curves are also constructed in Figure 5.3. It is noteworthy that the mean minus one standard deviation curves could be just as easily derived. It can be observed from both Figures 5.2 and 5.3 that in most circumstances except for systems with very short periods and low η values, the ratio of $E_h^{NR'}/E_h^{NR}$ is less than 1, which implies the predicted results under-predicting the normalized hysteretic energy demand. Therefore, an effective prediction method must take into account and correct this deficiency.

Assuming that the five earthquake records used to derive Figure 5.2 and 5.3 are representative earthquakes for many regions of the world, equations for the $E_h^{NR'}/E_h^{NR}$ ratio can be derived to allow direct and accurate prediction of hysteretic energy.

Hence, the results presented in Figure 5.2 and 5.3 can also be replaced by smoother ones defined by equations. Assuming curves of exponential form to be adequately representing the trends in data, best curve fitting is done based on linear regression analysis. The resulting equations for the six strength ratios are derived in Table 5.1.

Table 5.1 Best-fit equations for curves in Figures 5.2 and 5.3

η value	Mean $E_h^{NR'}/E_h^{NR}$	Mean Plus Standard Deviation $E_h^{NR'}/E_h^{NR}$
0.4	$\frac{E_h^{NR'}}{E_h^{NR}} = 1.29e^{-1.36T}$ (5.1)	$\frac{E_h^{NR'}}{E_h^{NR}} = 1.37e^{-1.07T}$ (5.2)
0.6	$\frac{E_h^{NR'}}{E_h^{NR}} = 1.16e^{-2.17T}$ (5.3)	$\frac{E_h^{NR'}}{E_h^{NR}} = 1.35e^{-1.84T}$ (5.4)
0.8	$\frac{E_h^{NR'}}{E_h^{NR}} = 1.99e^{-0.57T}$ (5.5)	$\frac{E_h^{NR'}}{E_h^{NR}} = 1.41e^{-1.74T}$ (5.6)
1.0	$\frac{E_h^{NR'}}{E_h^{NR}} = 2.23e^{-0.84T}$ (5.7)	$\frac{E_h^{NR'}}{E_h^{NR}} = 2.67e^{-5.04T}$ (5.8)
1.2	$\frac{E_h^{NR'}}{E_h^{NR}} = 1.81e^{-0.75T}$ (5.9)	$\frac{E_h^{NR'}}{E_h^{NR}} = 2.12e^{-5.93T}$ (5.10)
1.4	$\frac{E_h^{NR'}}{E_h^{NR}} = 1.36e^{-0.46T}$ (5.11)	$\frac{E_h^{NR'}}{E_h^{NR}} = 1.35e^{-6.66T}$ (5.12)

The accuracy of the resulting curve fitting for Figures 5.2 and 5.3 is quite acceptable, as illustrated in Figure 5.4 for an arbitrarily selected parameter-set. Interpolation between the curves for various η can also be performed if necessary.

To more explicitly demonstrate how the aforementioned procedure works to predict the hysteretic energy demand of a specific SDOF system, an example is given as following:

A SDOF system with period of 0.4 s and strength ratio of 0.6 is subjected to the El Centro earthquake. Using the computer program to automatically convert the earthquake into equivalent rectangular pulses, and the predicted normalized hysteretic energy obtained is 16.55. This value is only a preliminary predicted value of $E_h^{NR\prime}$ and need be revised to get the final result. According to Figure 5.2 or Eq. 5.3, the mean ratio of $E_h^{NR\prime}$ to E_h^{NR} is about 0.487, while the mean plus one standard deviation value from either Figure 5.3 or Eq. 5.4 is 0.647. Thus, for a one standard deviation of uncertainty, the true predicted normalized hysteretic energy demand of such a structure varies between 25.58 (16.55 over 0.647) and 50.61 (16.55 over 0.327), with an average value of 33.98 (16.55 over 0.487).

To obtain the predicted non-normalized hysteretic energy itself, the normalized value needs to be multiplied by structural yielding strength and displacement. Assuming the mass of the SDOF system in this example to be 1000 kg, its yield strength is then

$$R_y = \eta \times M\ddot{u}_{gmax} = 0.6 \times 1000 \times 3.417 \doteq 2050.2 \ (N) \qquad (5.13)$$

the maximum ground acceleration, $\ddot{u}_{gmax}$, is 3.417 m/s² for this earthquake. The

corresponding yield displacement is

$$\Delta_y = \frac{R_y}{K} = \frac{R_y}{(\frac{2\pi}{T})^2 M} = \frac{2050.2}{(\frac{2\pi}{0.4})^2 \times 1000} \doteq 8.32\times10^{-3}(m) \tag{5.14}$$

Thus, the predicted hysteretic energy demand for this SDOF system is

$$E_h' = E_h^{NR\prime}(R_y \Delta_y) \doteq 580\ (J) \tag{5.15}$$

where $E_h^{NR\prime}$ is taken as its mean value, i.e. 33.98.

The predicted value of E_h' can be easily checked by directly running NONSPEC computer program for this same SDOF system and the El Centro earthquake. The resulting exact hysteretic energy demand calculated is 555.4 Joule, an error of only about 4.4%.

This example illustrates that the concept and procedure of the equivalent rectangular pulses method is quite promising to predict hysteretic energy demand of a SDOF system. Eventually, more earthquake records, instead of the only five earthquakes considered in this research, should be taken into account to make the ratio-spectra more reliable. Moreover, earthquakes with frequency characteristics specific to certain geographic regions, as suggested by many researchers (Housner and Jennings 1964, Clough and Penzien 1975, Bertero and Mahin 1976, Chopra and Lopez 1979), could be considered to further improve, in the future, the prediction of normalized hysteretic energy.

5.4 Prediction of Seismic Hysteretic Energy Using Sine-wave Excitation Spectra

5.4.1 Equivalent Sine Pulses Method

By analogy with Section 5.3, real earthquakes could be modelled as a sequence of equivalent sine pulses. The procedure is identical to that previously described with the difference that two adjacent zero crossing points on the time axis of an earthquake ground motion record define a sine pulse of same maximum acceleration and duration as the actual irregular pulse from the earthquake record. Information on the previously constructed normalized hysteretic energy spectra for sine-wave excitation must also be used instead, interpreting each sine-pulse as a half-cycle duration sine-wave on that spectra. Computer programs were again written to facilitate the simulation work, and their listings are provided in Appendix A.

However, because of the limited range of β available on the normalized hysteretic energy spectra of Figure 4.13, i.e. the spectra obtained by the second normalized method for sine-wave excitations, not as many structural periods can be selected, as previously done for the equivalent rectangular pulses method, to construct mean ratio-spectra of $E_h^{NR\prime}$ to E_h^{NR} for the same five earthquakes. For example, the range of β on that Figure varies from 0.5 to 1.5 (a factor of 3), whereas the t_d/T used to derive the rectangular pulse excitations spectra ranged from 0.2 to 20 (a factor of 10). Nonetheless, it is possible to produce a partial ratio-spectra for structural periods from 0.3 s to 1.0 s, as shown in Figure 5.5. Beyond this range, for a given earthquake, some equivalent sine pulses fall outside the limits of the normalized hysteretic energy spectra constructed in Chapter 4 for sine-wave excitations, and a reliable result cannot be calculated as some contributions to the total hysteretic energy would be missing. In future research, the range of those normalized hysteretic energy spectra for sine-wave excitations would need to be extended.

Nevertheless, for the partial results obtained, Figure 5.4 appears to reveal the same trends as the ratio-spectra for rectangular pulse simulation. Unfortunately, curve fitting by regression analysis can not be meaningfully conducted over this limited range.

5.4.2 Prediction Method Based on the Use of Fourier Series

Another possible approach which has been considered to predict seismic hysteretic energy spectra consisted of trying to relate the Fourier Spectra of an actual earthquake to the previously derived normalized spectra for sine-wave excitation. Conceptually, an earthquake acceleration record can be perceived as a large number of simultaneously applied sine or cosine waves having different fundamental periods. By fast Fourier transform, the Fourier Spectra of the input excitation can be obtained. Unexpectedly, these resultant sine and cosine waves are all the ones with very small amplitudes which cannot cause a structure respond inelastically, and consequently no hysteretic energy is produced. Inverse Fourier Transform can obviously restore the actual time history earthquake record.

After performing a few such transforms, difficulties were encountered trying to relate the resulting Fourier Spectra to the normalized hysteretic energy spectra in any meaningful way. A first problem resides in the continuous nature of Fourier Spectra: the amplitude is a function of the number of digitization points. To remediate this shortcoming, values (areas) over a certain range of fundamental periods, ΔT, were lumped to an average value. However, for many practical values of ΔT considered, the amplitudes of the resulting pulses were still not sufficient intense to produce any inelastic response. Hence, attempts to use the Fourier Spectra have been, so far, inconclusive. The listings of fast Fourier transform computer program is provided also in Appendix A.

CHAPTER 6

CONCLUSIONS

In this thesis, assuming that earthquakes are complex sequences of rectangular puises and sine-waves, the energy methods proposed by Uang and Bertero are used to calculate energy demands of SDOF systems subjected to rectangular pulse and sine-wave excitations. Normalized energy spectra are constructed for both kinds of excitations by applying two new proposed energy normalization methods, and a methodology is formulated to predict hysteretic energy demands of SDOF systems of assumed elastic perfectly plastic model subjected to real earthquakes based on the availability of these normalized spectra for simple excitations. Some important conclusions of this research project are summarized below:

- The absolute energy method, which has been promoted by some researchers as superior to the relative energy method, has some practical shortcomings as illustrated herein, particularly regarding the definition of input and kinetic energies. As illustrated in the case of pulse excitation, a conceptual paradox

exists in that input energy can still fluctuate much past the end of the input (i.e. ground) excitation. The relative energy method, for its lack of such quirks and peculiarities but also for its close relationship to the parameters of engineering interest, seems a superior method.

- Energy methods produce good indicators of the nonlinear inelastic seismic structural performance.
- Hysteretic energy, which reflects the cumulative nonlinear inelastic cyclic response, is, by far, the most appropriate energy term to quantify energy dissipation demand of structures during earthquakes. This makes distinctions between absolute and relative energy methods less critical.
- The two new proposed energy normalization methods, one using maximum ground velocity square and structural mass as a normalization basis, the other structural yield strength and displacement, both produce useful dimensionless energy values; they are also very easily determined for simple rectangular pulse and sine-wave excitations.
- Normalized predicted hysteretic energy can be easily obtained for actual earthquakes excitations by (i) converting theses earthquakes into equivalent pulses, (ii) summing the values read for each pulse from the normalized hysteretic energy spectra constructed for simple rectangular pulse or sine-wave excitations, and (iii) adjusting the total values by ratio-spectra or equations statistically calibrated against a number of real earthquake records. The procedure is simple, has proven to work, and allows direct and reliable prediction of hysteretic energies without the need to resort to complex and time-consuming step-by-step nonlinear inelastic time-history analyses.

Future research on this topic is needed to extend the range of application of findings and improve the fundamental understanding of the behaviour of respective energy terms during earthquake excitations. In particular, and closer to the scope of this research project,

- The range of the normalized hysteretic spectra for sine-wave excitations would

benefit to be enlarged.

- More structural strength-displacement models other than the bilinear elastic perfectly plastic model are to be considered.
- More reliable or geographically dependant ratio-spectra could be constructed by the consideration of more earthquake records.
- Energy-based seismic design methods are desirable and must be developed for the evaluation and design of seismic-resistance of existing and new structures.

REFERENCES

Akiyama, H. (1985), "Earthquake resistant limit-state design for buildings", University of Tokyo Press.

Anderson, J.C. and Bertero, V.V. (1969), "Seismic behaviour of multi-story frames by different philosophies", *Report No. UCB/EERC-69/11*, Earthquake Engineering Research Centre, University of California, Berkeley, California.

Bertero, V.V. and Mahin, S.A. (1976), "Establishment of design earthquakes-evaluation of present methods", *International Symposium on Earthquake Structural Engineering.*

Bertero, V.V. and Popov, E.P. (1965), "Effect of large alternating strains on steel beams", *Proceedings*, Vol.91, No.ST1, ASCE, pp. 1-12.

Biggs, J.M. (1964), "Introduction to Structural Dynamics", McGraw-Hill, New York.

Bruneau, M. and Mahin, S.A. (1990a), "Ultimate behaviour of heavy steel section welded splices and design implications", *Journal of Structural Engineering*, Vol.116, No.8, ASCE.

Bruneau, M. and Mahin, S.A. (1990b), "Normalizing inelastic seismic response of structures having eccentricities in plan", *Journal of Structural Engineering*, Vol.116, No.12, ASCE.

Bruneau, M. and Mahin, S.A. (1992), "Inelastic seismic torsional response of simple symmetric structures", *Canadian Journal of Civil Engineering*, Vol.19, No.1.

Chopra, A.K. and Lopez, O.A. (1979), "Evaluation of simulated ground motions for predicting elastic response of long period structures and inelastic response of structures", *Earthquake Engineering and Structural Dynamics.*

Clough, R.W. and Penzien, J. (1975), "Dynamics of Structures", McGraw-Hill, New

York.

Conte, J.P., Pister, K.S. and Mahin, S.A. (1990), "Influence of the earthquake ground motion process and structural properties on response characteristics of simple structures", *Report No. UCB/EERC-90/09*, Earthquake Engineering Centre, University of California, Berkeley.

Fajfar, P. and Fischinger, M. (1990), "Earthquake design spectra considering duration of ground motion", *Proceedings of Fourth U.S. National Conference on Earthquake Engineering*, EERI, Vol.2, pp. 15-24.

Fajfar, P., Vidic, T., and Fischinger, M. (1990), "A measure of earthquake motion capacity to damage medium-period structures", *Soil Dynamics of Earthquake Engineering*, Vol.9, pp. 236-242.

Goel, S.C. and Berg, G.V. (1968), "Inelastic earthquake response of tall steel frames", *Journal of the Structural Division*, Vol.94, No.ST8, pp. 1907-1914, ASCE.

Hadjian, A.H. (1982), "A re-evaluation of equivalent linear models for simple yielding systems", *Earthquake Engineering and Structural Dynamics*, Vol. 10, pp. 759-767.

Housner, G.W. (1956), "Limit design of structures to resist earthquakes", *Proceedings of the First World Conference on Earthquake Engineering*, pp. 5:1-11, Berkeley, California.

Housner, G.W. and Jennings, P.C. (1964), "Generation of artificial earthquakes", *Journal of the Engineering Mechanics Division*, ASCE, EM1, pp. 113-150.

Housner, G.W. and Jennings, P.C. (1977), "The capacity of extreme earthquake motions to damage structures", *Structural and Geotechnical Mechanics*, pp. 102-116, W.J. Hall, Prentice-Hall, Englewood Cliffs, New Jersey.

Iwan, W.D. (1980), "Estimating inelastic response spectra from elastic spectra", *Earthquake Engineering and Structural Dynamics*, Vol. 8, pp. 375-388.

Jennings, P.C. (1965), "Earthquake response of a yielding structure", *Journal of the Engineering Mechanics Division*, Vol.90, No.EM4, pp. 41-68, ASCE.

Kato, B. and Akiyama, H. (1982), "Seismic design of steel buildings", *Journal of the Structural Division*, Vol.108, No.ST8, pp. 1709-1721, ASCE.

Kuwamura, H. and Galambos, T.V. (1989), "Earthquake load for structural reliability", *Journal of Structural Engineering*, ASCE, 115, pp. 1446-1462.

Leger, P. and Dussault, S. (1991), "Seismic energy dissipation in MDOF structures", *Journal of Structural Engineering*, ASCE.

Mahin, S.A. and Lin, J. (1983), "Construction of Inelastic Response Spectra for Single-degree-of-freedom Systems", *Report No. UCB/EERC-83/17*, Earthquake Engineering Centre, University of California, Berkeley.

McCabe, S.L. and Hall, W.J. (1989), "Assessment of seismic structural damage", *Journal of Structural Engineering*, ASCE, Vol.115.

McKevitt, W.E., Anderson, D.L., Nathan, N.D. and Cherry, S. (1979), "Towards a simple energy method for seismic design of structures", *Proceedings of the Second U.S. National Conference on Earthquake Engineering*, pp. 383-392, EERI.

Naeim, F. et al (1989), "The seismic design handbook", Van Nostrand Reinhold, New York.

National Building Code of Canada 1990, (1990), Associate Committee on the National Building Code, National Research Council of Canada, Ottawa.

Newmark, N.M. and Hall, W.J. (1973), "Procedures and criteria for earthquake resistant design", *Building Science Series No.46*, pp.209-236, Building Practices for Disaster Mitigation, National Bureau of Standards.

Pecknold, D.A. and Riddle, R. (1978), "Effect of initial base motion on response spectra", *Journal of the Engineering Mechanics Division*, Vol. 104, No. EM2, ASCE, pp. 485-491.

Sedarat, H. and Bertero, V.V. (1990), "Effects of torsion on the linear and nonlinear seismic response of structures", *Report No. UCB/EERC-90/12*, Earthquake Engineering Research Centre, University of California, Berkeley.

Tembulkar, J.M. and Nau, J.M. (1987), "Inelastic modelling and seismic energy dissipation", *Journal of Structural Engineering*, ASCE, Vol.113, pp. 1373-1377.

Trifunac, M.D. and Brady, A.G. (1975), "A study on the duration of strong earthquake ground motion", *Bulletin of the Seismological Society of America*, Vol.65, No.3, pp. 581-626.

Uang, C.M. (1991), "Establishing R (or R_w) and C_D factors for building seismic provisions", *Journal of Structural Engineering*, ASCE, Vol.117, pp. 1446-1462.

Uang, C.M. and Bertero, V.V. (1986), "Earthquake simulation tests and associated studies of a 0.3-scale model of a 6-story concentrically braced steel structure", *Report*

No. UCB/EERC-86/10, Earthquake Engineering Research Centre, University of California, Berkeley.

Uang, C.M. and Bertero, V.V. (1988a), "Use of energy as a design criterion in earthquake-resistant design", *Report No. UCB/EERC-88/18*, Earthquake Engineering Research Centre, University of California, Berkeley.

Uang, C.M. and Bertero, V.V. (1988b), "Implication of recorded earthquake ground motions on seismic design of building structures", *Report No. UCB/EERC-88/13*, Earthquake Engineering Research Centre, University of California, Berkeley.

Uang, C.M. and Bertero, V.V. (1990), "Evaluation of seismic energy in structures", *Journal of Earthquake Engineering and Structural Dynamics*, Vol.19, pp.77-90.

Veletsos, A.S., Newmark, N.M. and Chelapati, C.V. (1965), "Deformation spectra for elastic and elasto-plastic systems subjected to ground shock and earthquake motions", *Proceedings of the Third World Conference on Earthquake Engineering*, pp. II-663 to II-678.

Wu, J. and Hanson, R.D. (1989), "Study of inelastic spectra with high damping", *Journal of Structural Engineering*, ASCE, Vol.115, pp. 1412-1431.

Zahrah, T.F. and Hall, W.J. (1984), "Earthquake energy absorption in SDOF structures", *Journal of Structural Engineering*, ASCE, Vol.110, pp. 1757-1772.

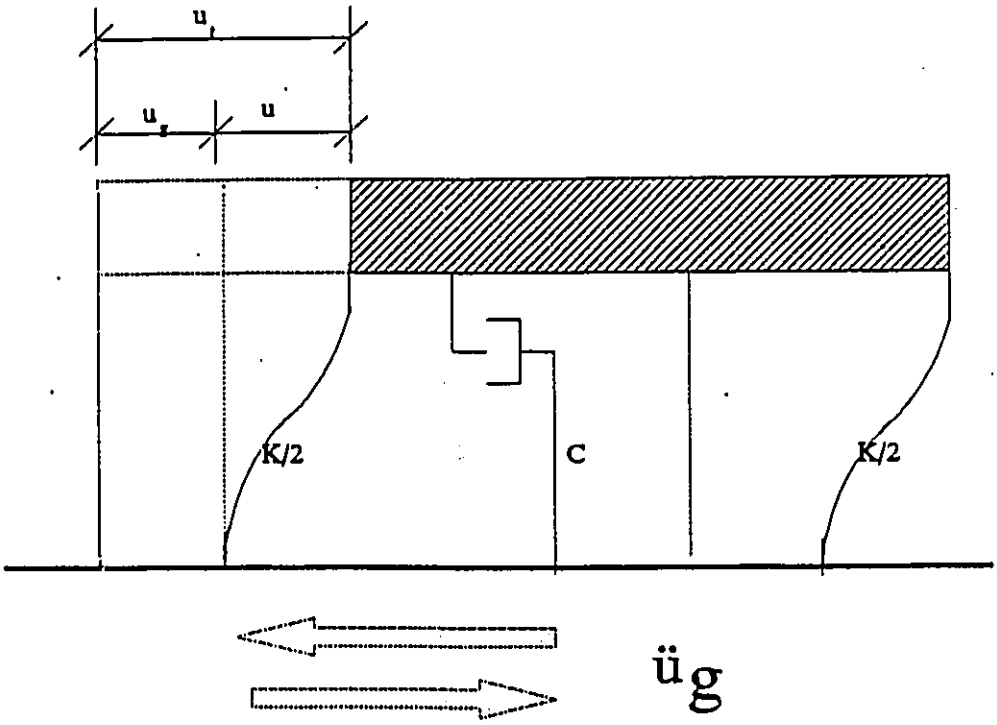

Figure 2.1 SDOF system subjected to ground excitation

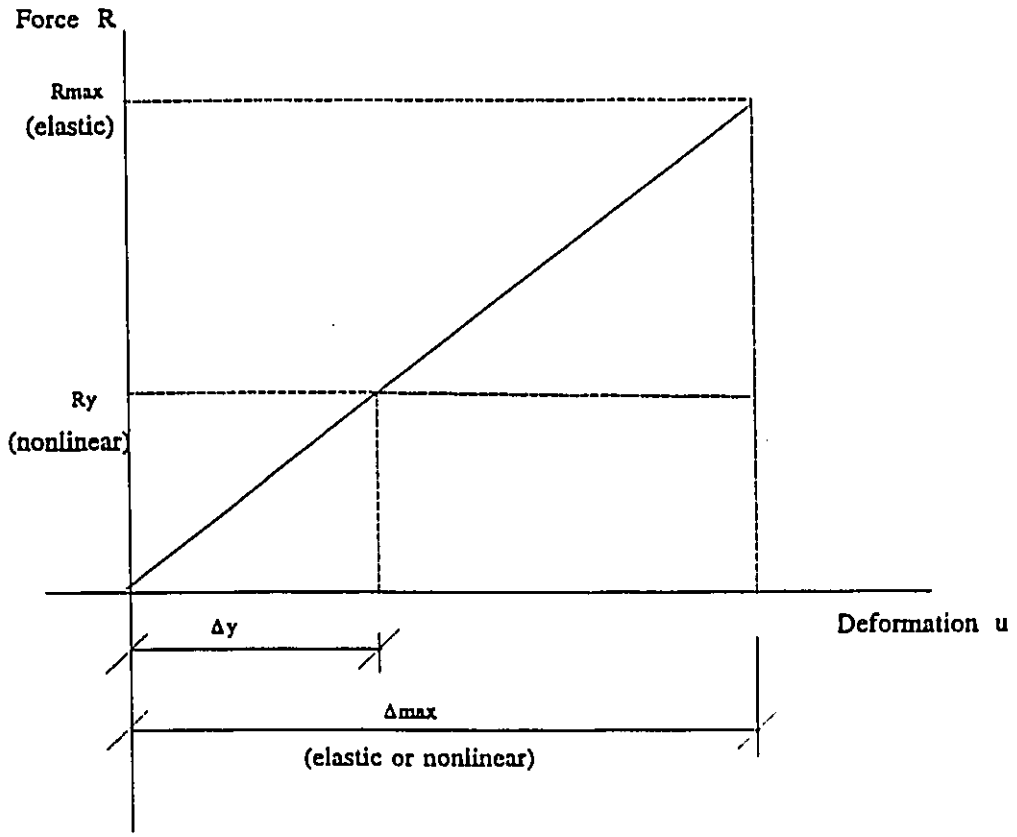

Figure 2.2 Ideal monotonic nonlinear inelastic sample member force-displacement relationship

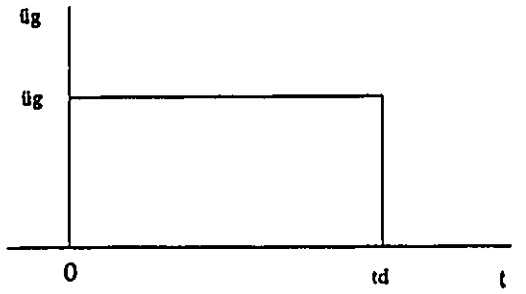

(a) acceleration

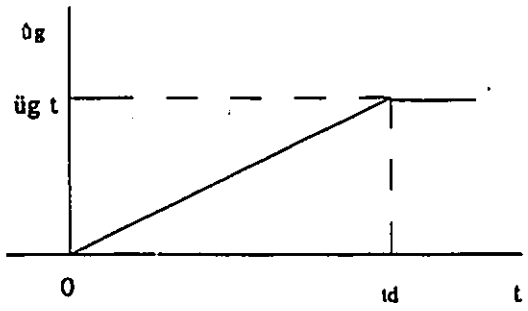

(b) velocity

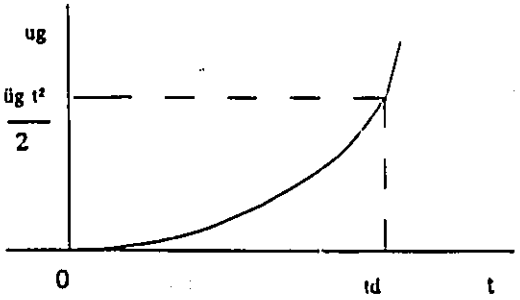

(c) displacement

Figure 2.3 Ground excitation information for example of Section 2.2.3

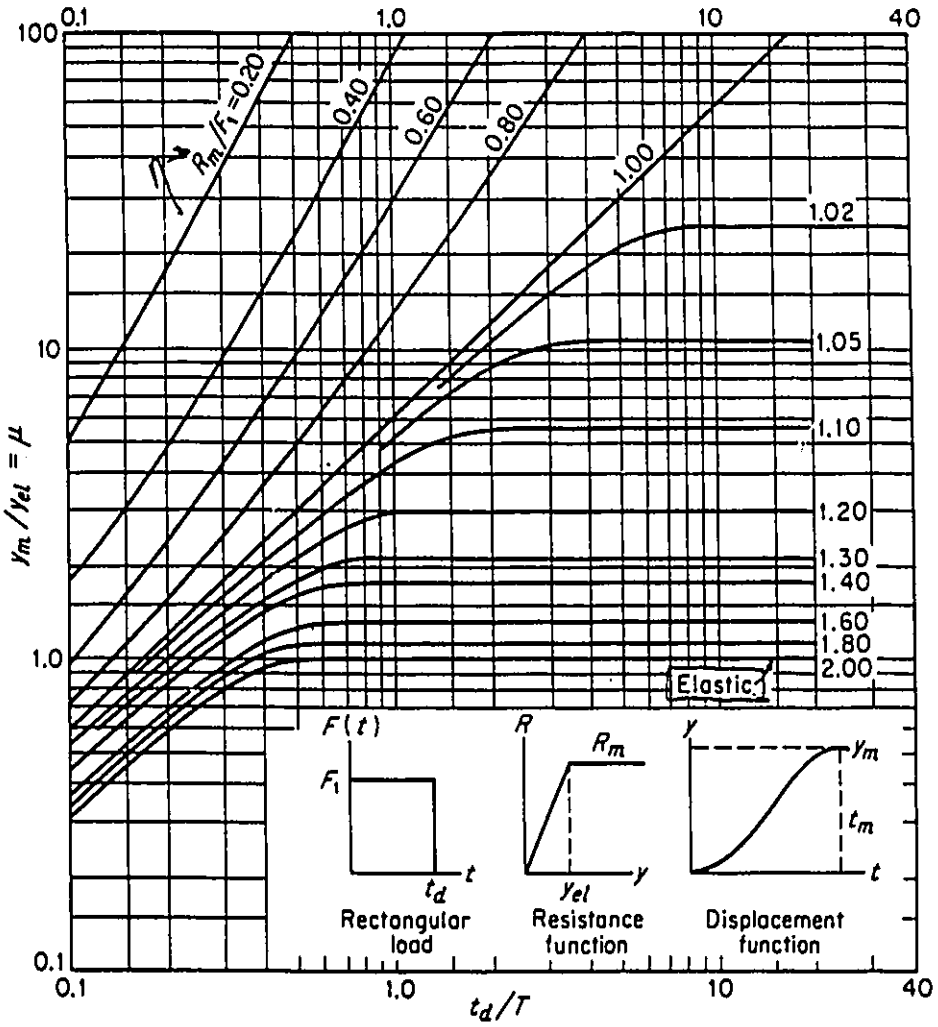

Figure 3.1a Maximum response of SDOF systems (undamped) due to rectangular load pulses (Biggs, 1964)

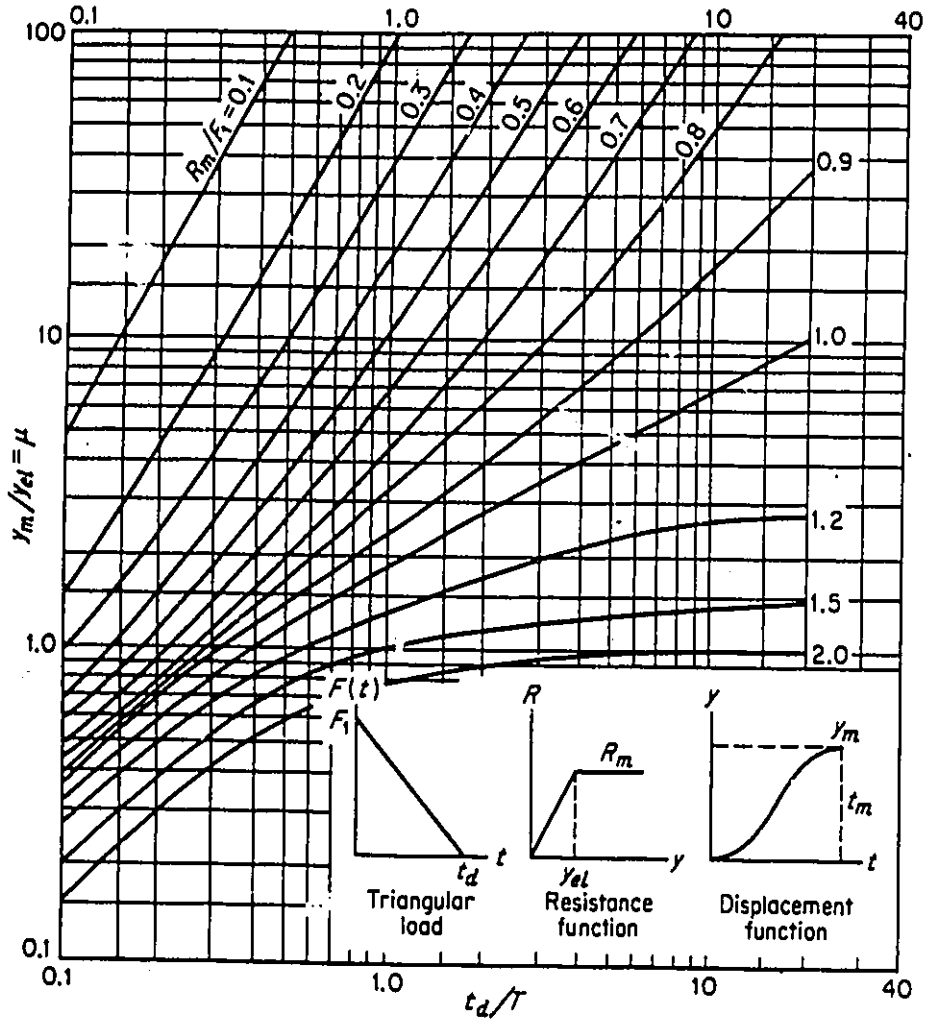

Figure 3.1b Maximum response of SDOF systems (undamped) due to triangular load pulses with zero rise time (Biggs, 1964)

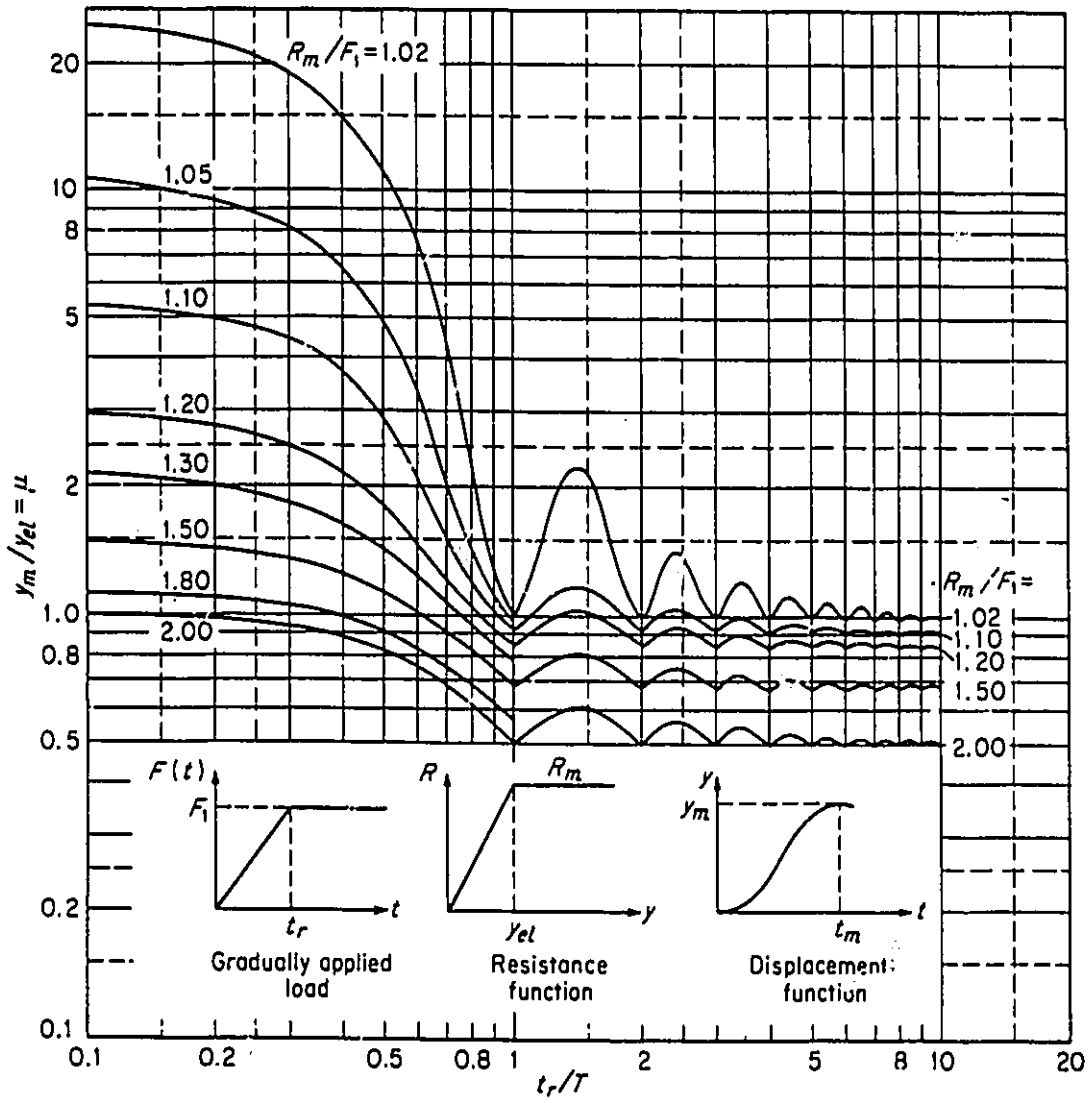

Figure 3.1c Maximum response of SDOF systems (undamped) due to constant force with finite rise time (Biggs, 1964)

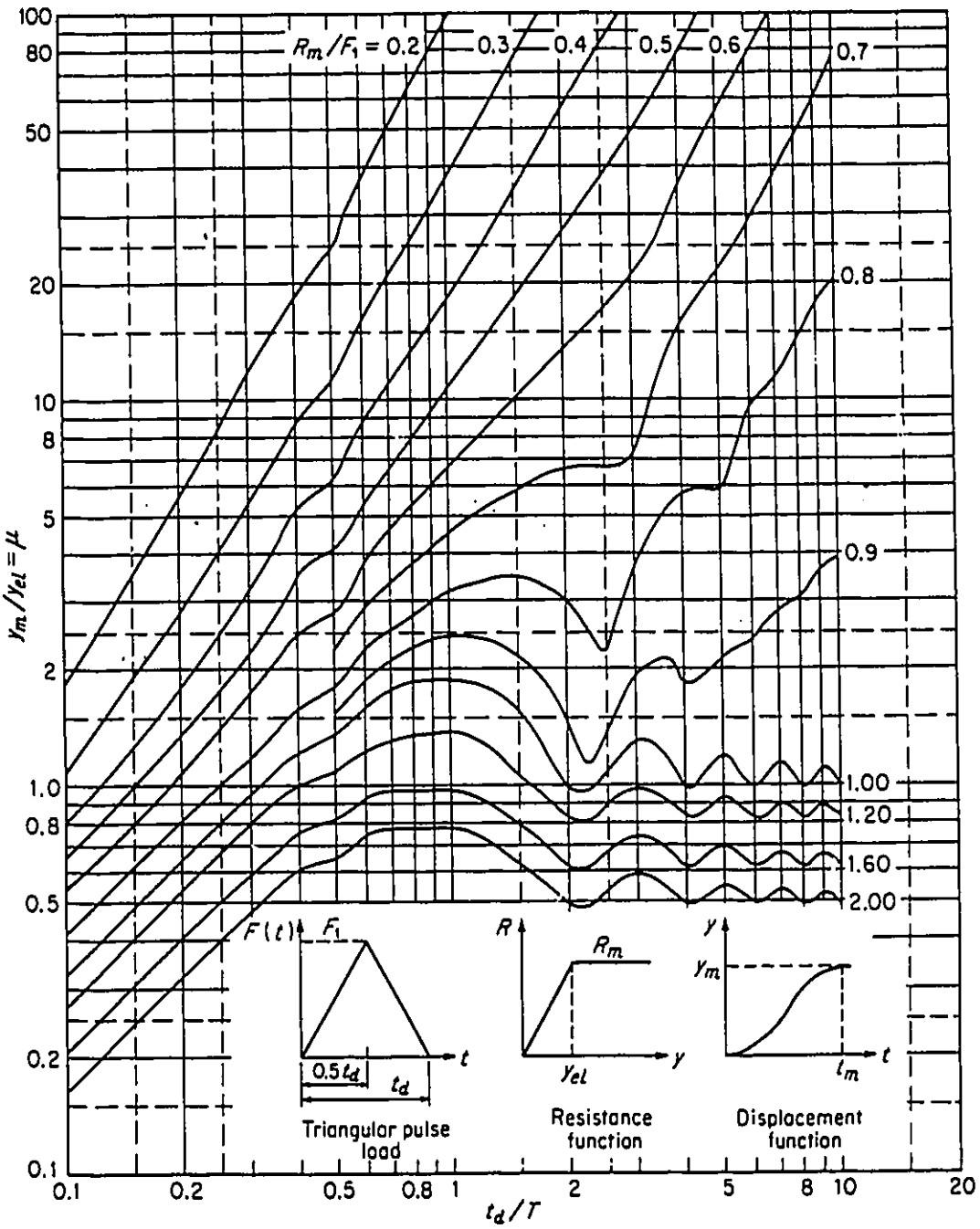

Figure 3.1d Maximum response of SDOF systems (undamped) due to triangular load pulses with finite rise time (Biggs, 1964)

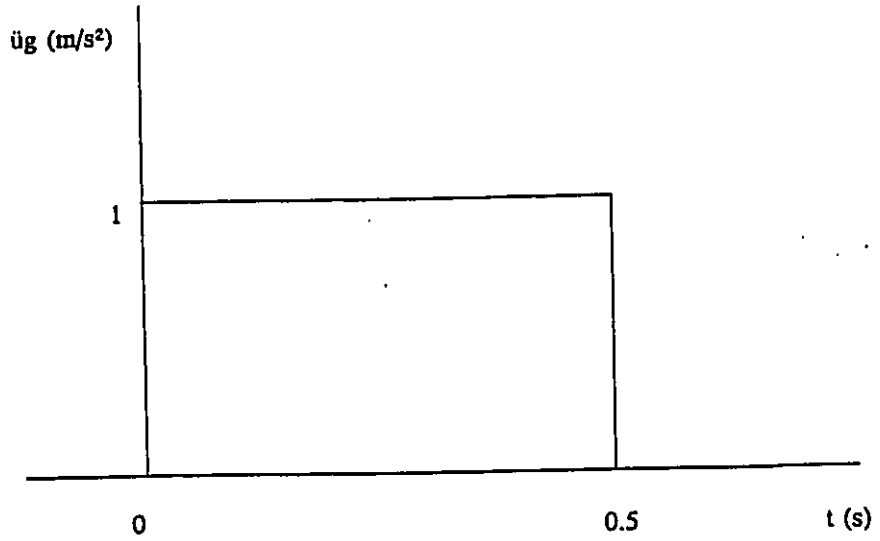

Figure 3.2 An arbitrarily selected rectangular pulse

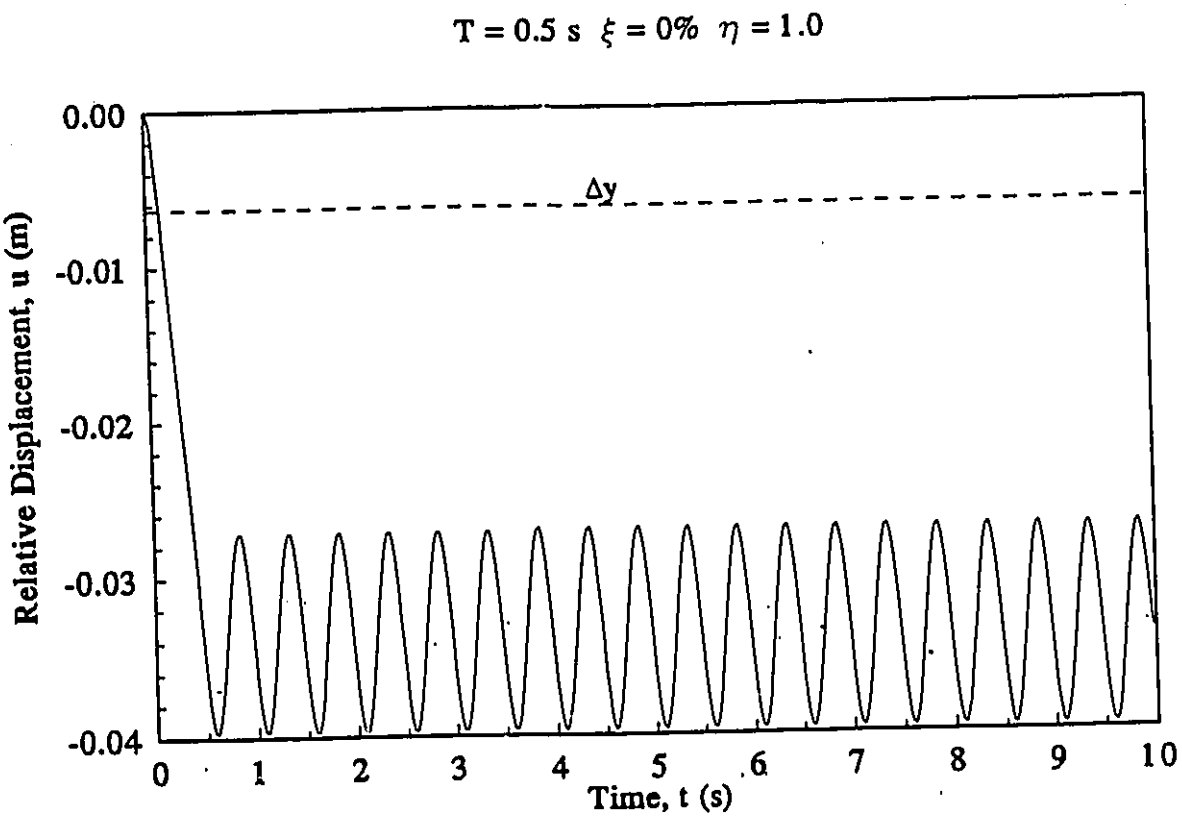

Figure 3.3 Relative displacement time history in Example 1

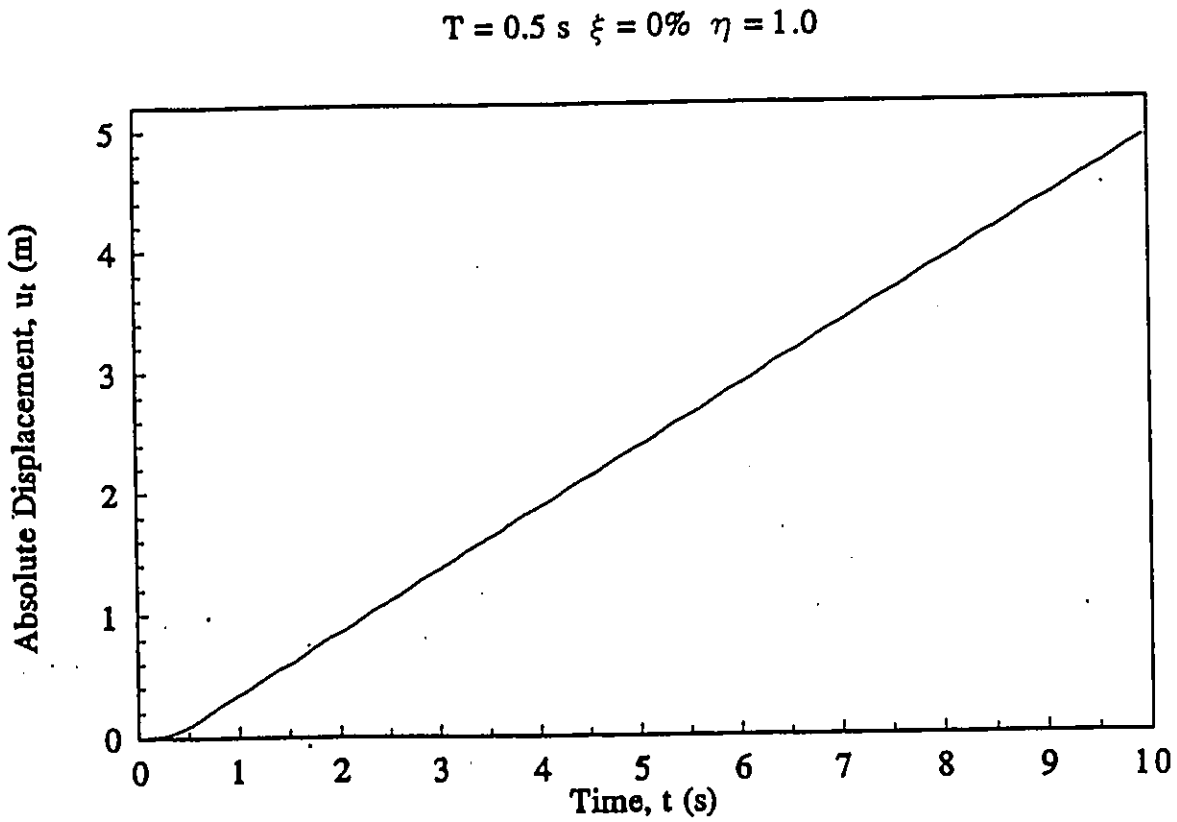

Figure 3.4 Absolute displacement time history in Example 1

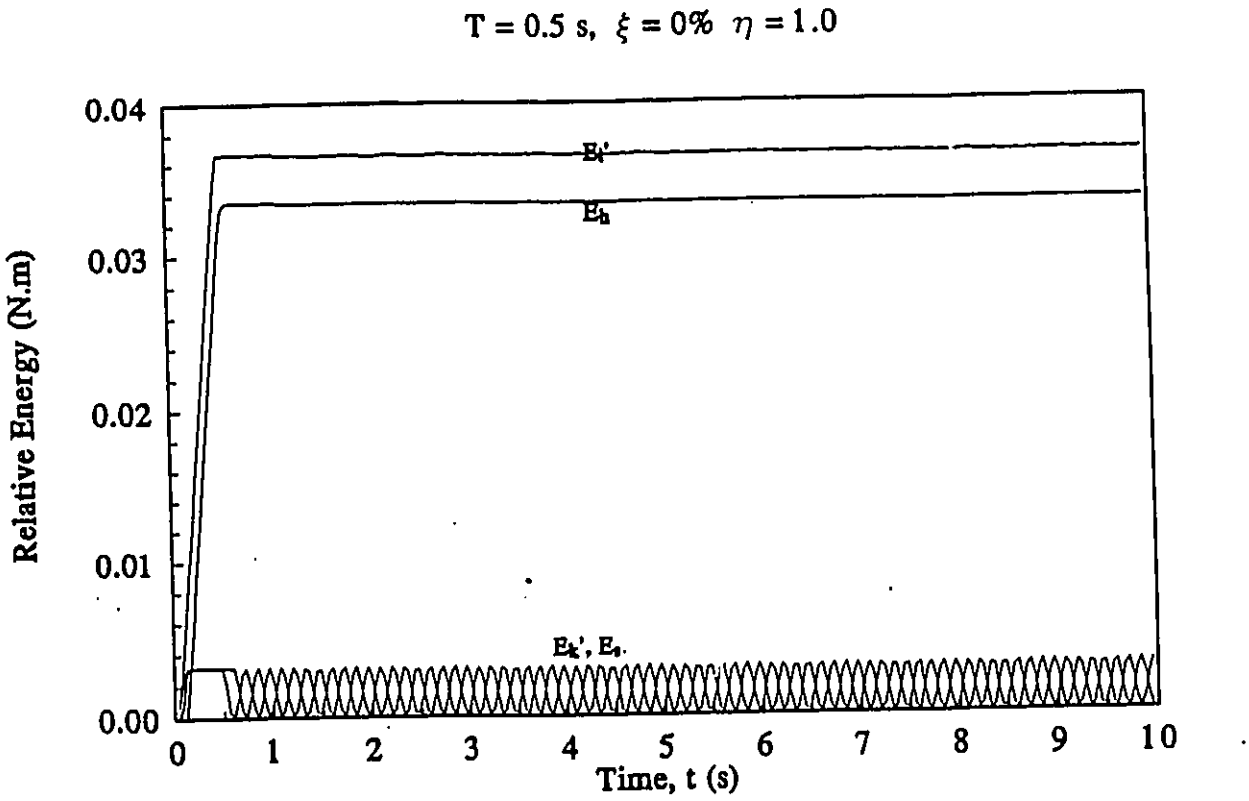

Figure 3.5 Relative energy time histories in Example 1

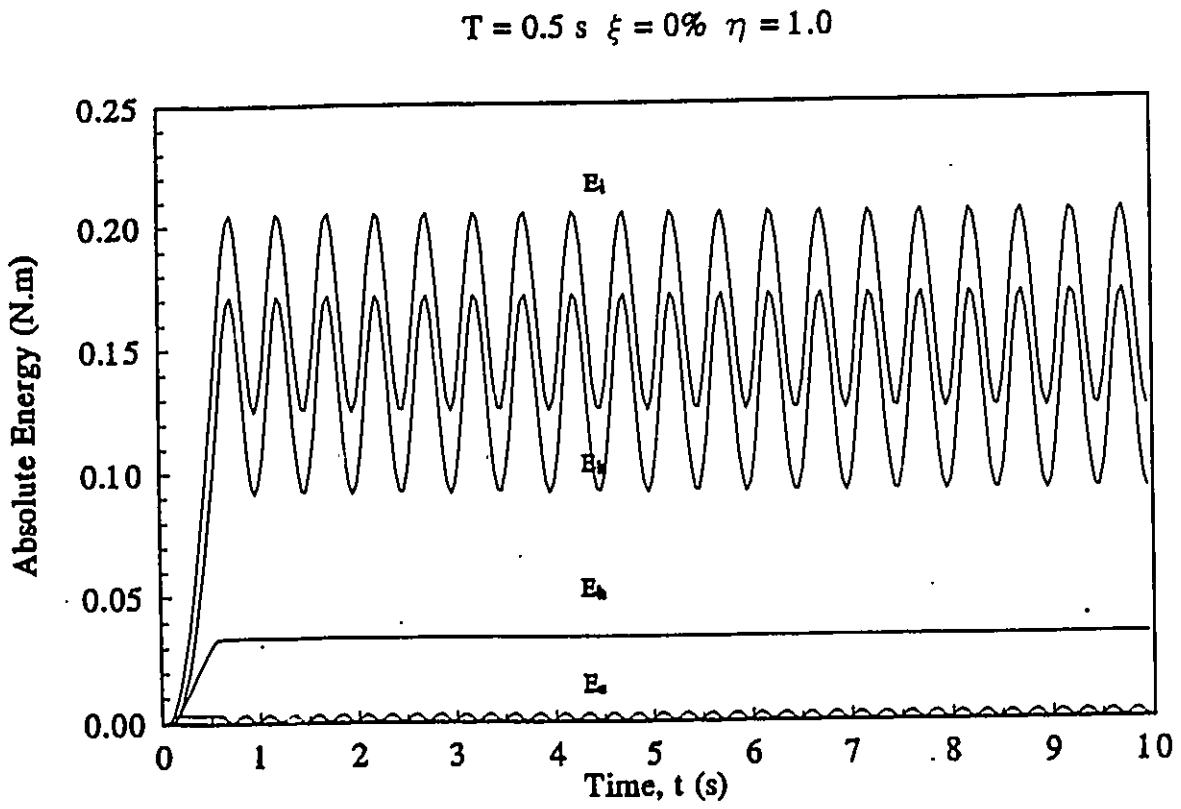

Figure 3.6 Absolute energy time histories in Example 1

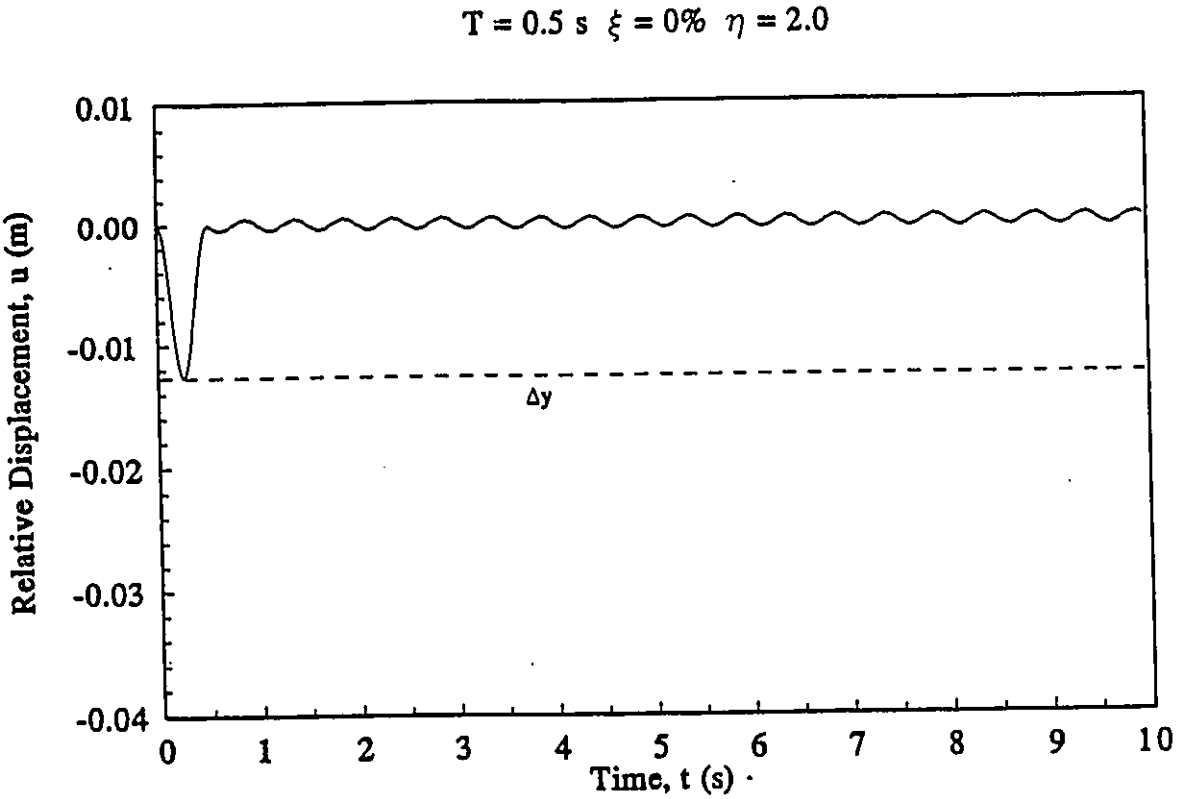

Figure 3.7 Relative displacement time history in Example 2

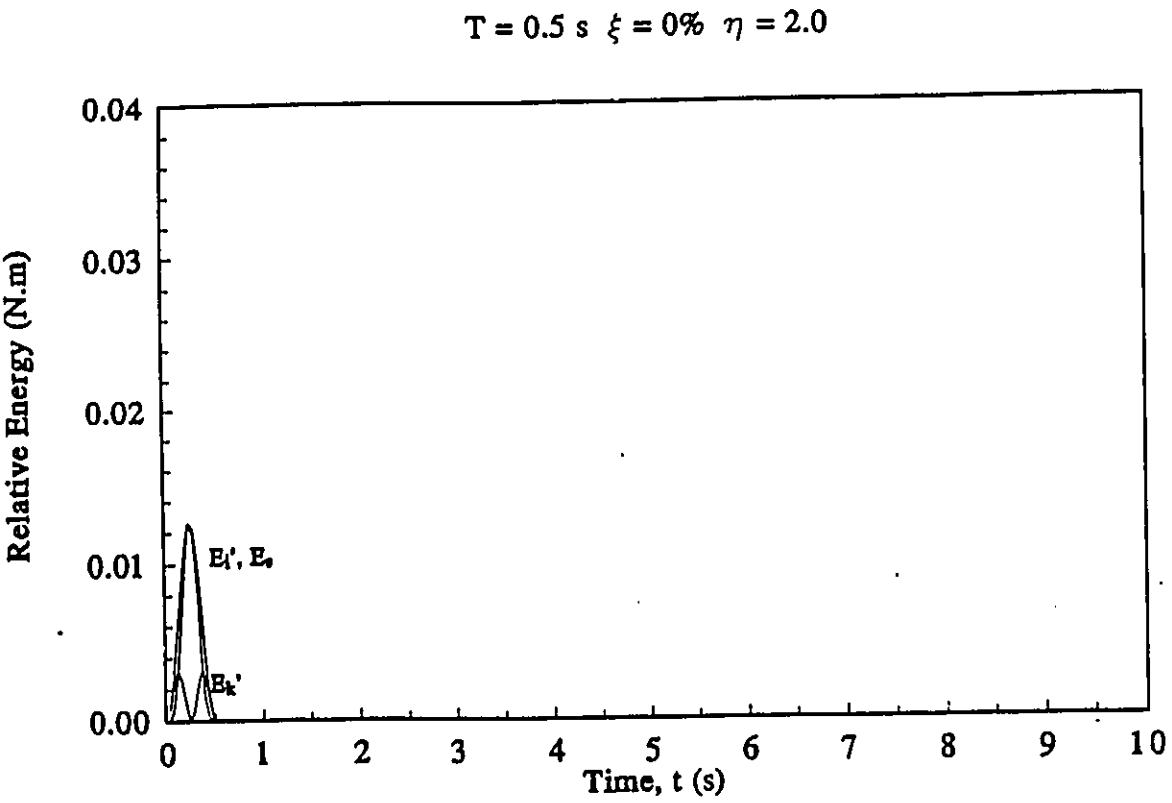

Figure 3.8 Relative energy time histories in Example 2

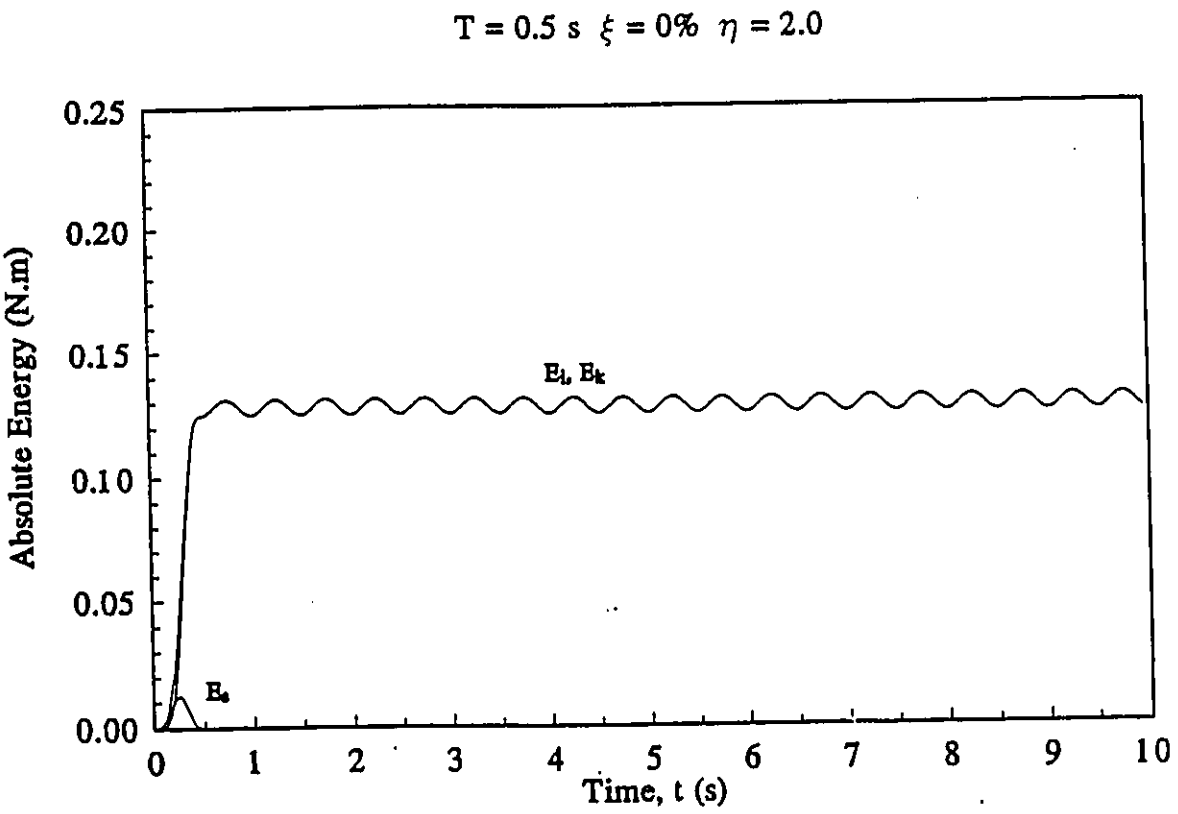

Figure 3.9 Absolute energy time histories in Example 2

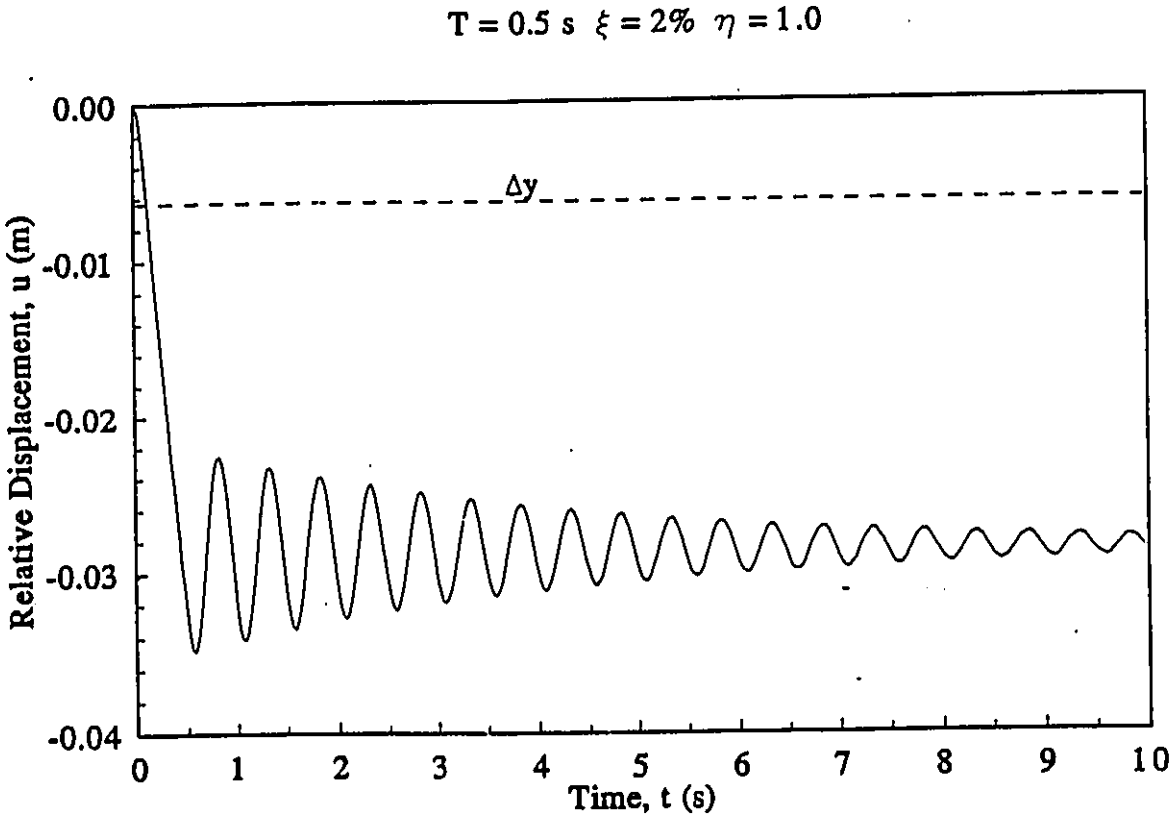

Figure 3.10 Relative displacement time history in Example 3

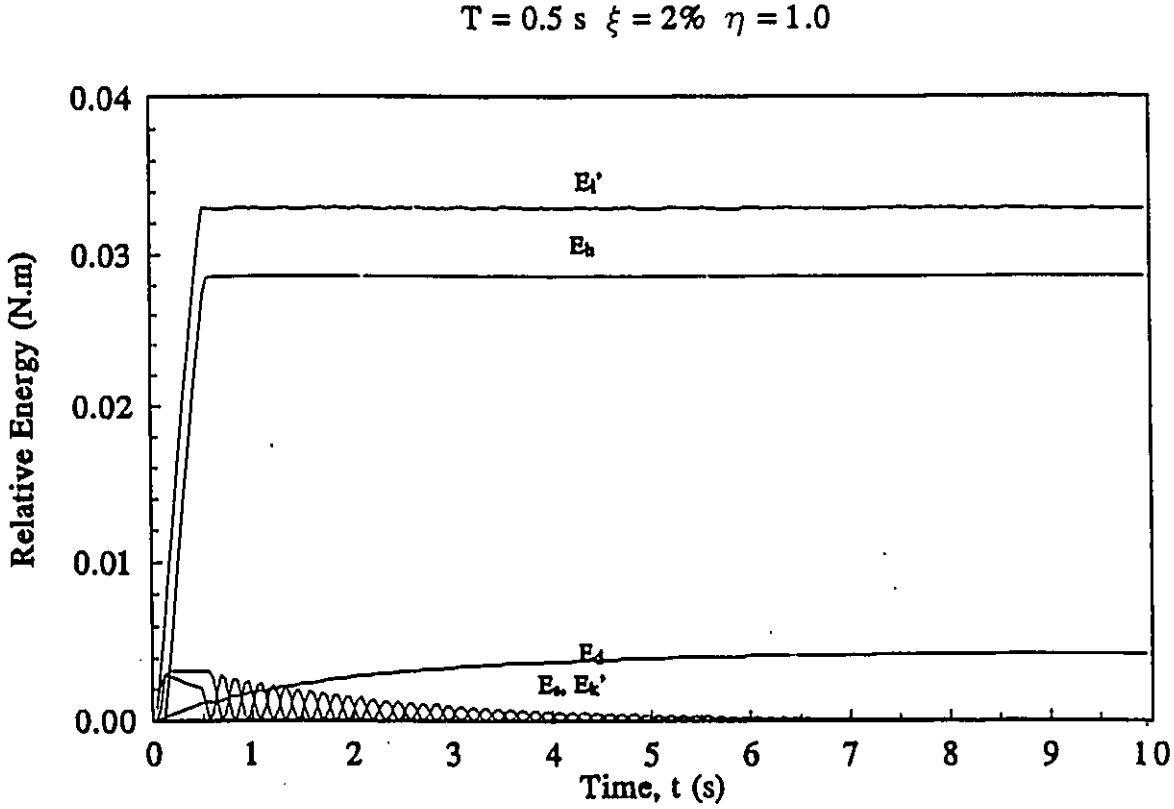

Figure 3.11 Relative energy time histories in Example 3

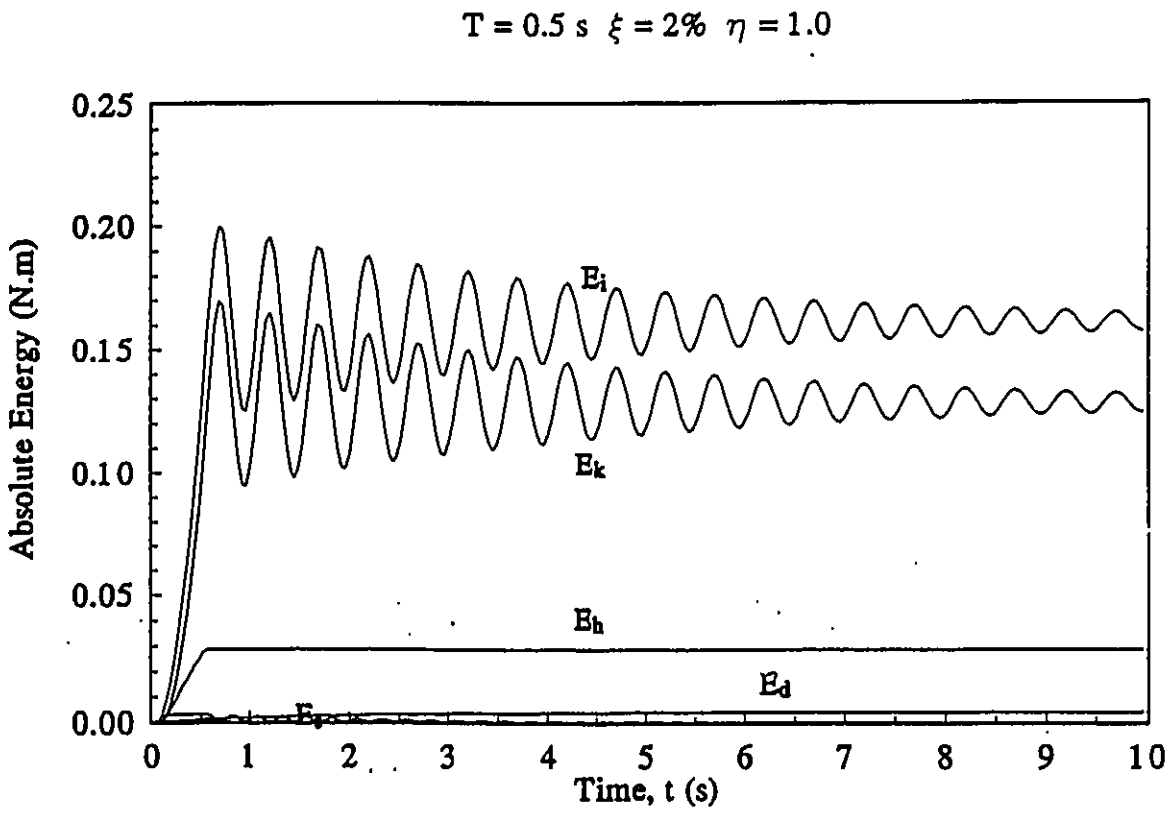

Figure 3.12 Absolute energy time histories in Example 3

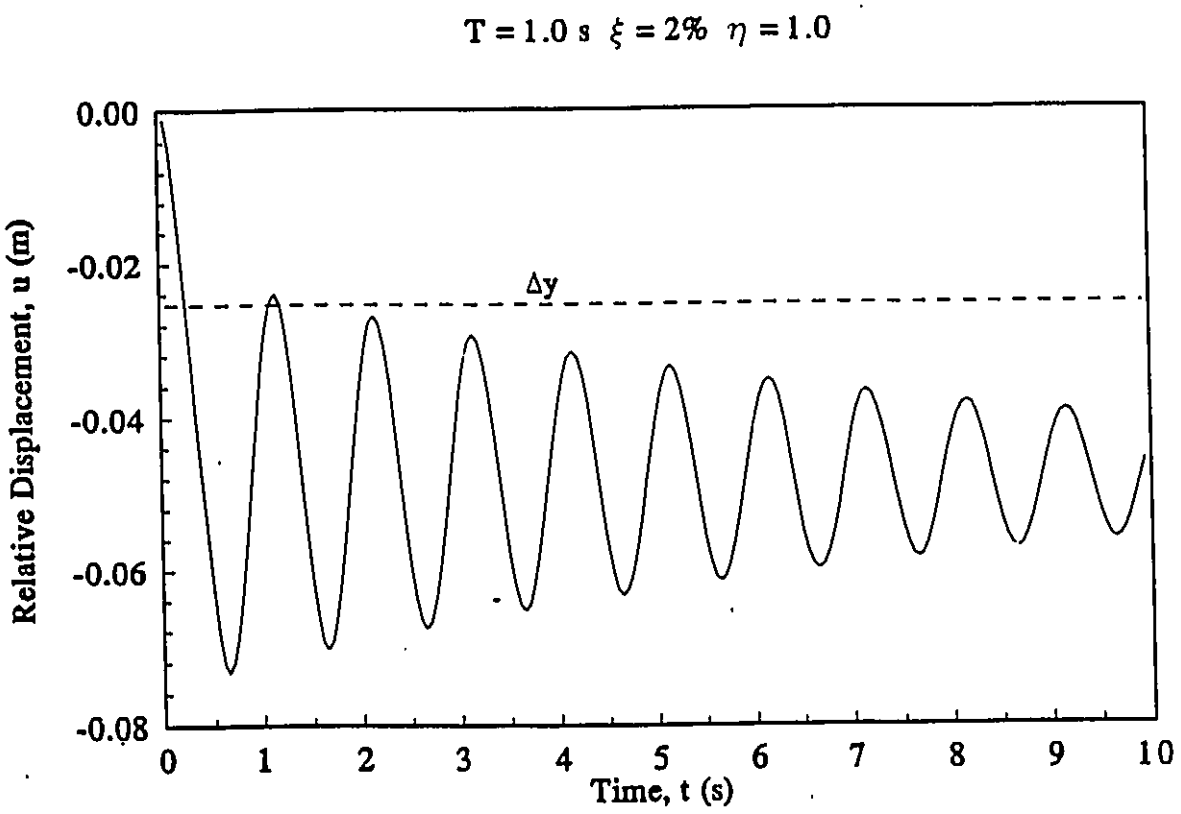

Figure 3.13 Relative displacement time history in Example 4

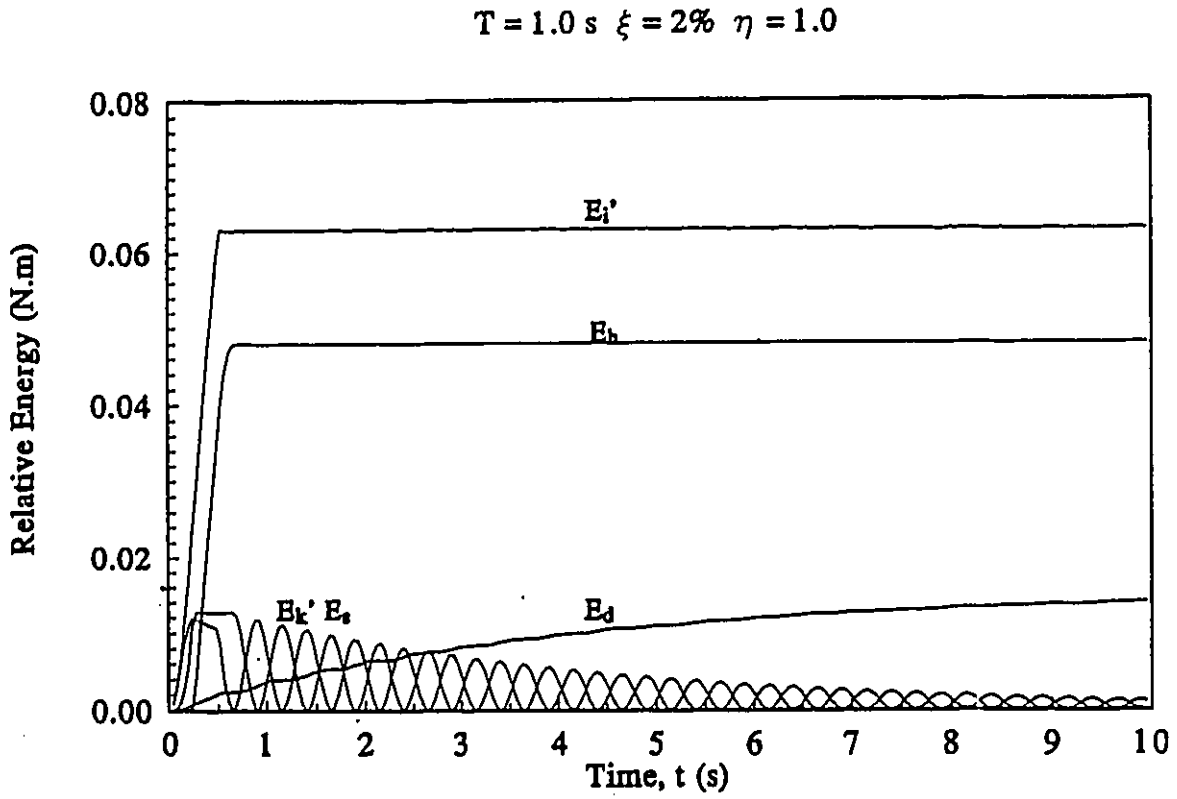

Figure 3.14 Relative energy time histories in Example 4

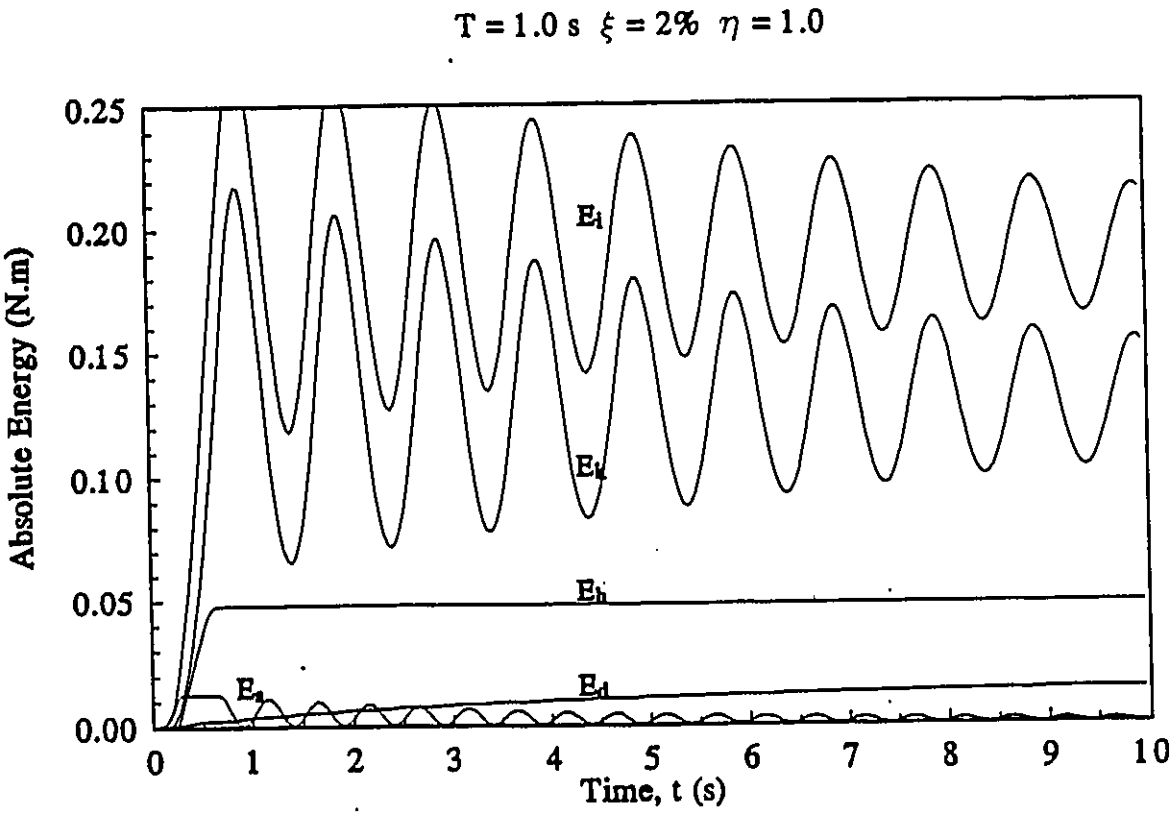

Figure 3.15 Absolute energy time histories in Example 4

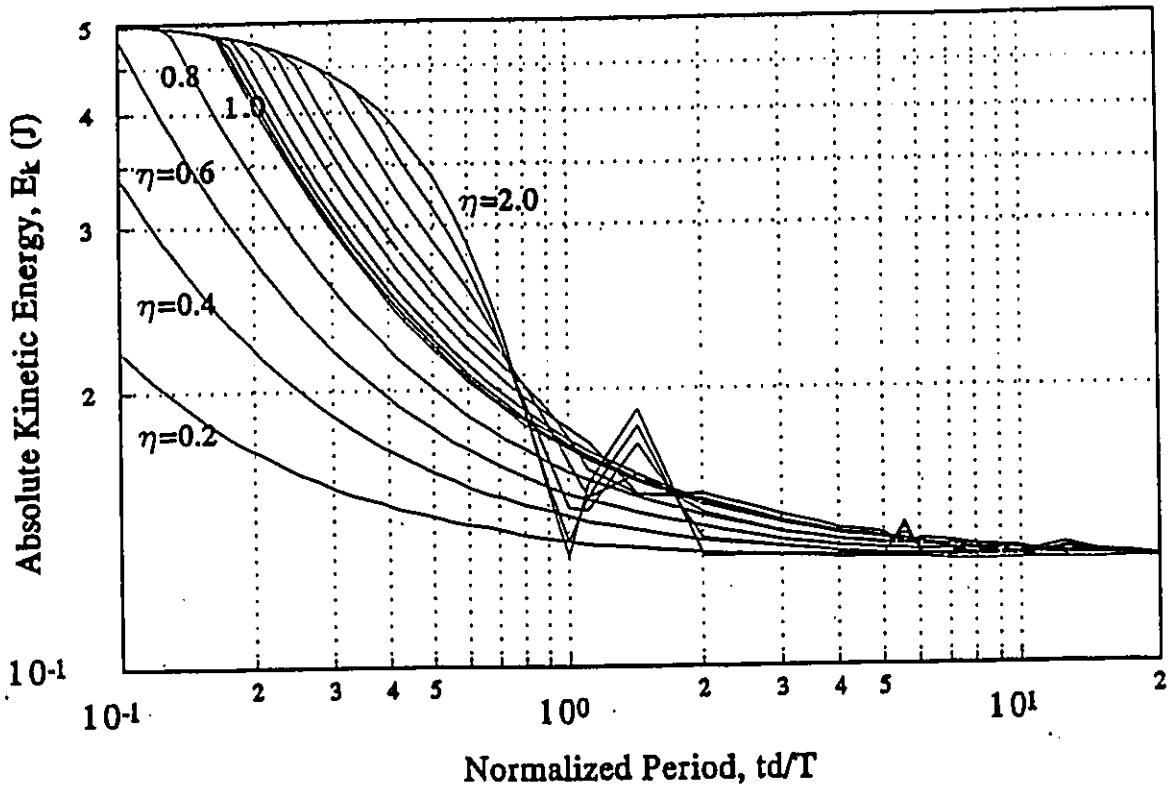

Figure 3.16 Absolute kinetic energy spectra under a rectangular pulse excitation (ξ = 0%)

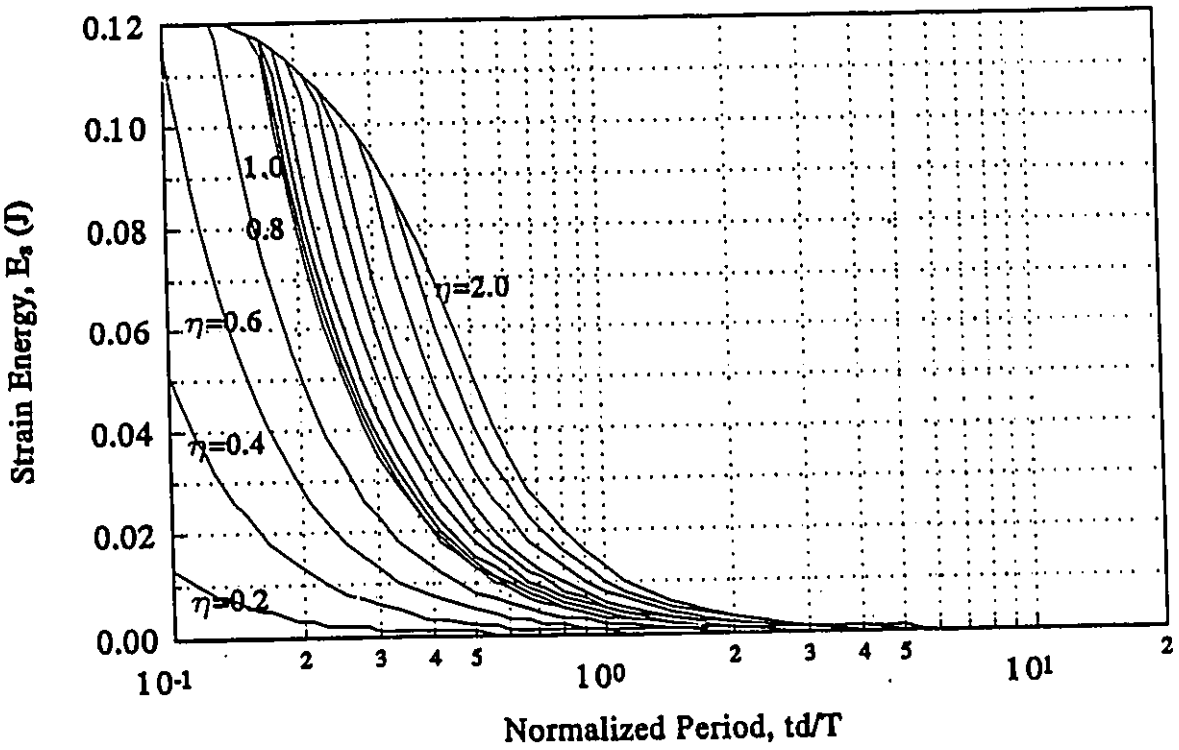

Figure 3.17 Strain energy spectra under a rectangular pulse excitation (ξ = 0%)

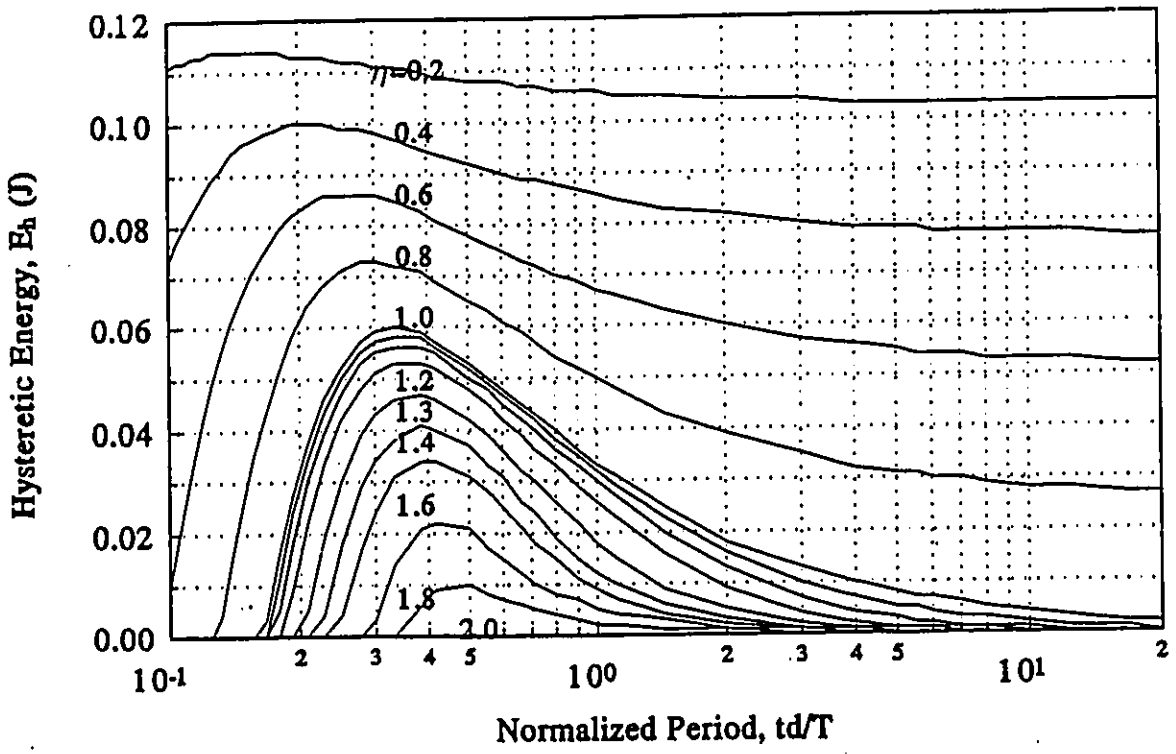

Figure 3.18 Hysteretic energy spectra under a rectangular pulse excitation (ξ = 0%)

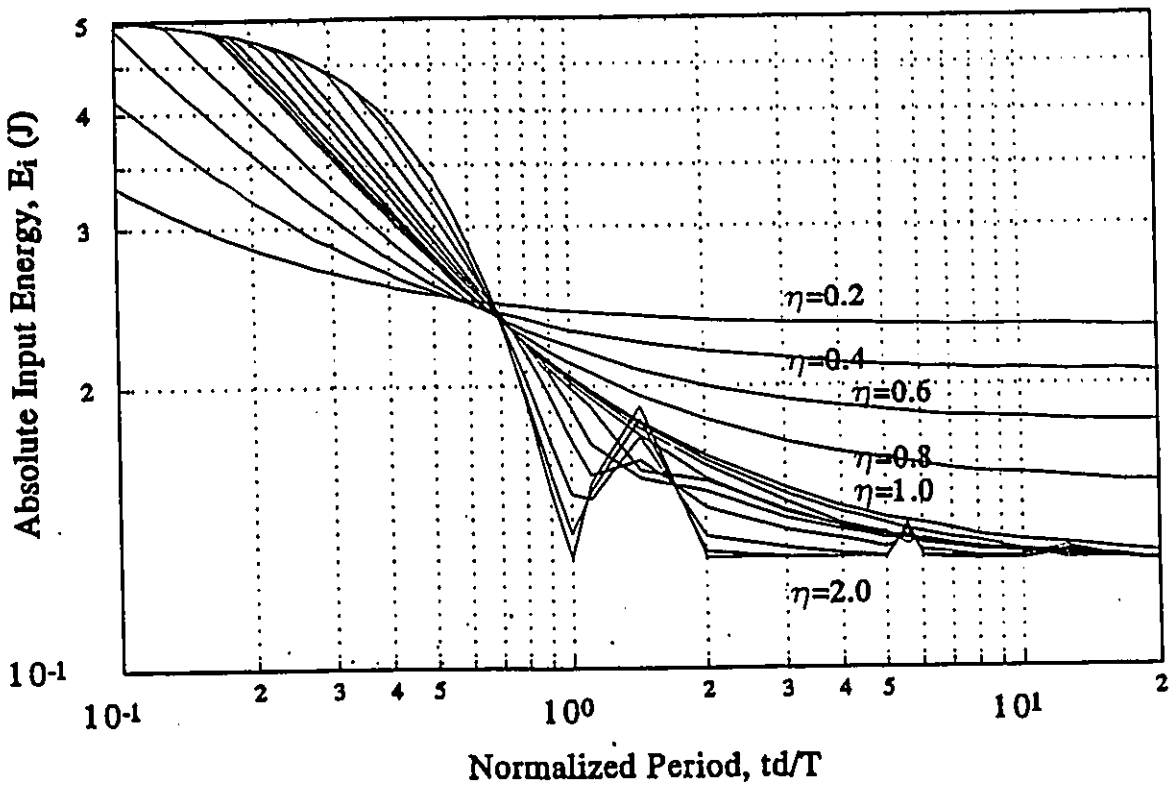

Figure 3.19 Absolute input energy spectra under a rectangular pulse excitation (ξ = 0%)

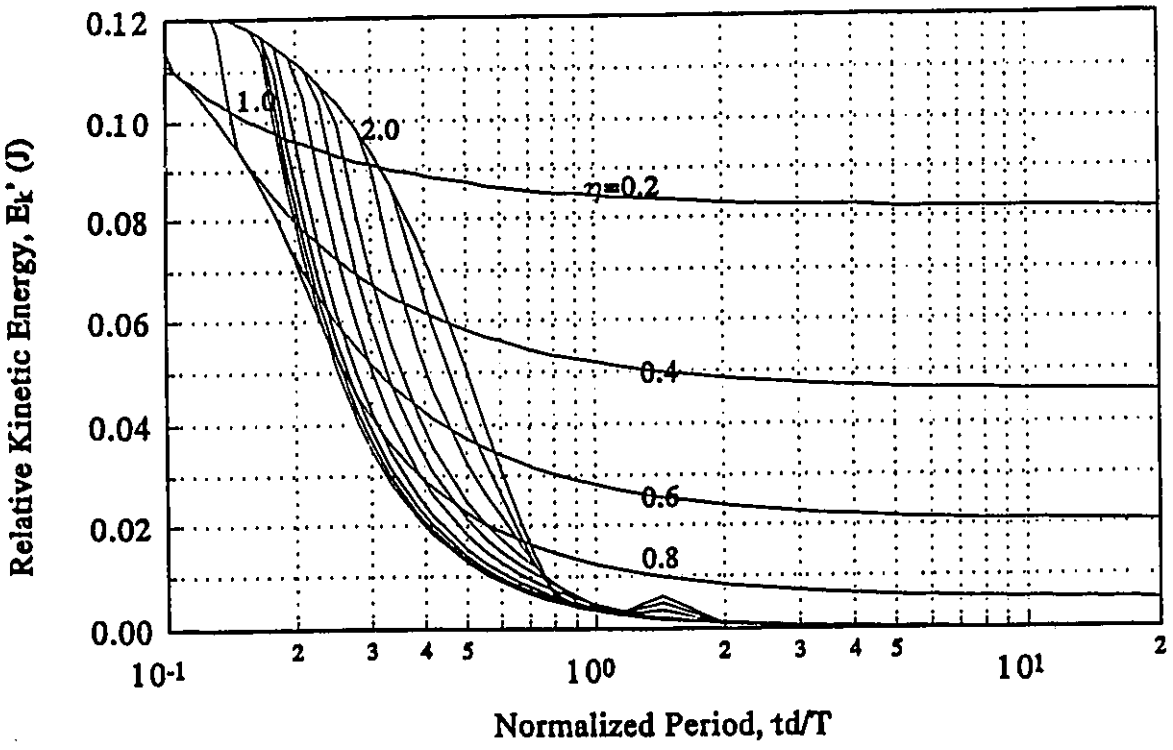

Figure 3.20 Relative kinetic energy spectra under a rectangular pulse excitation (ξ = 0%)

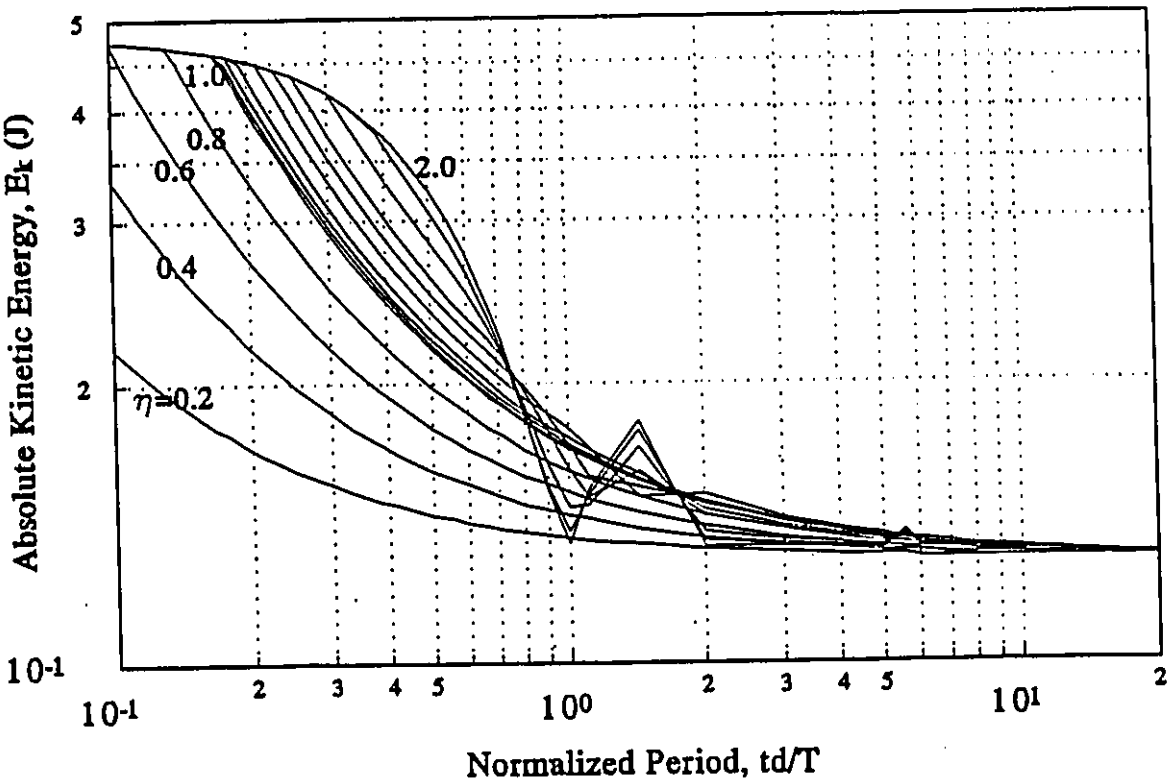

Figure 3.21 Absolute kinetic energy spectra under a rectangular pulse excitation (ξ = 2%)

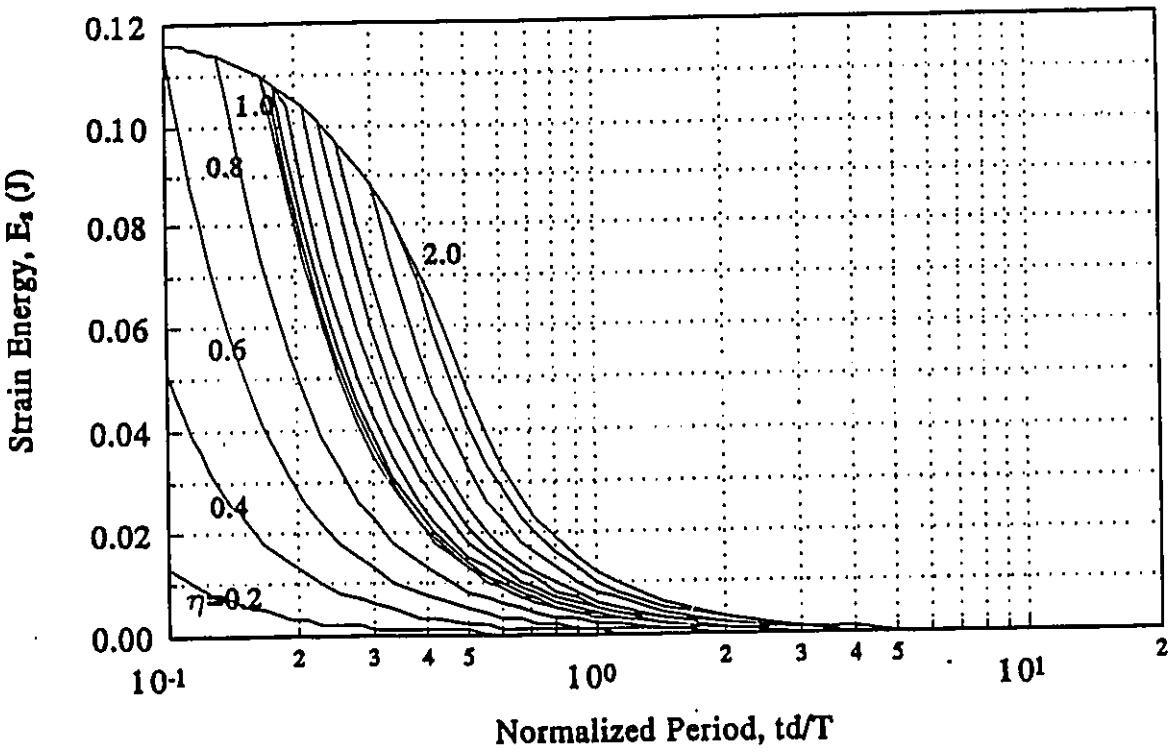

Figure 3.22 Strain energy spectra under a rectangular pulse excitation (ξ = 2%)

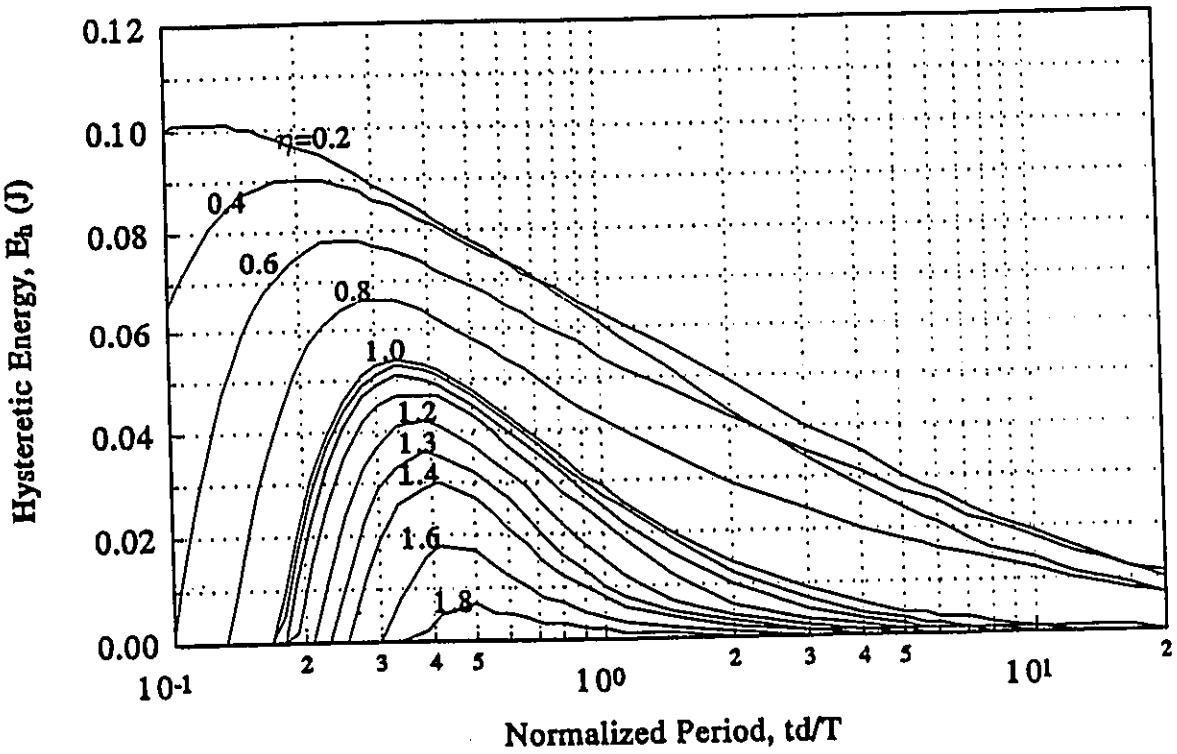

Figure 3.23 Hysteretic energy spectra under a rectangular pulse excitation (ξ = 2%)

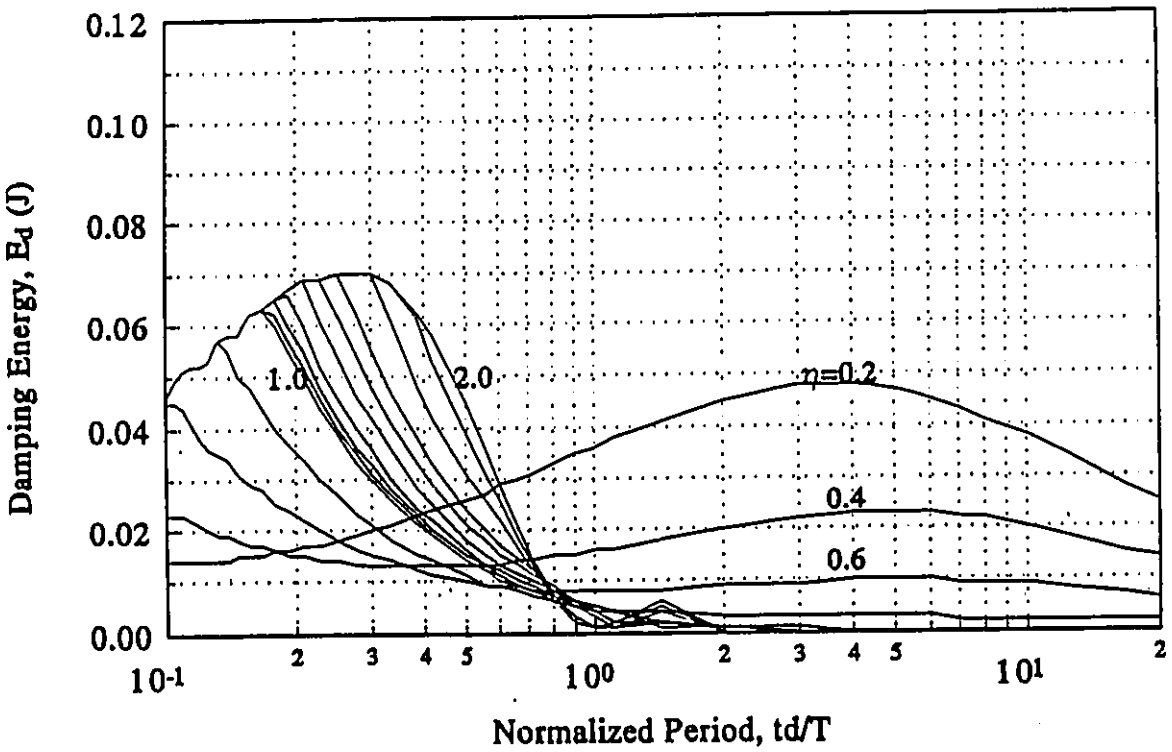

Figure 3.24 Damping energy spectra under a rectangular pulse excitation (ξ = 2%)

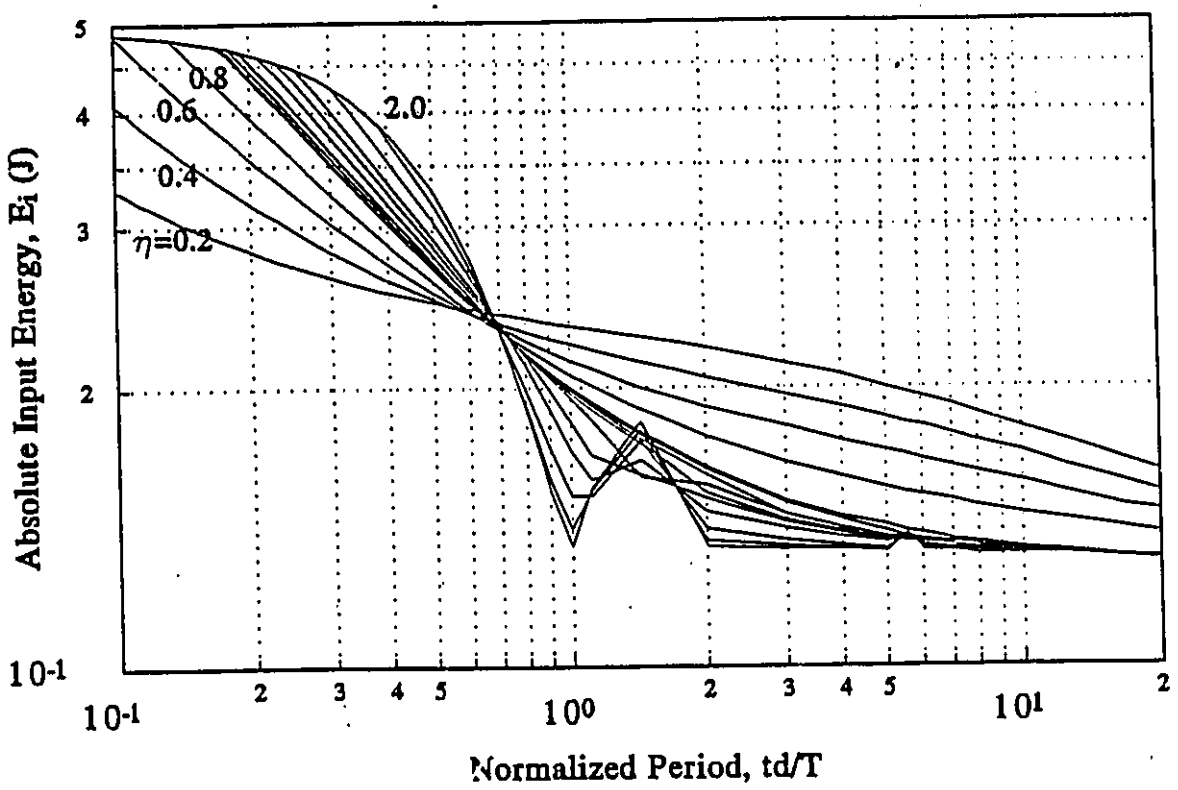

Figure 3.25 Absolute input energy spectra under a rectangular pulse excitation (ξ = 2%)

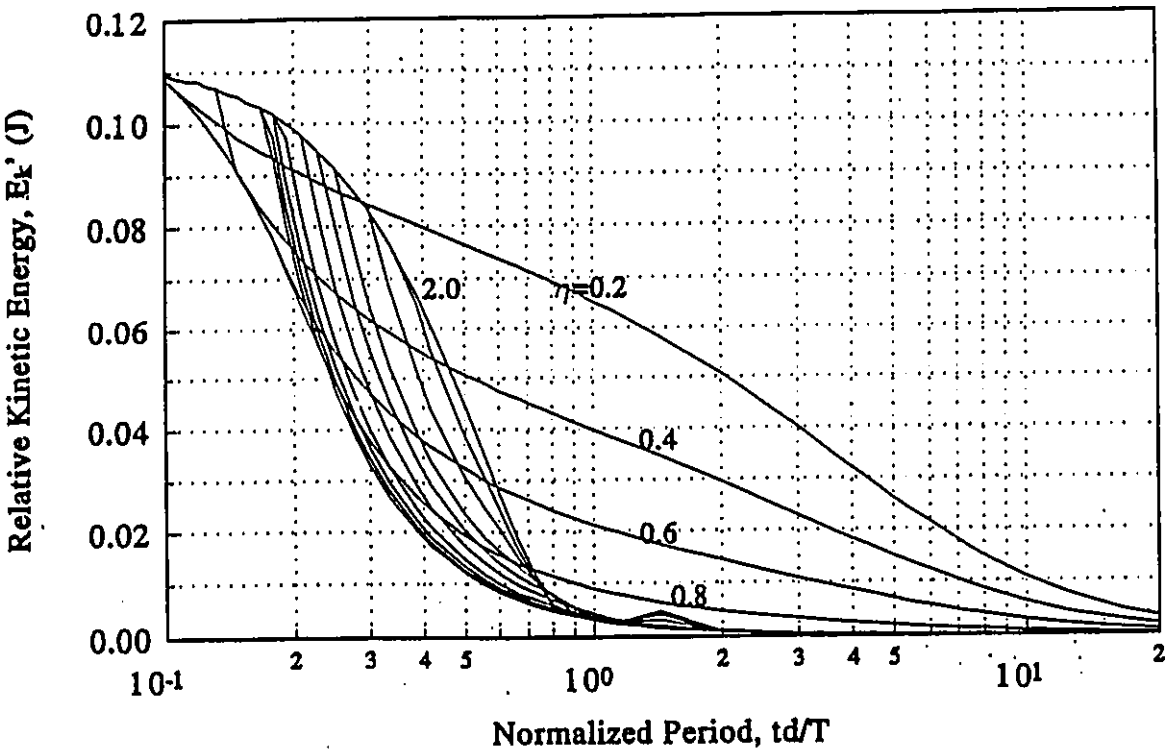

Figure 3.26 Relative kinetic energy spectra under a rectangular pulse excitation (ξ = 2%)

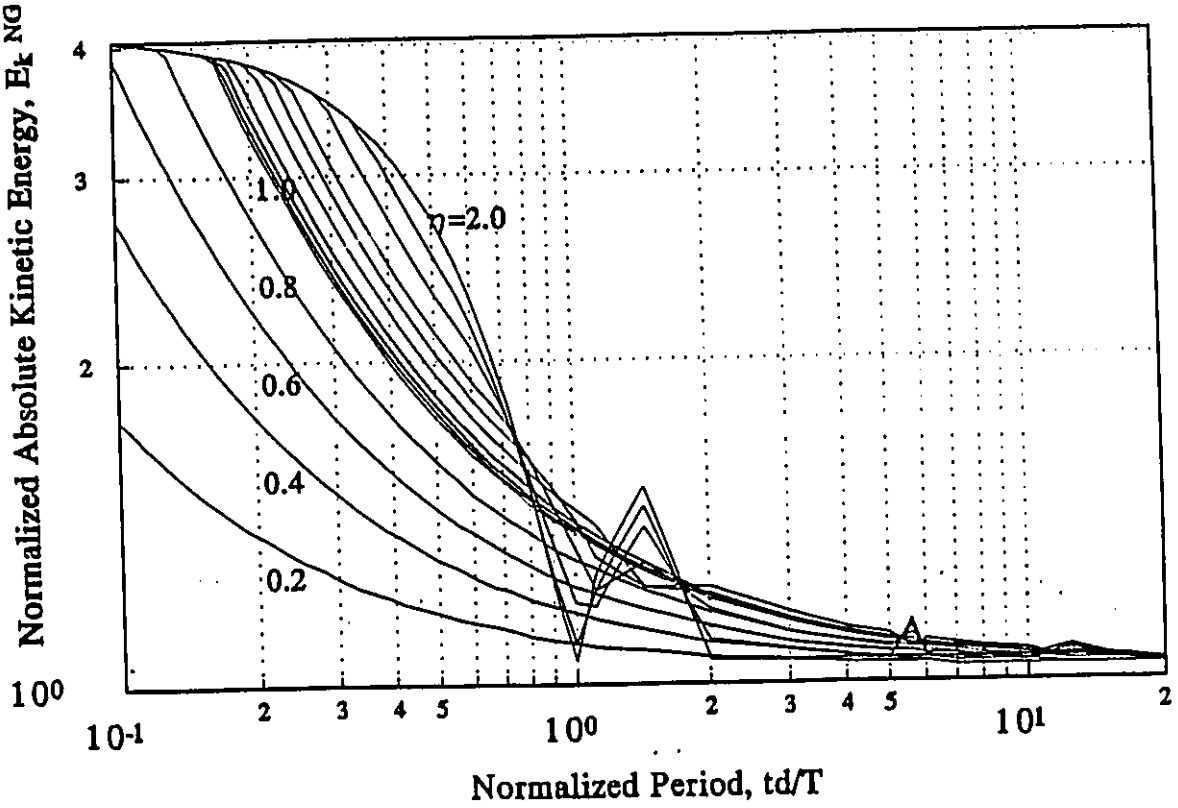

Figure 3.27 Normalized absolute kinetic energy spectra for rectangular pulse excitation (ξ = 0%)

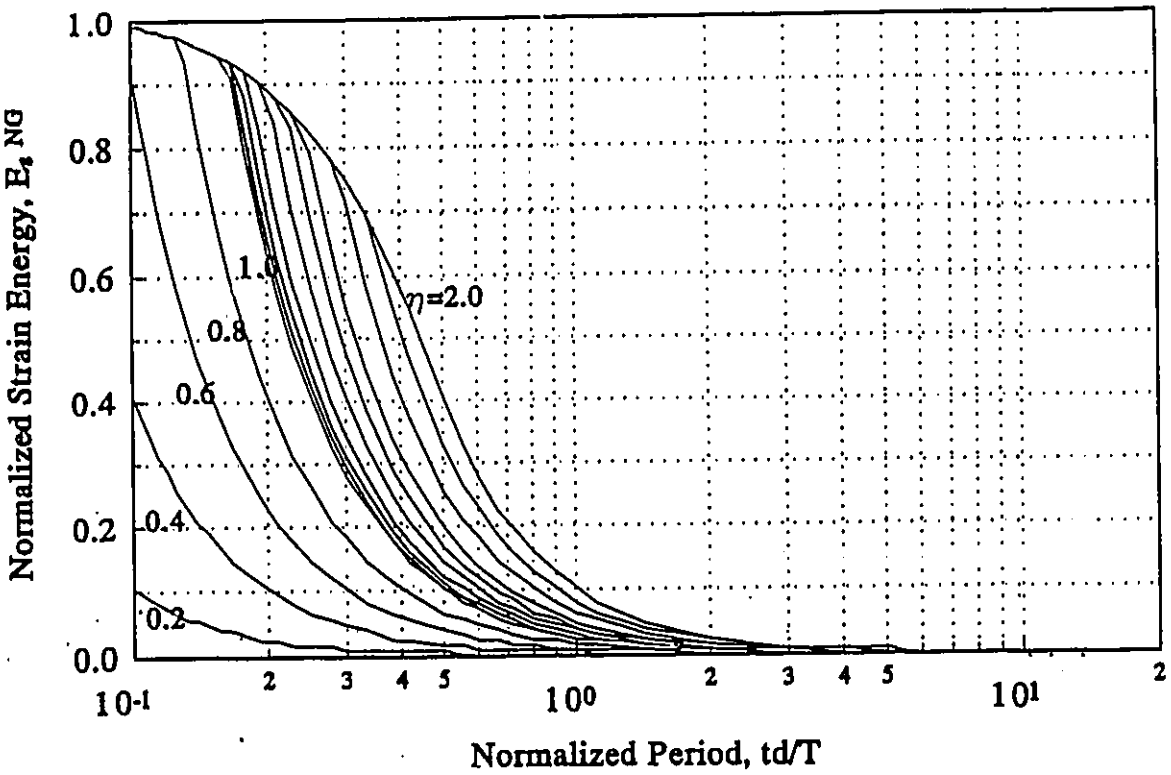

Figure 3.28 Normalized strain energy spectra for rectangular pulse excitation (ξ = 0%)

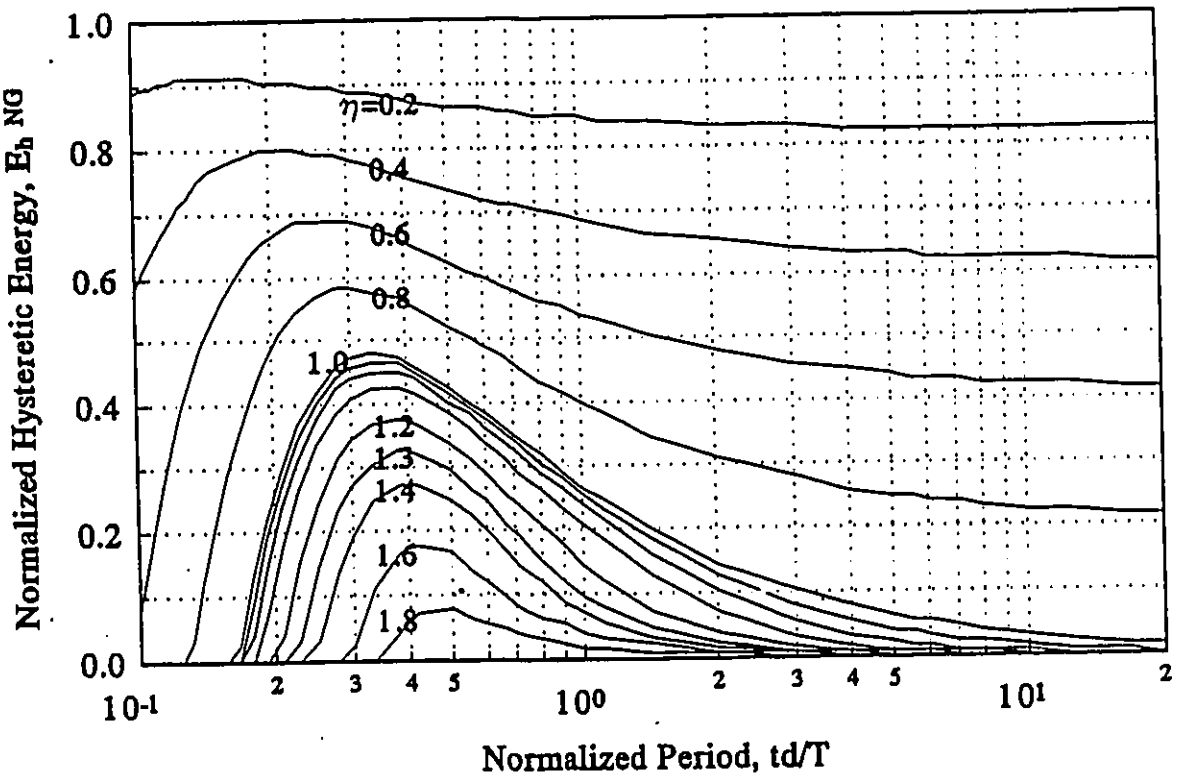

Figure 3.29 Normalized hysteretic energy spectra for rectangular pulse excitation (ξ = 0%)

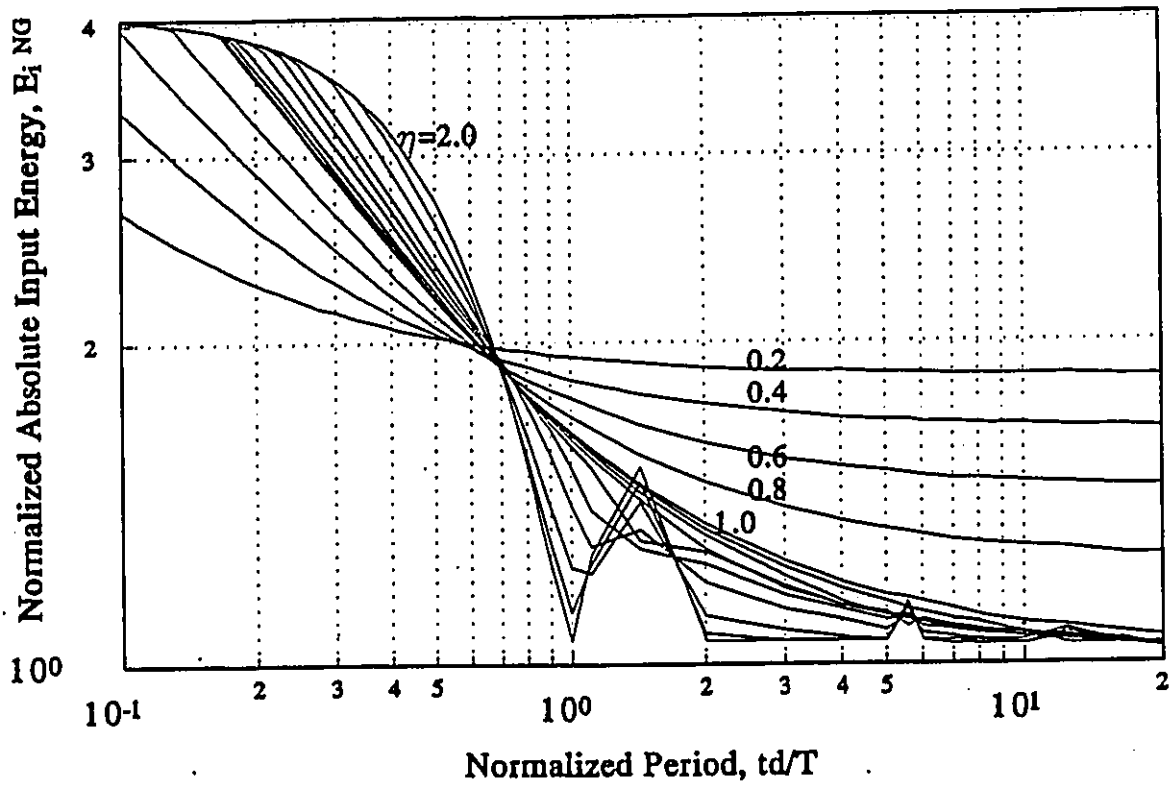

Figure 3.30 Normalized absolute input energy spectra for rectangular pulse excitation (ξ = 0%)

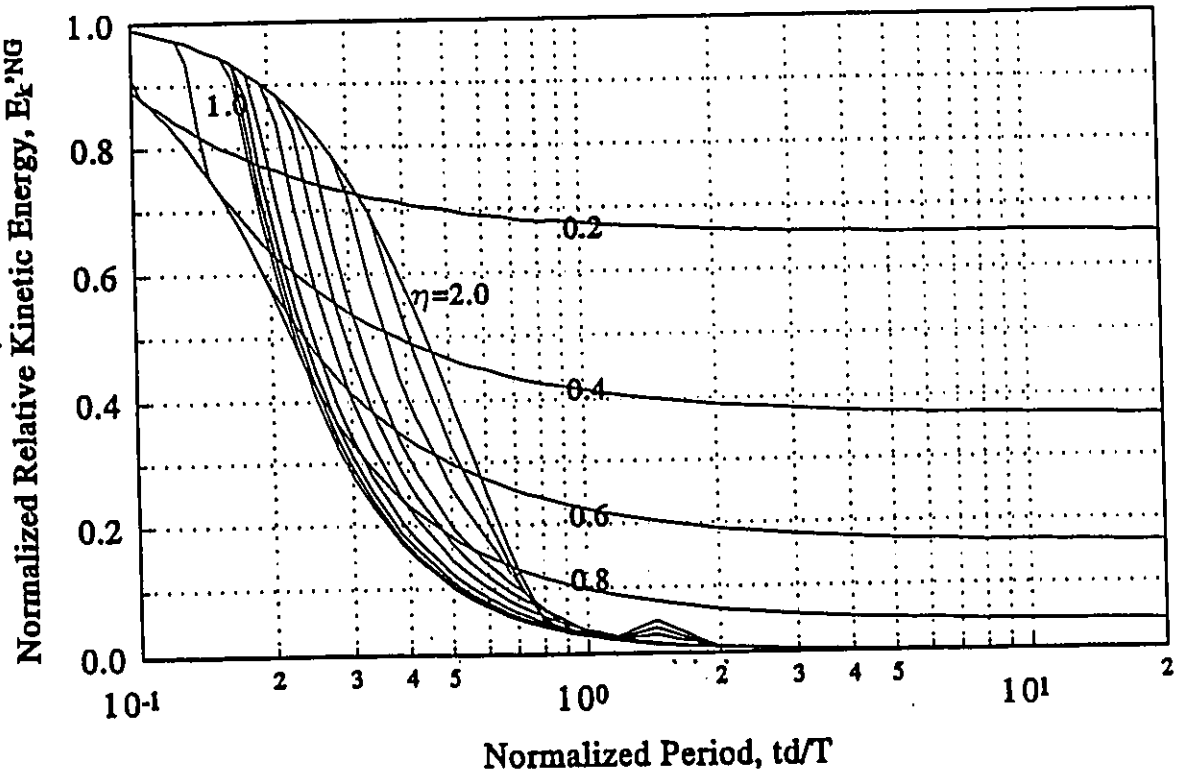

Figure 3.31 Normalized relative kinetic energy spectra for rectangular pulse excitation (ξ = 0%)

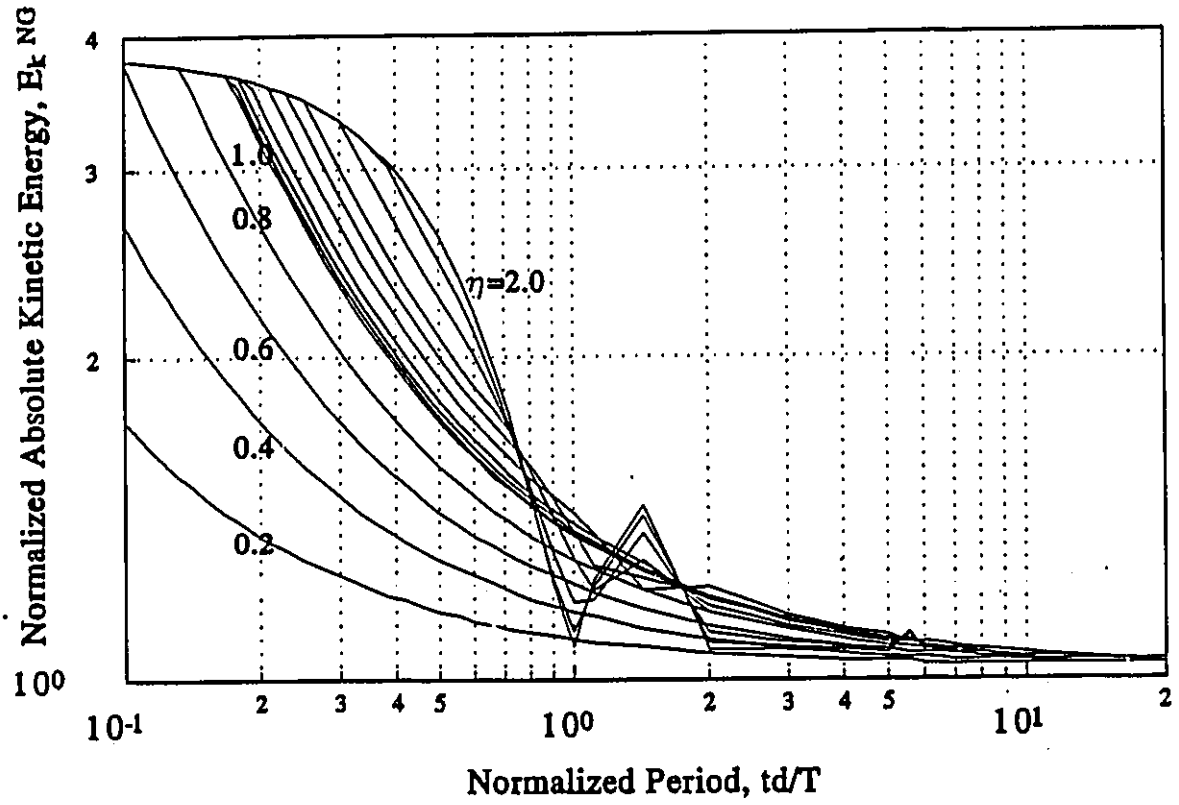

Figure 3.32 Normalized absolute kinetic energy spectra for rectangular pulse excitation (ξ = 2%)

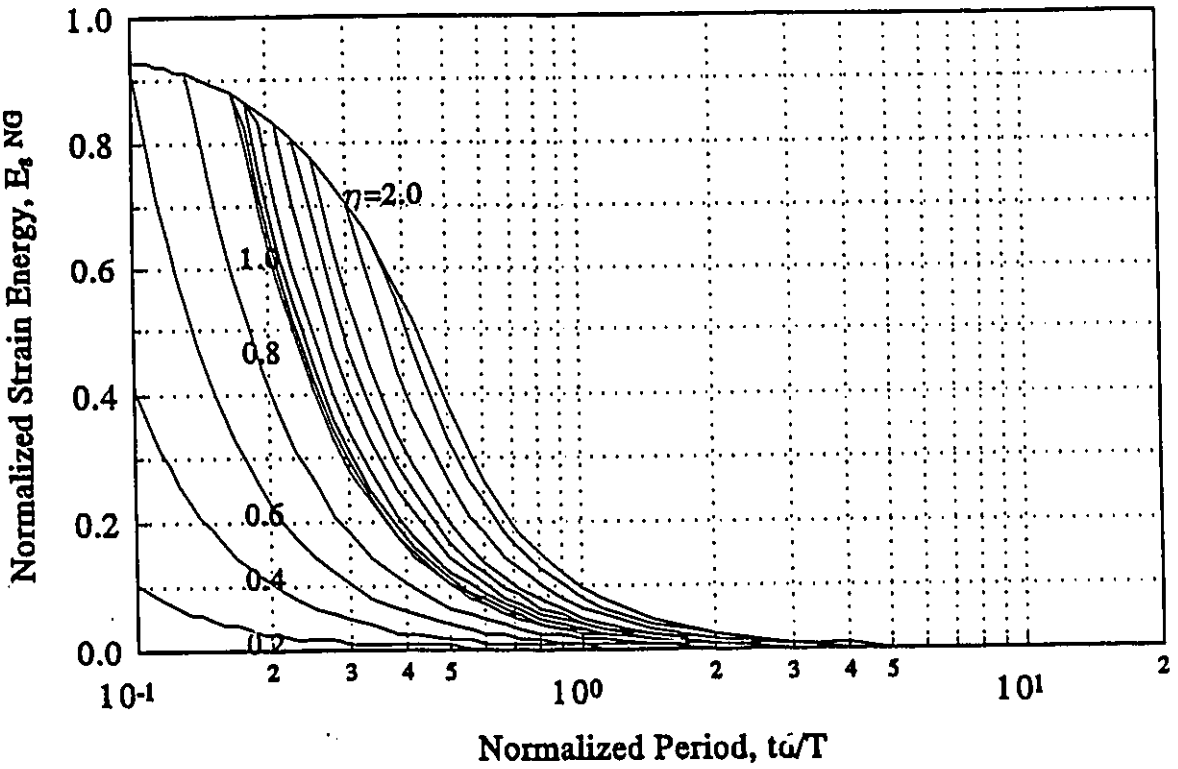

Figure 3.33 Normalized strain energy spectra for rectangular pulse excitation (ξ = 2%)

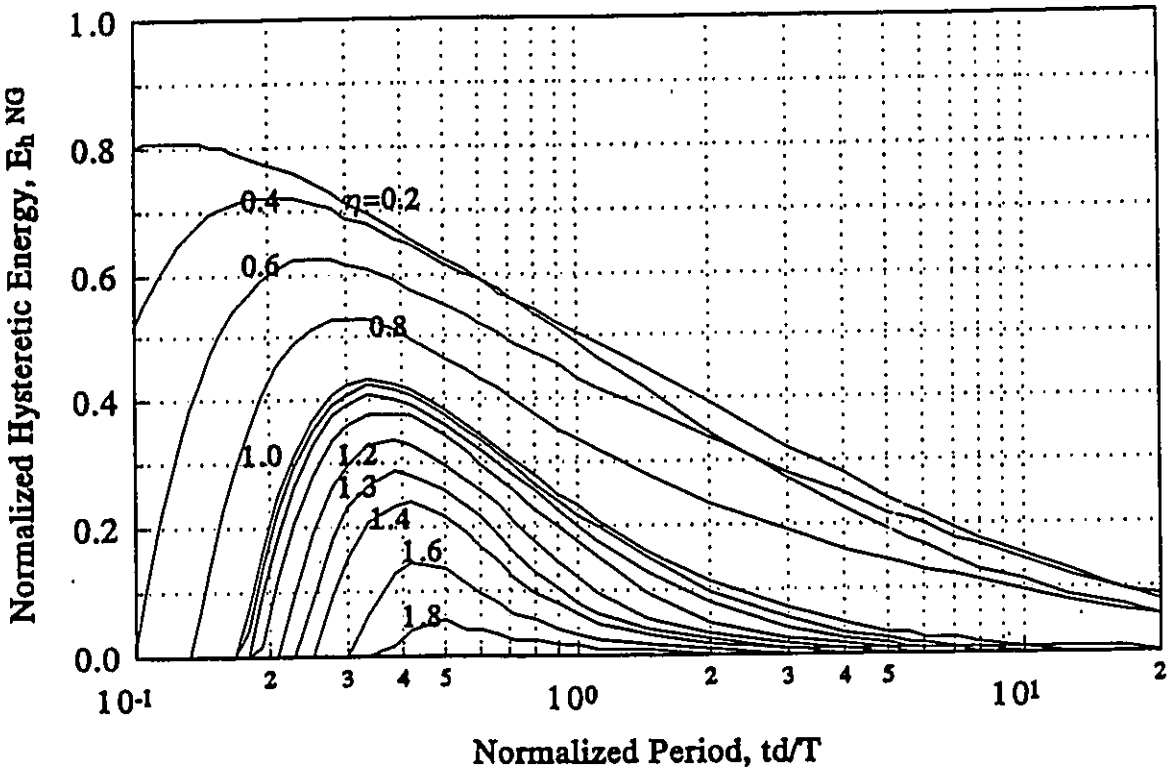

Figure 3.34 Normalized hysteretic energy spectra for rectangular pulse excitation (ξ = 2%)

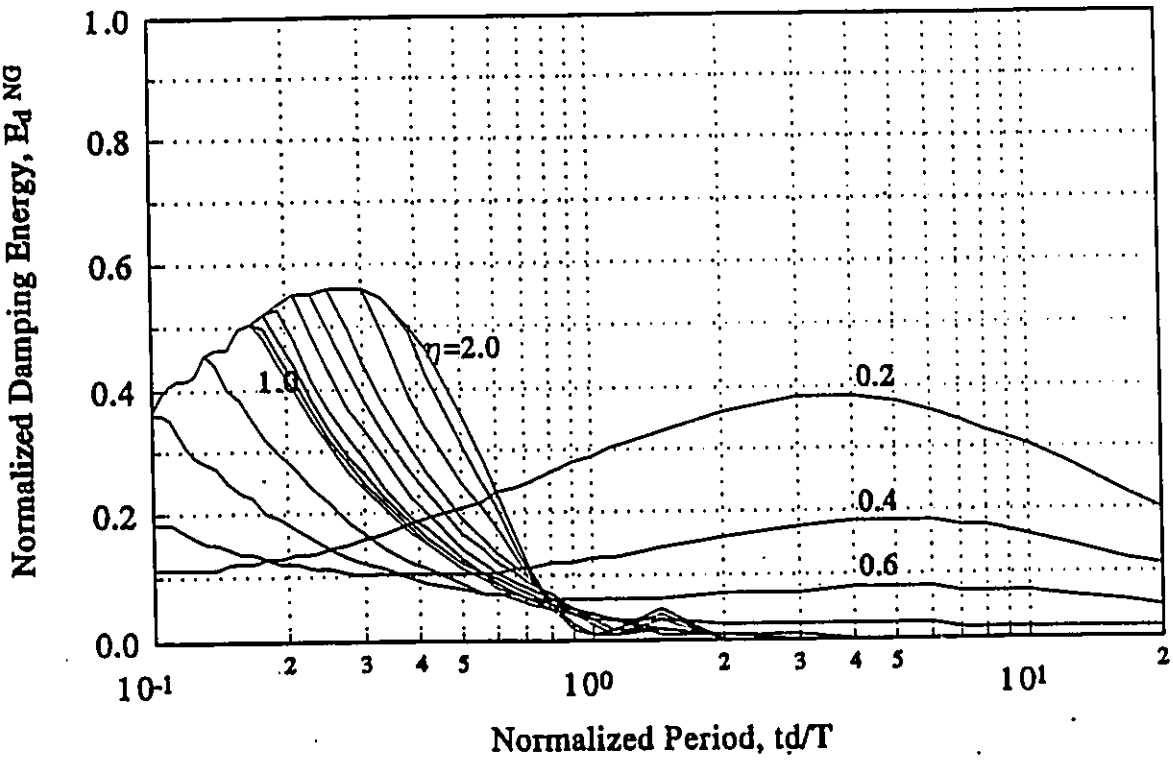

Figure 3.35 Normalized damping energy spectra for rectangular pulse excitation (ξ = 2%)

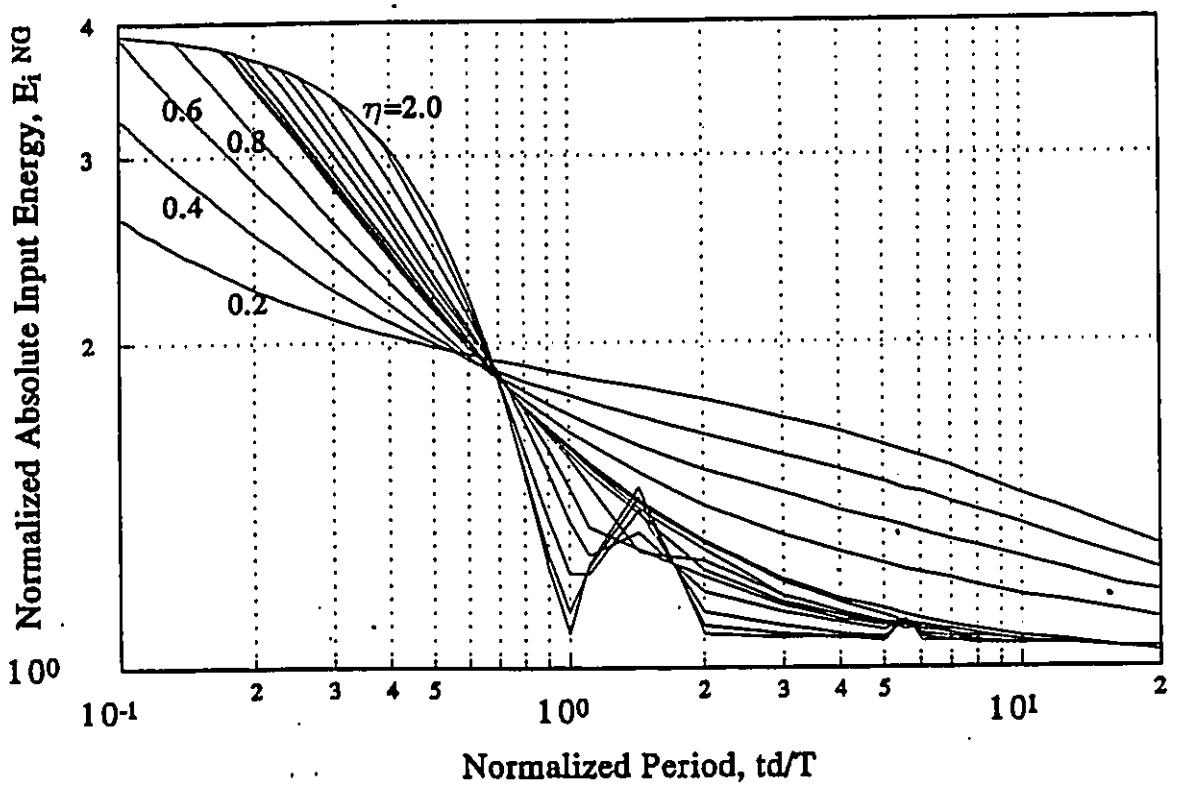

Figure 3.36 Normalized absolute input energy spectra for rectangular pulse excitation (ξ = 2%)

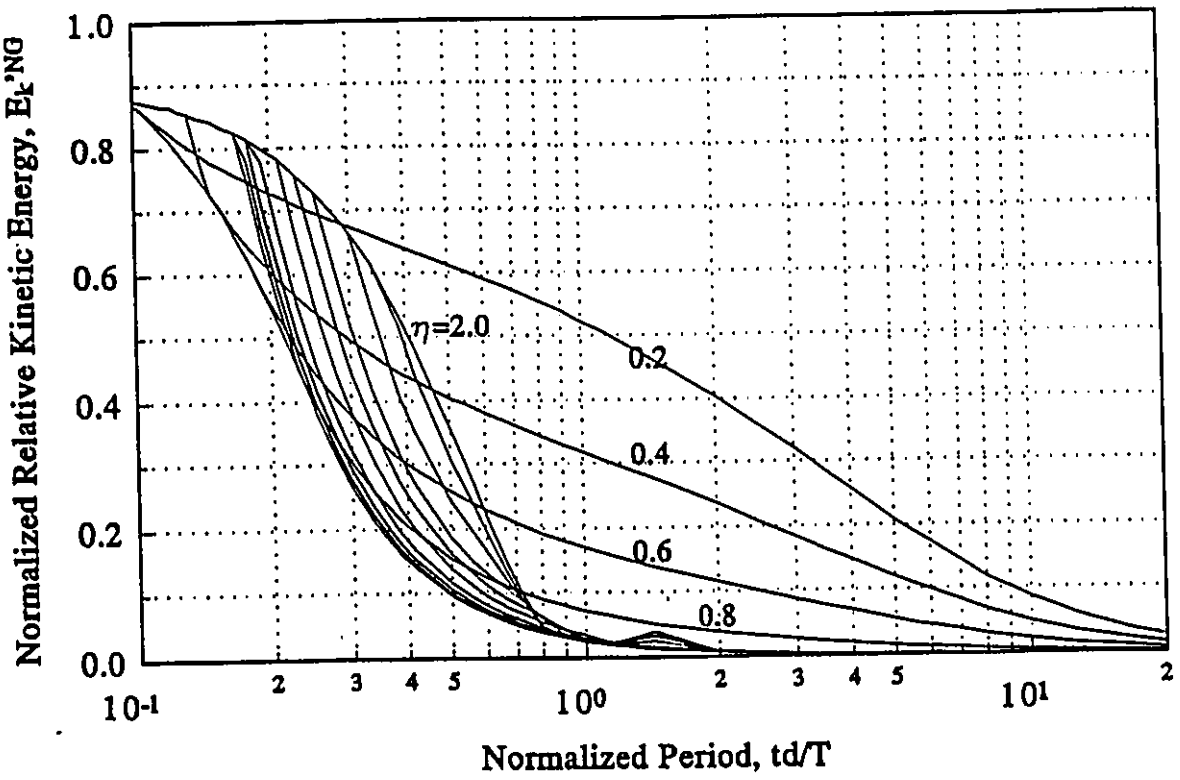

Figure 3.37 Normalized relative kinetic energy spectra for rectangular pulse excitation (ξ = 2%)

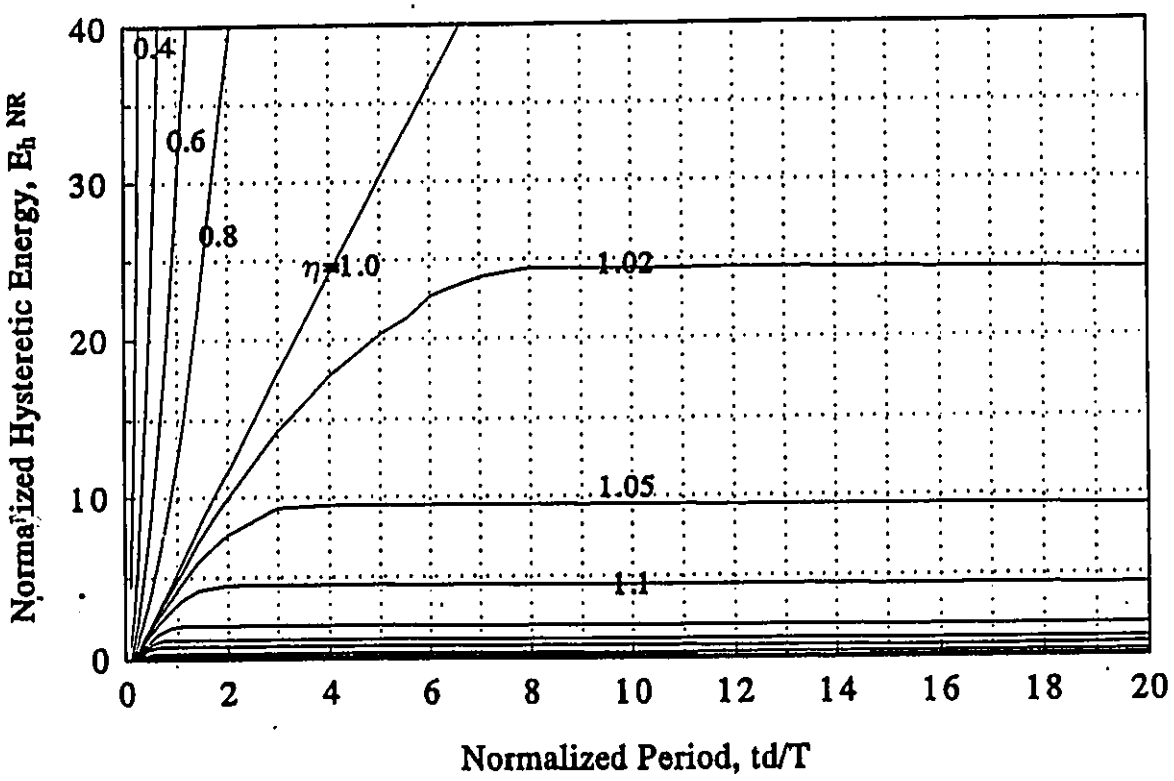

Figure 3.38 Normalized hysteretic energy spectra for rectangular pulse excitation ($\xi = 0\%$)

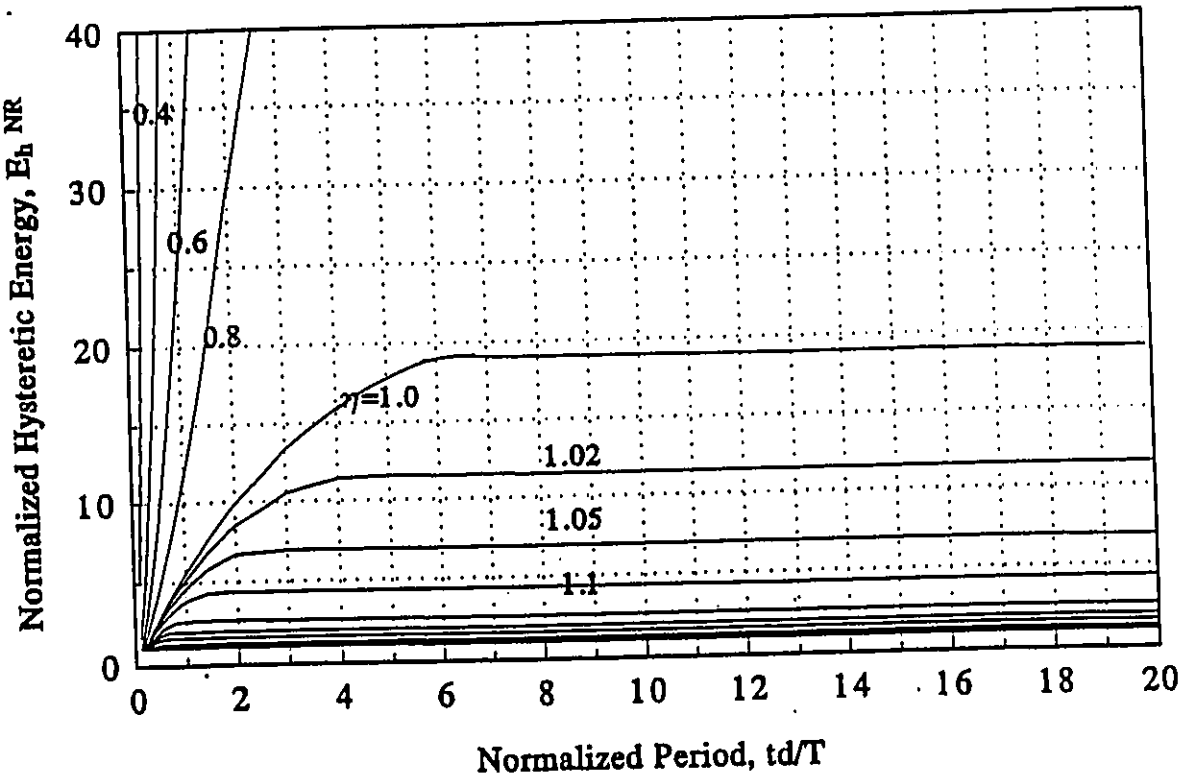

Figure 3.39 Normalized hysteretic energy spectra for rectangular pulse excitation (ξ = 2%)

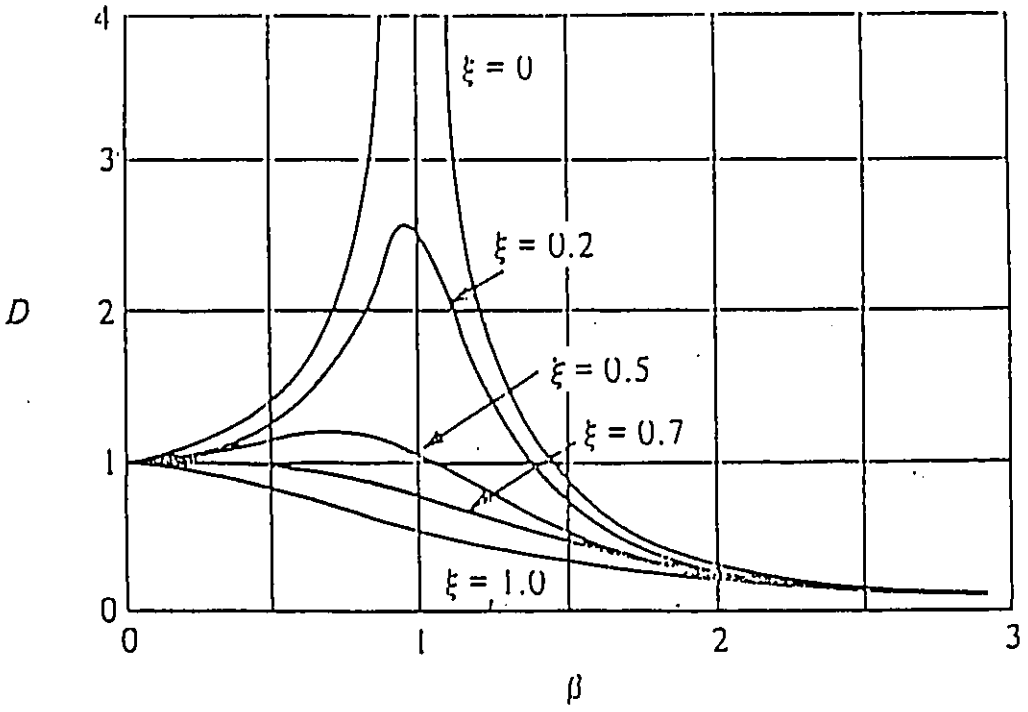

Figure 4.1 Variation of dynamic magnification factor with damping and frequency (Clough and Penzien 1975)

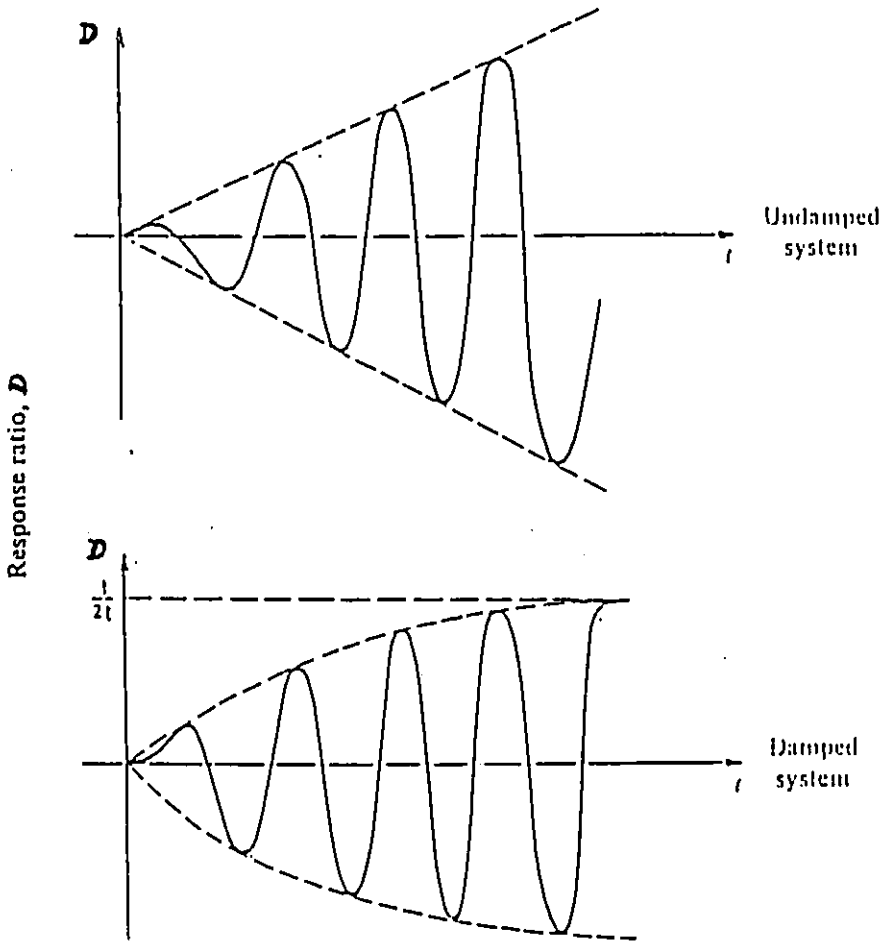

Figure 4.2 Response to resonant loading $\beta = 1$ for at-rest initial conditions (Clough and Penzien 1975)

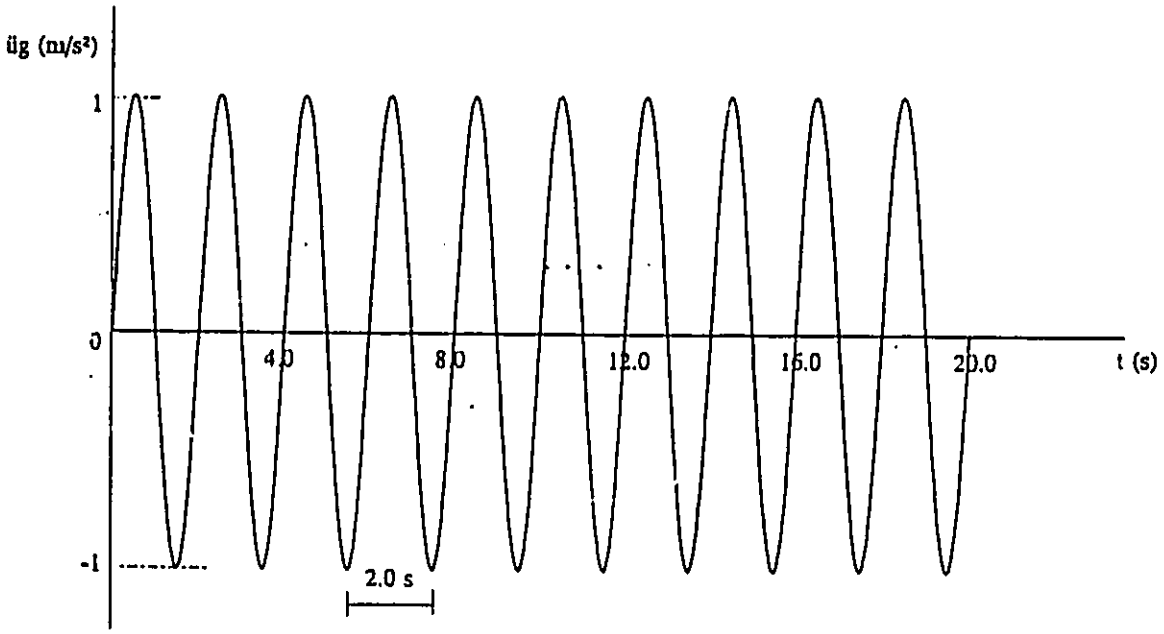

Figure 4.3 An arbitrarily selected sine-wave excitation

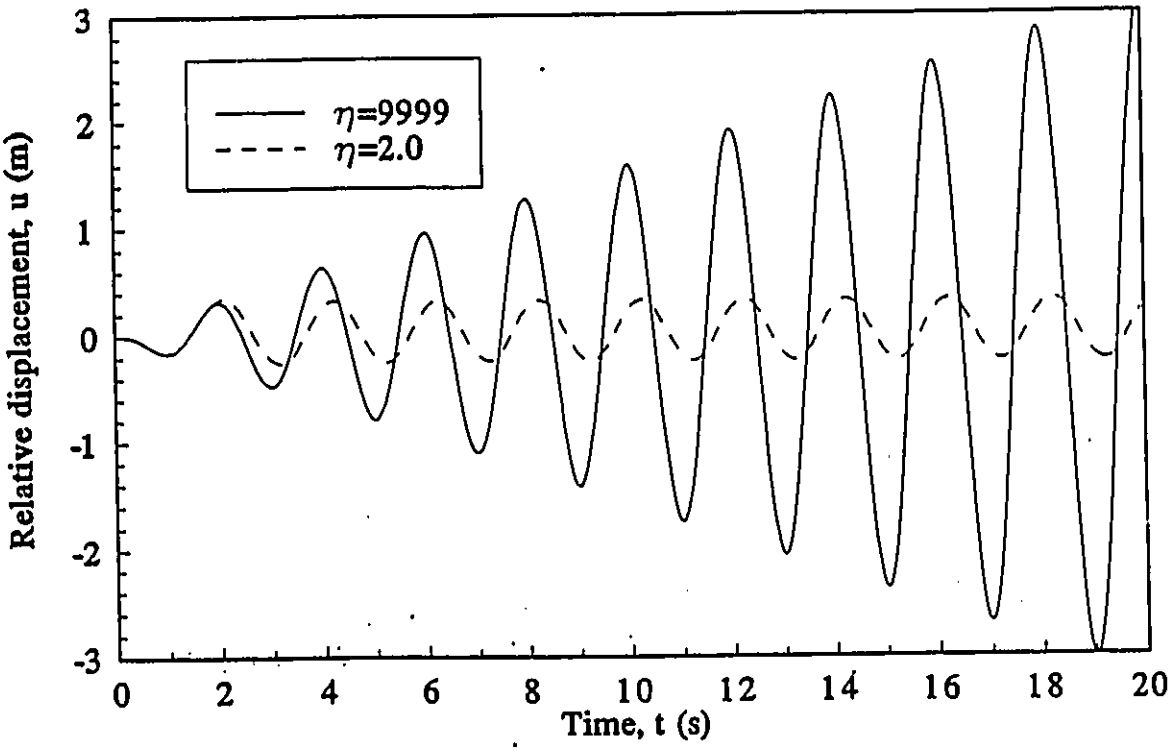

Figure 4.4 Relative displacement time histories in Example 1
(β = 1.0, ξ = 0%)

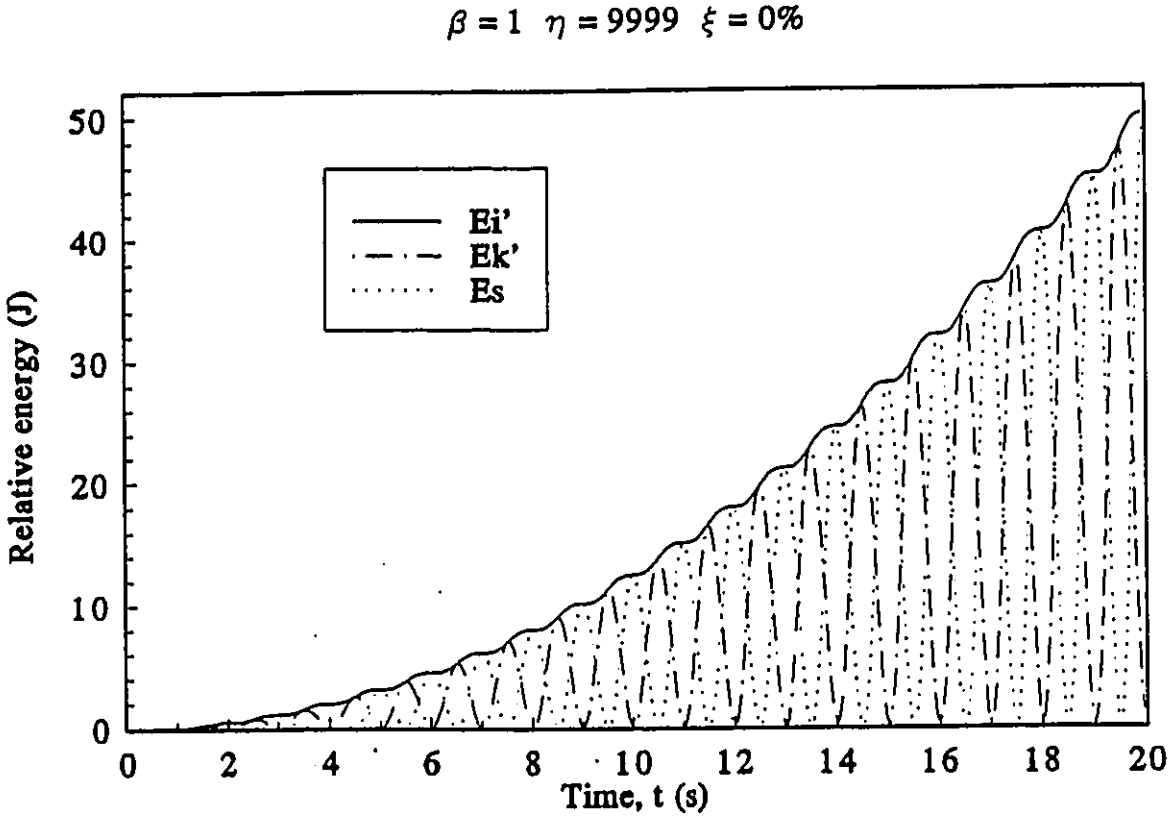

Figure 4.5 Relative energy time histories for η of 9999 in Example 1

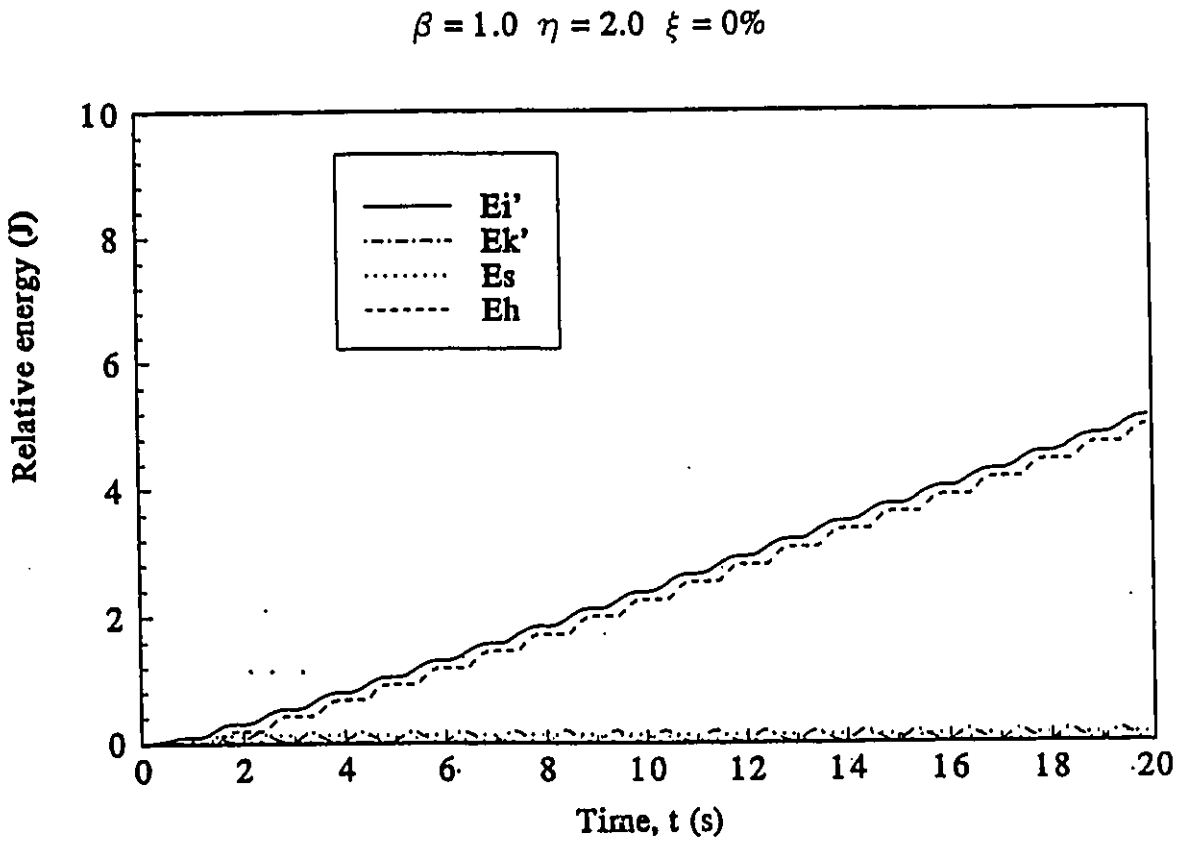

Figure 4.6 Relative energy time histories for η of 2.0 in Example 1

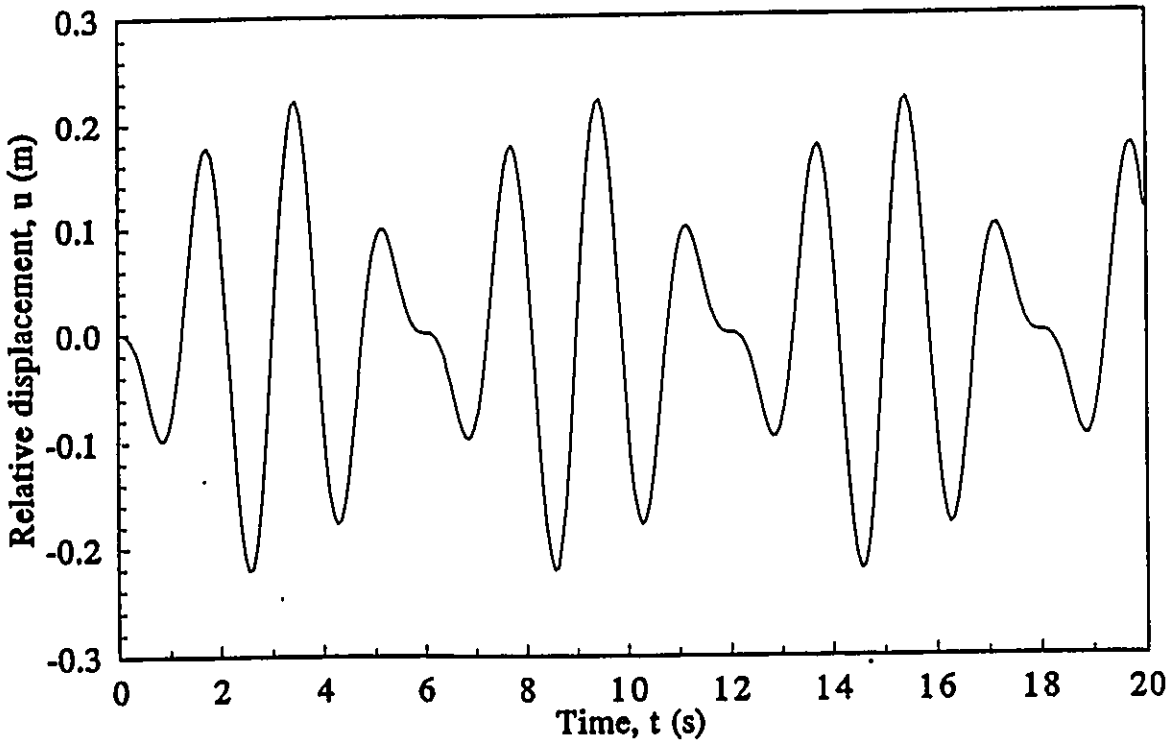

Figure 4.7 Relative displacement time history in Example 2
($\beta = 0.75$, $\eta = 9999$, $\xi = 0\%$)

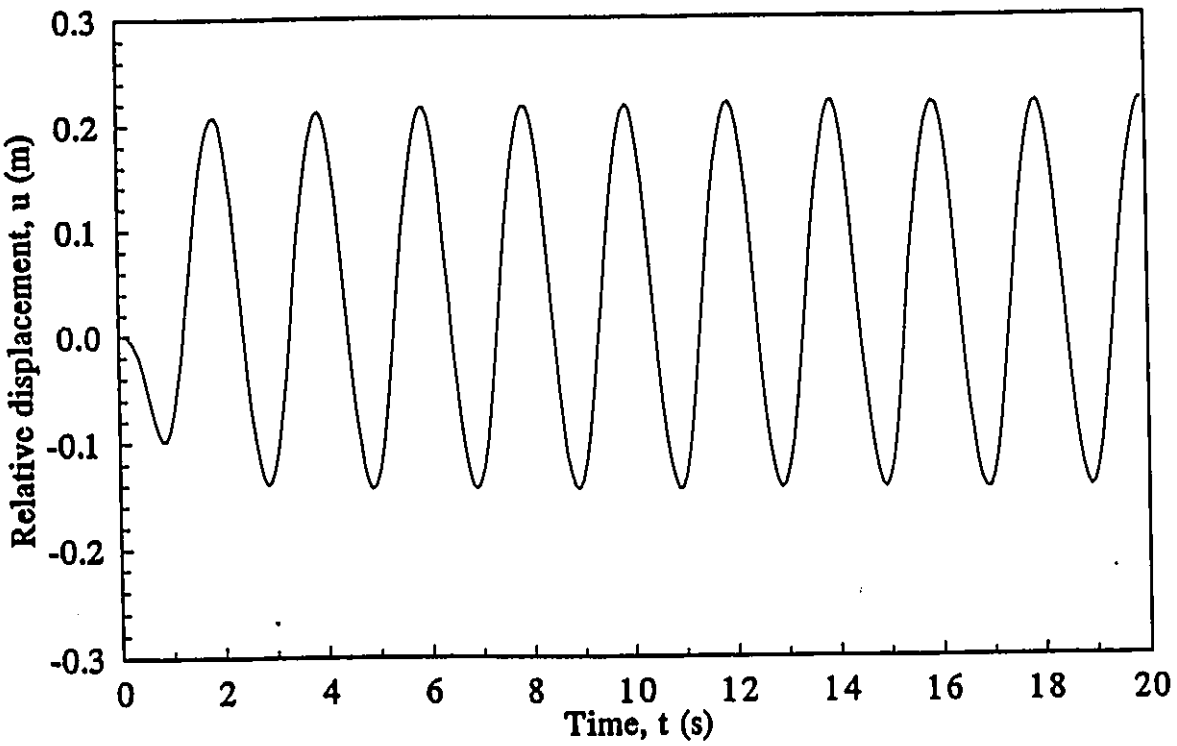

Figure 4.8 Relative displacement time history in Example 2
($\beta = 0.75$, $\eta = 2.0$, $\xi = 0\%$)

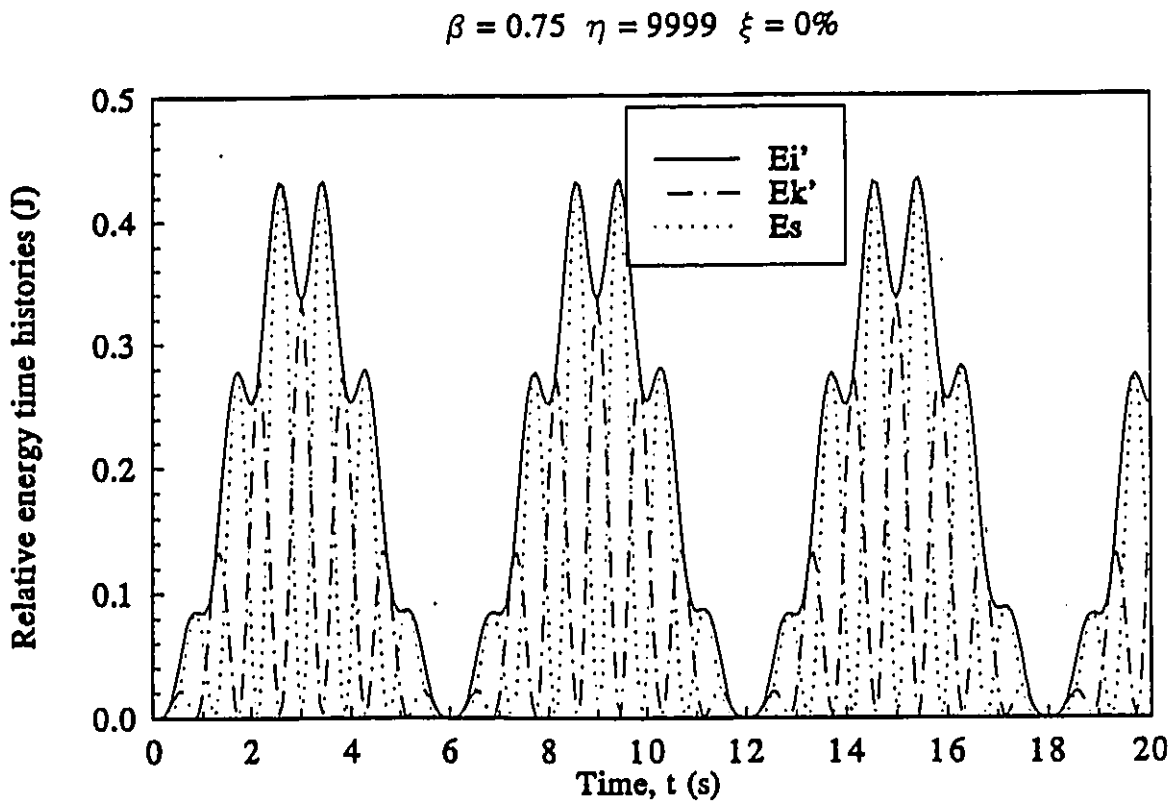

Figure 4.9 Relative energy time histories for η of 9999 in Example 2

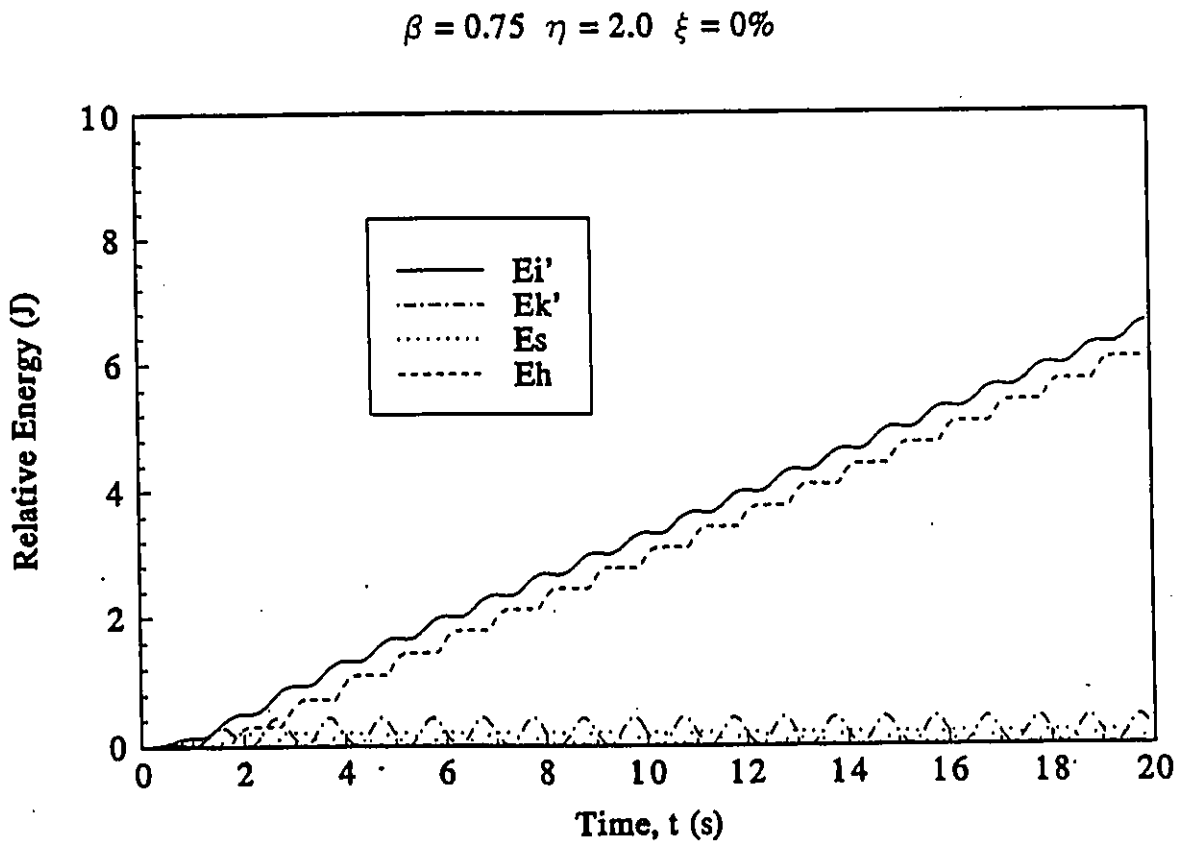

Figure 4.10 Relative energy time histories for η of 2.0 in Example 2

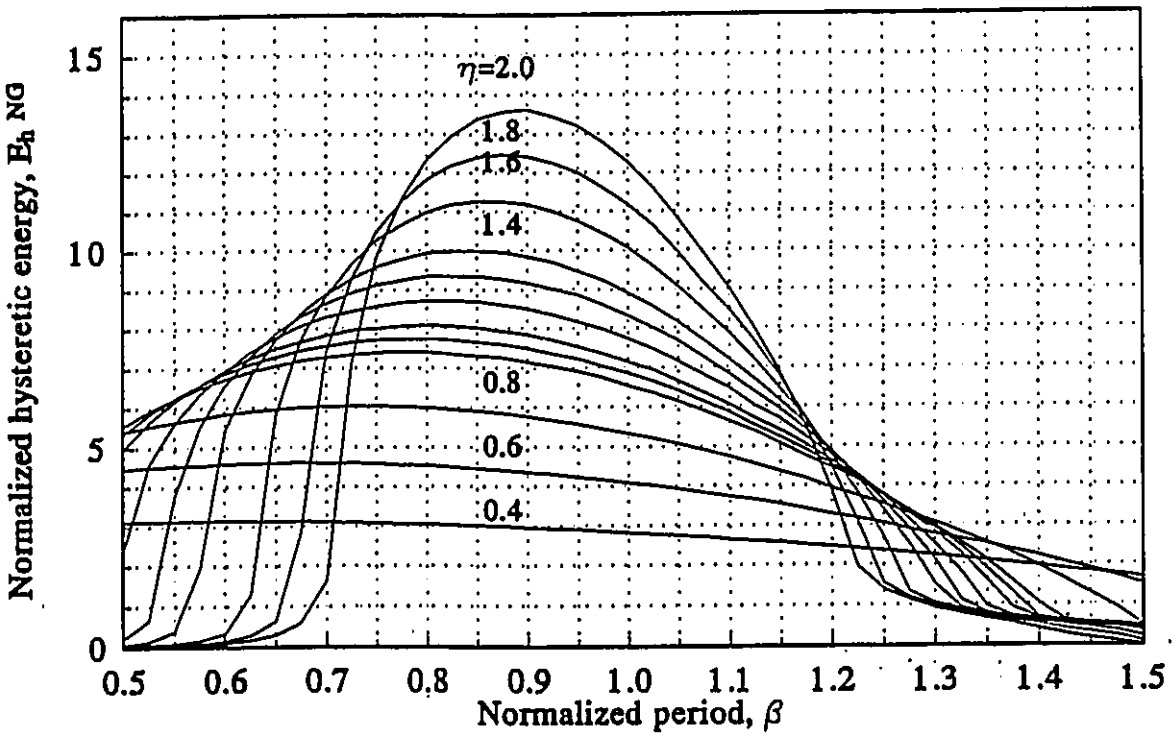

Figure 4.11 Normalized hysteretic energy spectra (ξ = 0%)

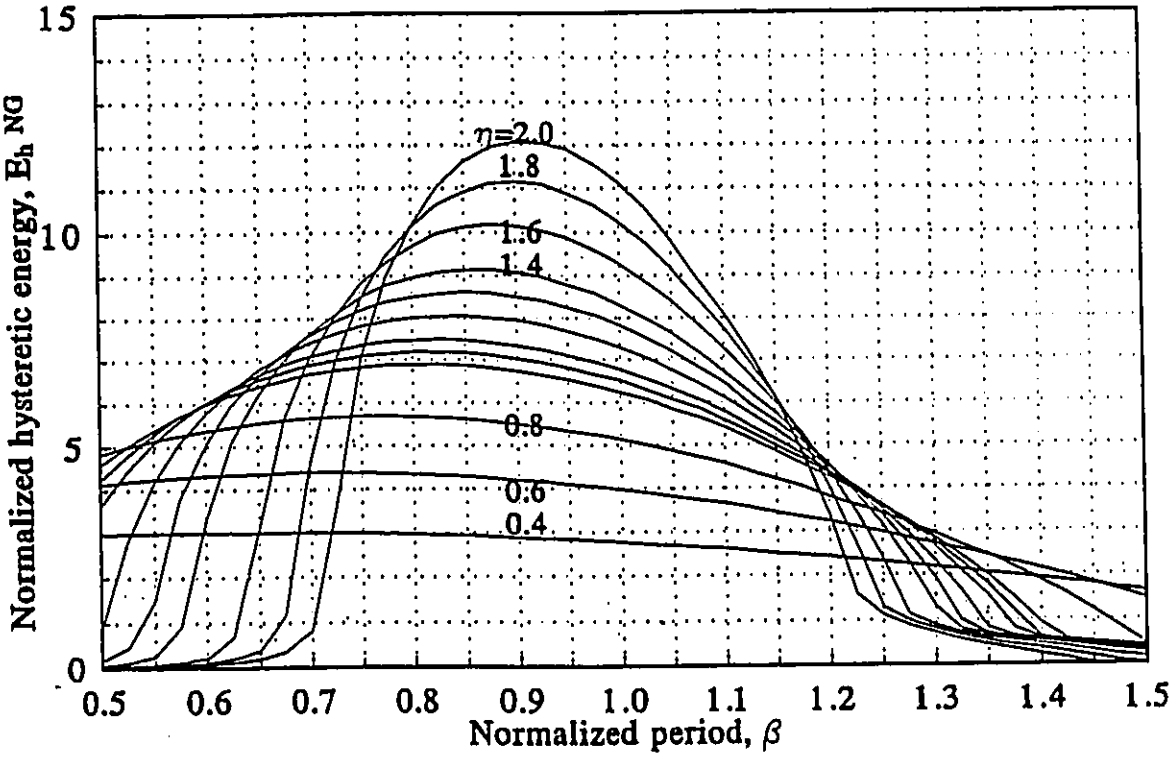

Figure 4.12 Normalized hysteretic energy spectra (ξ = 2%)

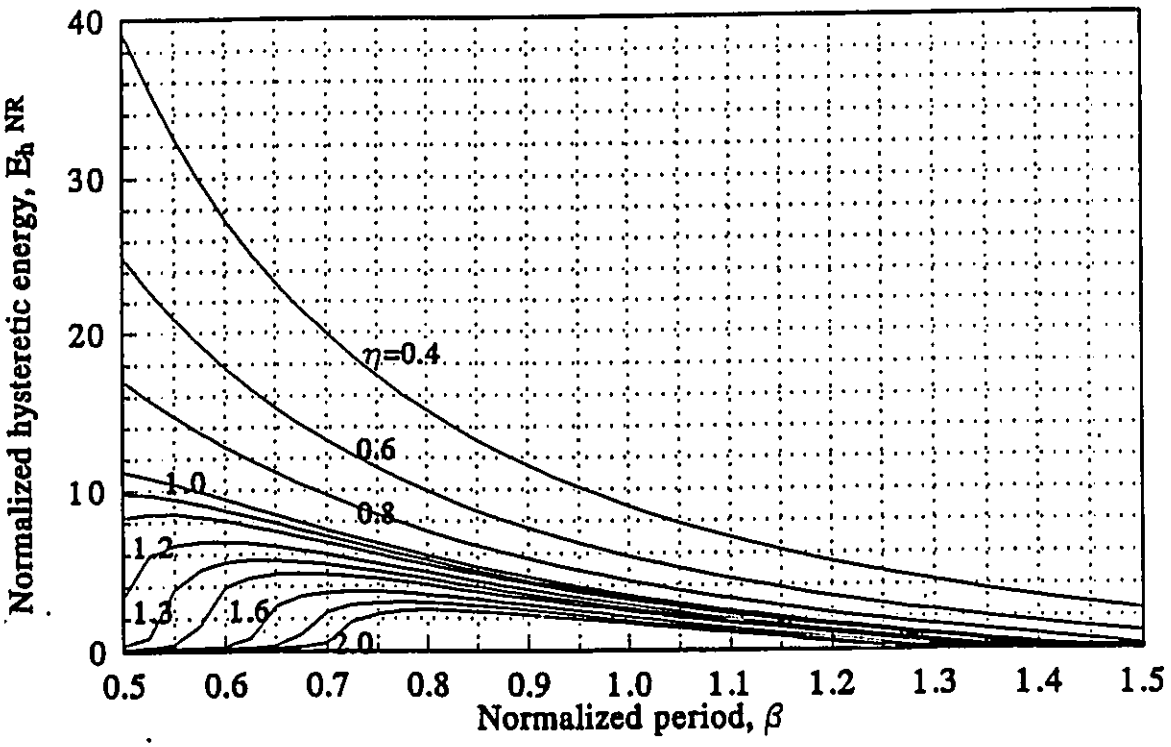

Figure 4.13 Normalized hysteretic energy spectra (ξ = 0%)

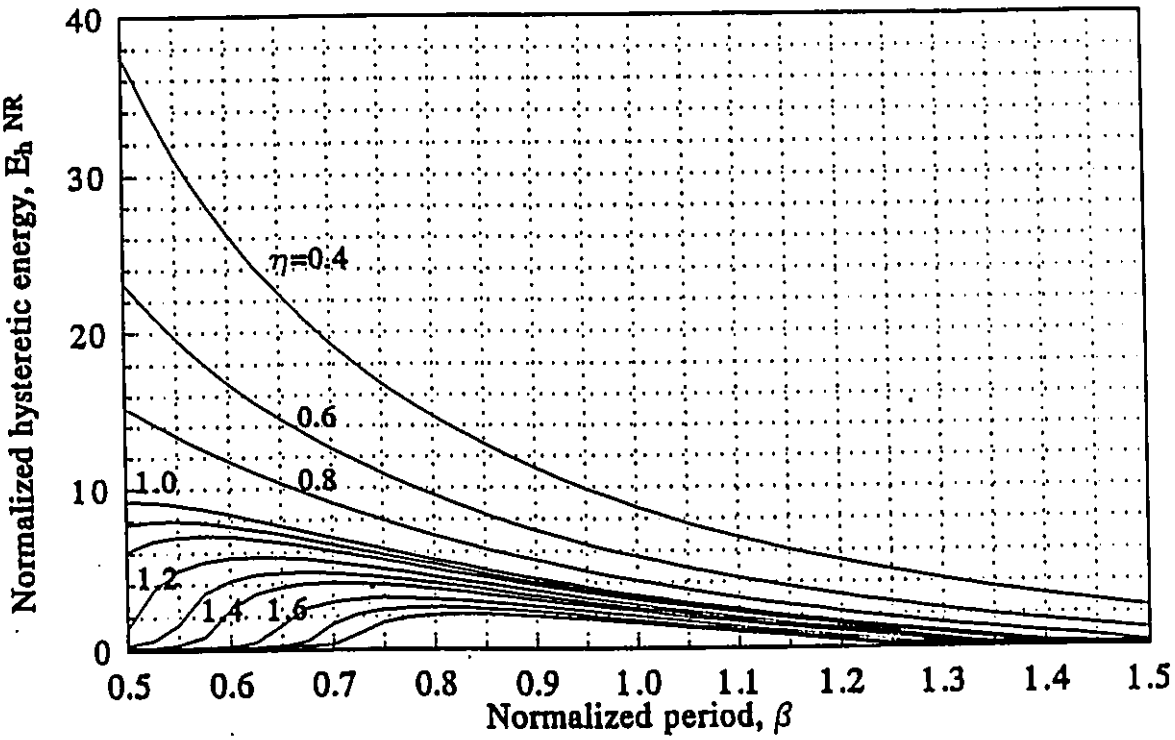

Figure 4.14 Normalized hysteretic energy spectra (ξ = 2%)

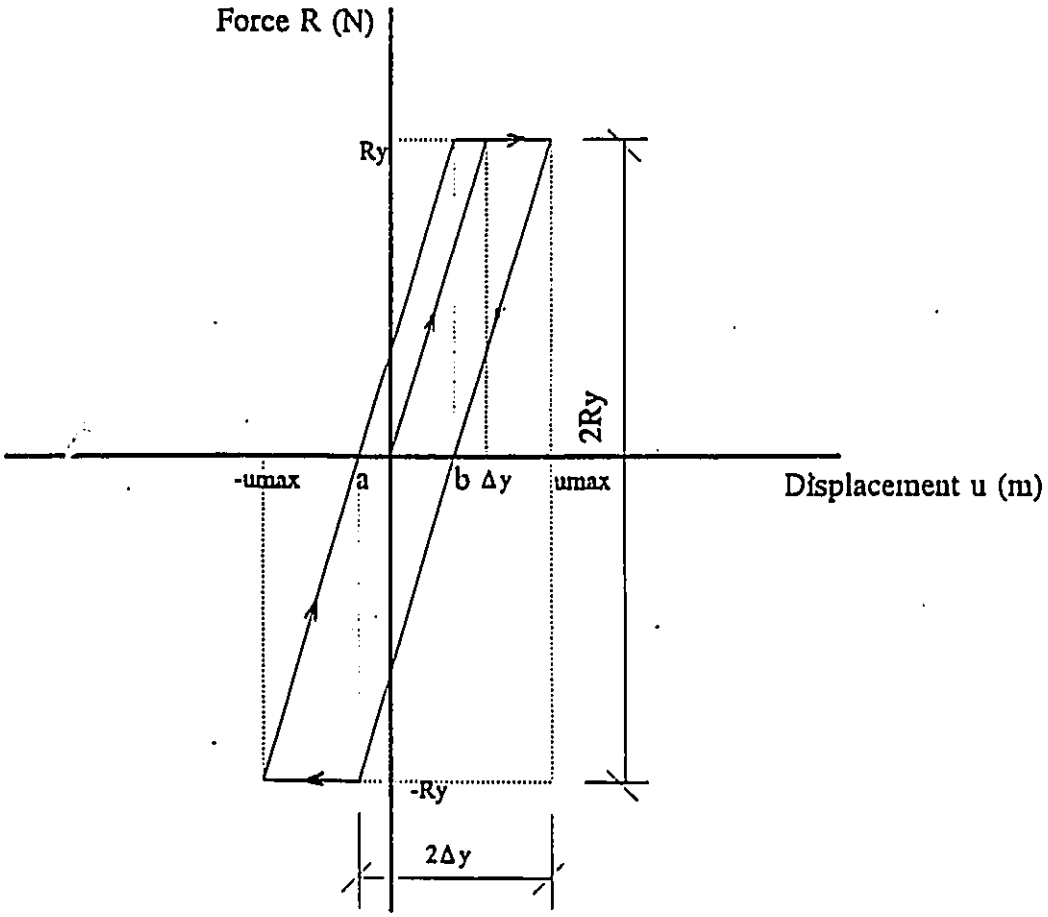

a --- yield displacement of cyclic response for reverse loading;

b --- yield displacement of cyclic response for reloading.

Figure 4.15 Bilinear hysteresis loop model of SDOF system subjected to a sine-wave loading

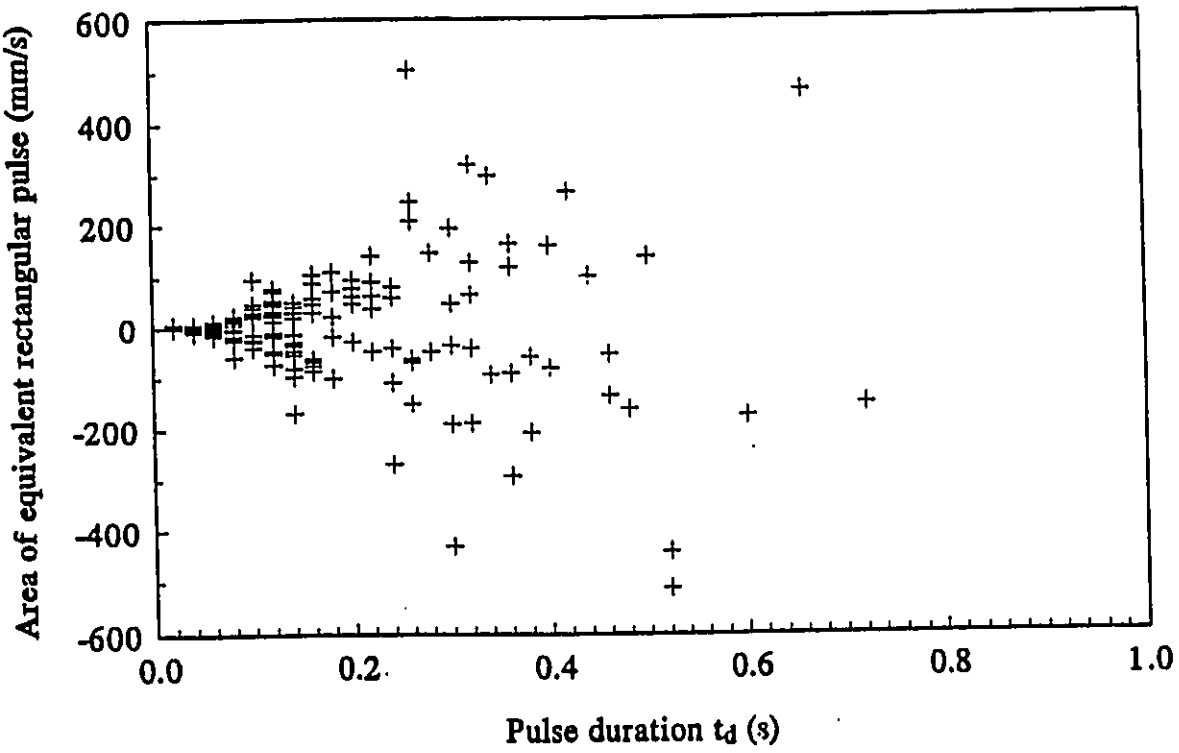

Figure 5.1 Distribution of equivalent pulses of El Centro earthquake

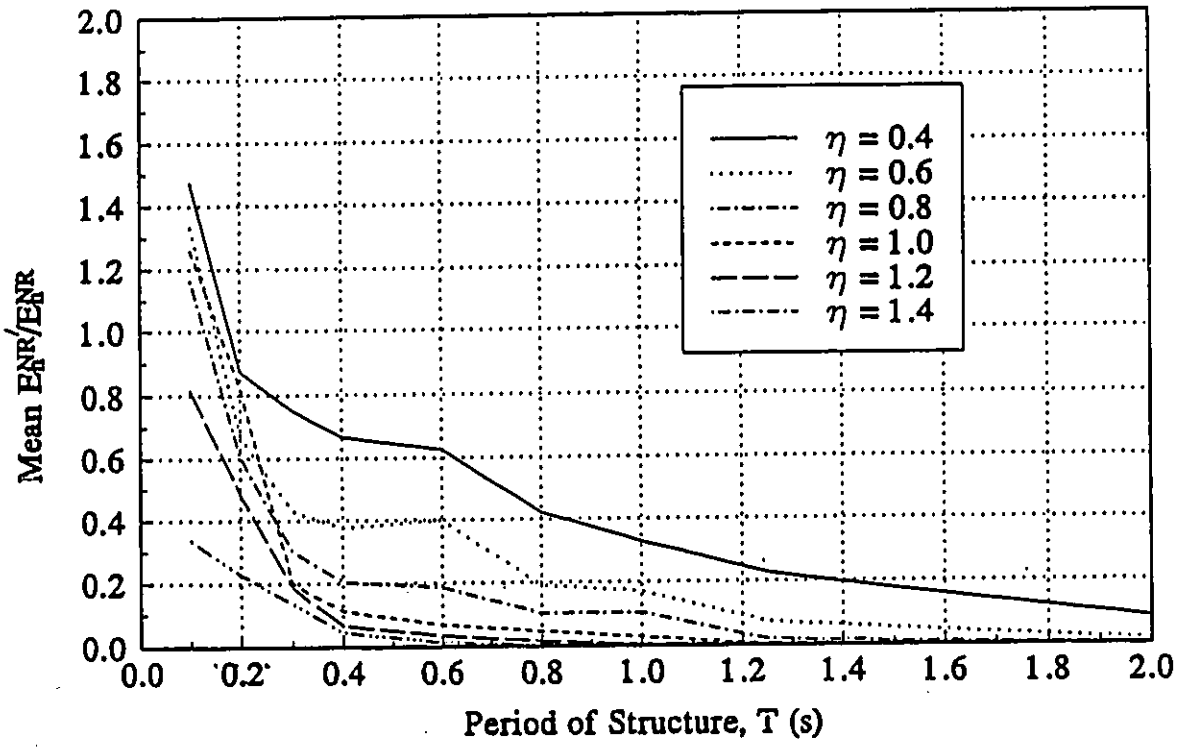

Figure 5.2 Mean ratio-spectra based on five earthquakes converted to rectangular pulses

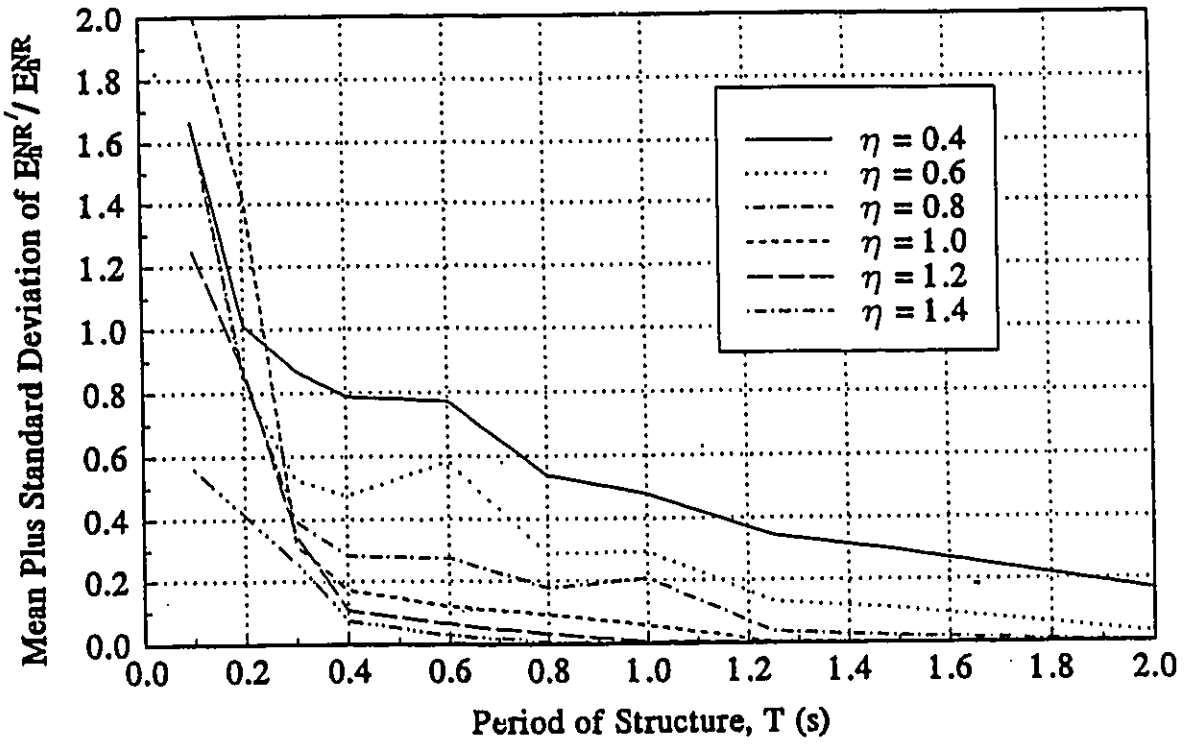

Figure 5.3 Mean plus one standard deviation ratio-spectra for five earthquakes

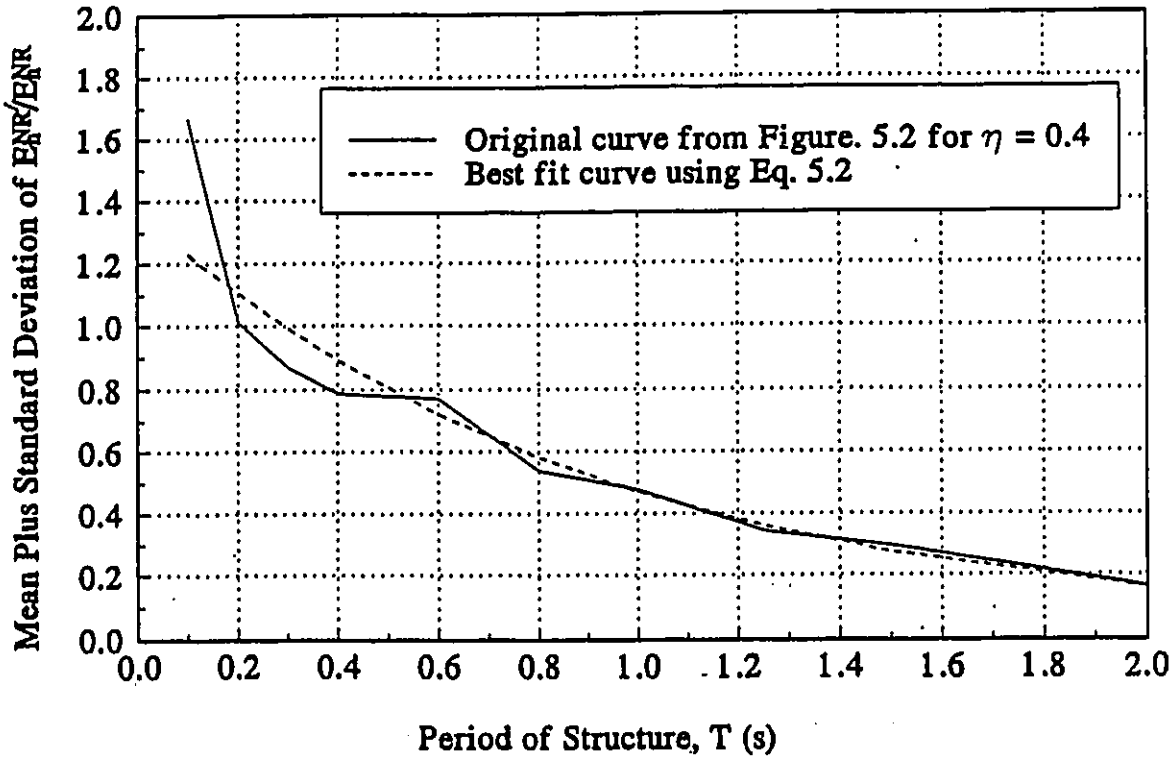

Figure 5.4 Sample best fitting condition

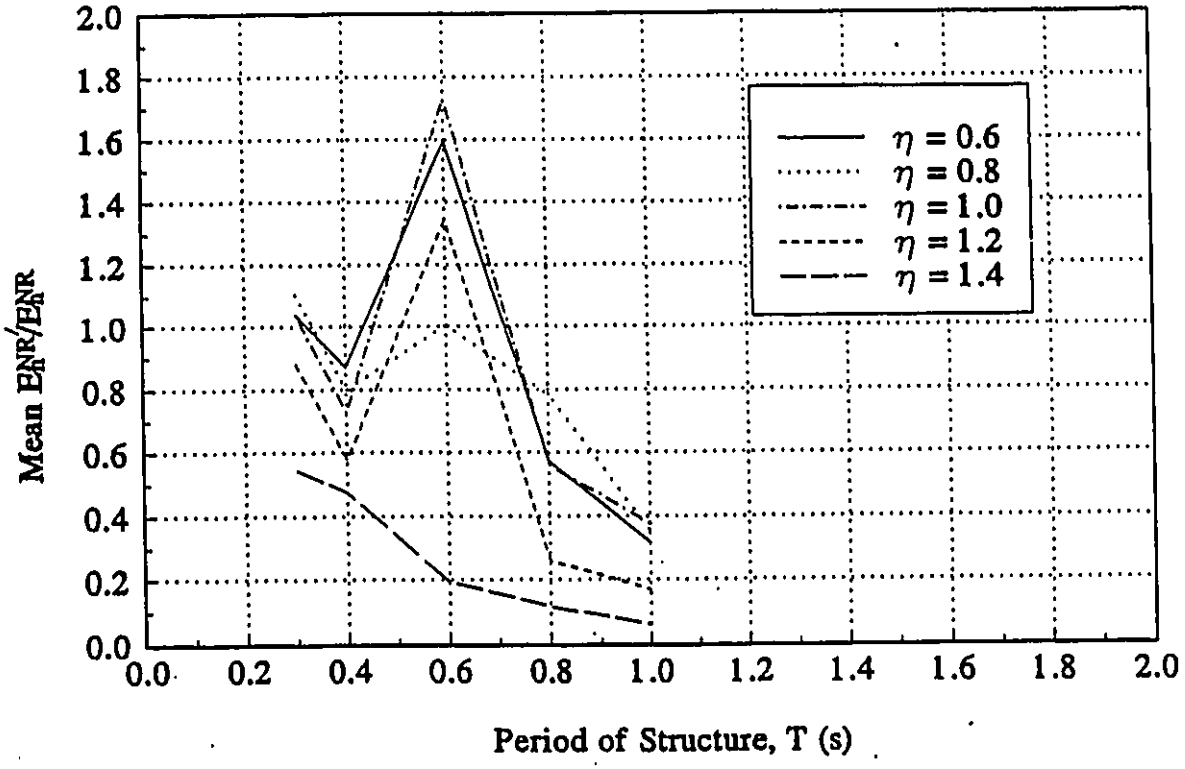

Figure 5.5 Mean ratio-spectra based on five earthquakes converted to sine pulses

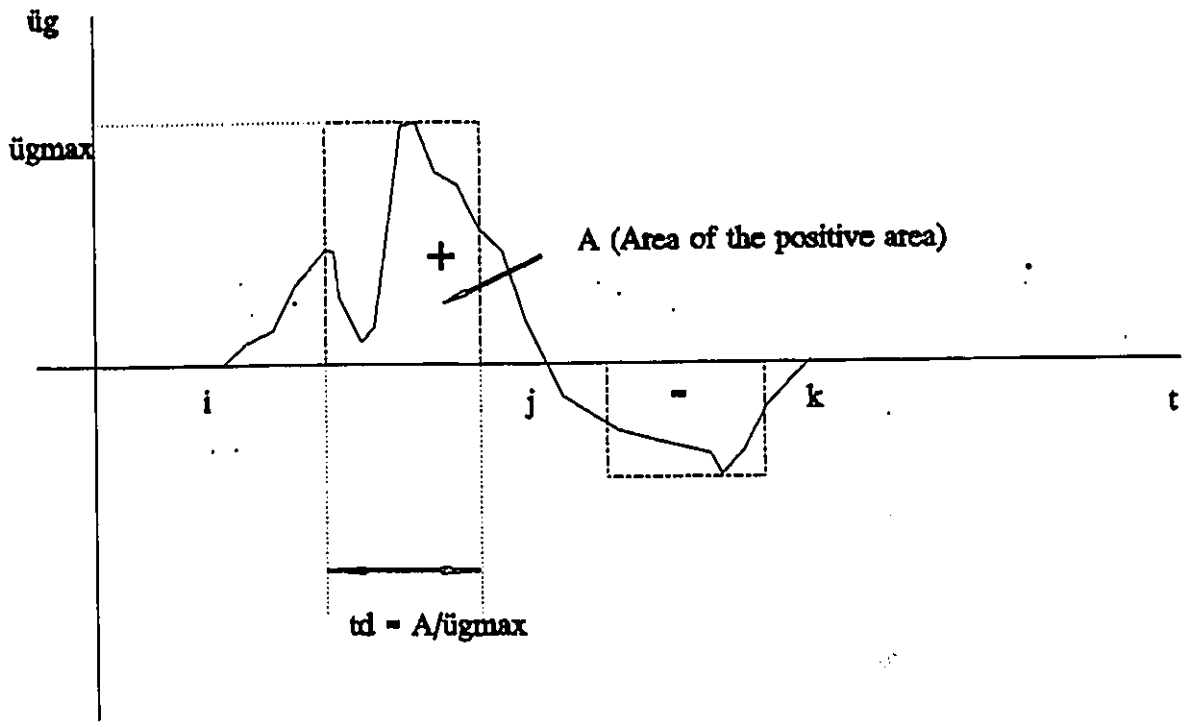

Figure 5.6 Illustration of the converted rectangular pulse method

Appendix A
List of Computer Programs

Program to convert a real earthquake ground acceleration record to equivalent rectangular pulses

Line# Source Line Microsoft FORTRAN Optimizing Compiler Version 5.00

```
 1            PROGRAM AREA
 2
 3   C       AUTO SIMULATE RAW E.Q. DATA TO RECTAGULAR PULSES
 4   C       N:       NUMBER OF RAW DATA READIN
 5   C       RY:      YIELD STRENGTH OF STRUCTURE
 6   C       T:       RAW DATA TIME
 7   C       X1:      READIN ACC. IN RAW DATA
 8   C       XMAX:    ABSOLUTE MAX ACC. IN ONE ORIGINAL PULSE
 9   C       A:       CUMULATED AREA IN EACH ORIGINAL PULSE
10   C       TD:      DURATION OF THE INDIVIDUAL RECTANGULAR PULSE
11   C       ETA:     EQUIVALENT ETA FOR EACH RECTANGULAR PULSE
12
13            OPEN (UNIT=11,FILE='PULSES',STATUS='UNKNOWN')
14            OPEN (UNIT=12,FILE='ELSES',STATUS='UNKNOWN')
15            READ (5,*) N, RY
16            T=0.00
17            X=0.00
18            A=0.00
19            XMAX=X
20            DO 20 I=1,N
21            READ (5,*) X1
22               IF (ABS(X1). GT. XMAX) THEN
23               XMAX=ABS(X1)
24               ENDIF
25            IF (X1*X. GE. 0) THEN
26                     XM=(X1+X)/2
27                     X=X1
28                     T=T+0.02
29                     A1=0.02*XM
30                     A=A+A1
31                     WRITE (12,100) X, T
32  100                FORMAT (1X, F14.6, F14.6)
33            ELSE
34                     DELTAT=0.02*ABS(X)/(ABS(X1)+ABS(X))
35                     T=T+DELTAT
36                     DELTAA=0.5*ABS(X)*DELTAT
37                     A=A+DELTAA
38                     TD=(ABS(A))/XMAX
39                     ETA=RY/XMAX
40                     X=0.00
41                     WRITE (12,200) X, T, A, XMAX, TD, ETA
42                     WRITE (11,200) X, T, A, XMAX, TD, ETA
43  200                FORMAT (1X, 6F12.4)
44                     XMAX = 0.0
45                     A = 0.0
46            END IF
47  20        CONTINUE
48            STOP
49            END
```

main Local Symbols

Name	Class	Type	Size	Offset
A	local	REAL*4	4	0002
X1	local	REAL*4	4	0006
I	local	INTEGER*4	4	000a

Microsoft FORTRAN Optimizing Compiler Version 5.00

main Local Symbols

Name	Class	Type	Size	Offset
N	local	INTEGER*4	4	000e
T	local	REAL*4	4	0012
TD	local	REAL*4	4	0016
X	local	REAL*4	4	001a
ETA	local	REAL*4	4	001e
XM	local	REAL*4	4	0022
DELTAA	local	REAL*4	4	0026
RY	local	REAL*4	4	002a
A1	local	REAL*4	4	002e
DELTAT	local	REAL*4	4	0032
XMAX	local	REAL*4	4	0036

Global Symbols

Name	Class	Type	Size	Offset
main	FSUBRT	***	***	0000

Code size = 0313 (787)
Data size = 00a0 (160)
Bss size = 003a (58)

No errors detected
No errors detected

Program to calculate the raw predicted normalized hysteretic energy for rectangular pulses method

Line# Source Line Microsoft FORTRAN Optimizing Compiler Version 5.00

```
 1
 2            PROGRAM AUTOREAD
 3            DIMENSION DATA (43,15), PUT (375,2), DETA(14)
 4
 5  C       DATA:    AXUM DATA
 6  C       PUT:     INPUT TD AND ETA FROM TDAREA'S RESULT 'PULSES'
 7  C       ETA:     STRENGTH RATIO
 8  C       PERIOD:  PERIOD OF STRUCTURE
 9  C       NTD:     NUMBER OF TD
10  C       RY:      YIELD SHEAR OF STRUCTURE
11  C       TDT:     READIN TD/T
12  C       DETA:    14 ETA VALUES IN DATA
13
14            OPEN (UNIT=11, FILE='DETA', STATUS='OLD')
15            OPEN (UNIT=8, FILE='DATA', STATUS='UNKNOWN')
16            OPEN (UNIT=9, FILE='NEH', STATUS='UNKNOWN')
17            OPEN (UNIT=10, FILE='PUT',STATUS='UNKNOWN')
18
19            DO 1 II=1,43
20            READ(8,*) (DATA(II,JJ),JJ=1,15)
21     1      CONTINUE
22
23            SUM = 0
24            READ (5,*) PERIOD, NTD, RY
25            DO 15 I = 1, NTD
26            READ (10,*) PUT(I,1),PUT(I,2)
27    30              ETA = PUT(I,2)
28               IF ((ETA .LT. 0.2) .OR. (ETA .GT. 2.0)) GOTO 15
29    40              TDT = PUT(I,1) / PERIOD
30               IF ((TDT .LT. 0.1) .OR. (TDT .GT. 20.0)) GOTO 15
31    55       CONTINUE
32  C
33            IFOUND = 0
34    75       DO 25 M = 1,43
35             IF (IFOUND.EQ.0.AND.DATA(M,1).GT.TDT) THEN
36                     MA = M - 1
37                     MB = M
38                     IF(MA.EQ.0) MA=1
39                     XLARG = DATA(MB,1)
40                     SMAL = DATA(MA,1)
41                     IFOUND=1
42              ENDIF
43    25        CONTINUE
44
45            IFOUND=0
46    85       DO 35 L = 1,14
47             N = L + 1
48             K = L - 1
49             READ (11,*) DETA(L)
50             IF (IFOUND.EQ.0.AND.ETA .GT. DETA(L)) THEN
51                  XA = DATA(MA,L)
52                  XB = DATA(MB,L)
53                  XC = DATA(MA,N)
54                  XD = DATA(MB,N)
55                  XAB = - ((XLARG - TDT)/(XLARG - SMAL)) * (XB - XA) + XB
56                  XCD = - ((XLARG - TDT)/(XLARG - SMAL)) * (XD - XC) + XD
57                  YL = DETA(K)
58                  YS = DETA(L)
```

Line# Source Line Microsoft FORTRAN Optimizing Compiler Version 5.00

```
   59                X=-((YL - ETA)/(YL - YS)) * (XAB - XCD)+XAB
   60                      WRITE (9,150) PUT(I,1), PUT(I,2),X
   61   150                 FORMAT (1X, 3F14.6)
   62             SUM = SUM + X
   63             IFOUND=1
   64             ENDIF
   65   35        CONTINUE
   66            REWIND(11)
   67   15        CONTINUE
   68            WRITE (9,160) SUM
   69   160       FORMAT (1X, 'SUM OF NHE IS', F20.6)
   70            STOP
   71            END
```

main Local Symbols

Name	Class	Type	Size	Offset
PERIOD.	local	REAL*4	4	0002
IFOUND.	local	INTEGER*4	4	0006
I	local.	INTEGER*4	4	000a
K	local	INTEGER*4	4	000e
L	local	INTEGER*4	4	0012
M	local	INTEGER*4	4	0016
N	local	INTEGER*4	4	001a
MA.	local	INTEGER*4	4	001e
MB.	local	INTEGER*4	4	0022
II.	local	INTEGER*4	4	0026
JJ.	local	INTEGER*4	4	002a
X	local	REAL*4	4	002e
XA.	local	REAL*4	4	0032
XB.	local	REAL*4	4	0036
ETA	local	REAL*4	4	003a
DATA.	local	REAL*4	2580	003e
XAB	local	REAL*4	4	0a52
XC.	local	REAL*4	4	0a56
XD.	local	REAL*4	4	0a5a
DETA.	local	REAL*4	56	0a5e
XCD	local	REAL*4	4	0a96
YL.	local	REAL*4	4	0a9a
NTD	local	INTEGER*4	4	0a9e
RY.	local	REAL*4	4	0aa2
YS.	local	REAL*4	4	0aa6
TDT	local	REAL*4	4	0aaa
SMAL.	local	REAL*4	4	0aae
SUM	local.	REAL*4	4	0ab2
PUT	local	REAL*4	3000	0ab6
XLARG	local	REAL*4	4	166e

Global Symbols

Name	Class	Type	Size	Offset
main.	FSUBRT	***	***	0000

Code size = 05f9 (1529)

Microsoft FORTRAN Optimizing Compiler Version 5.00

```
Data size = 0087 (135)
Bss size  = 1672 (5746)

No errors detected
```

Program to convert a real earthquake ground acceleration record to equivalent sine pulses

Line# Source Line Microsoft FORTRAN Optimizing Compiler Version 5.00

```
     1            PROGRAM AREA
     2
     3  C        AUTO SIMULATE RAW E.Q. DATA TO RECTAGULAR PULSES
     4  C        N:       NUMBER OF RAW DATA READIN
     5  C        RY:      YIELD STRENGTH OF STRUCTURE
     6  C        T:       RAW DATA TIME
     7  C        X1:      READIN ACC. IN RAW DATA
     8  C        XMAX:    ABSOLUTE MAX ACC. IN ONE ORIGINAL PULSE
     9  C        A:       CUMULATED AREA IN EACH ORIGINAL PULSE
    10  C        TD:      DURATION OF THE INDIVIDUAL RECTANGULAR PULSE
    11  C        ETA:     EQUIVALENT ETA FOR EACH RECTANGULAR PULSE
    12
    13            OPEN (UNIT=13,FILE='SPULSE',STATUS='UNKNOWN')
    14            OPEN (UNIT=14,FILE='SELSE',STATUS='UNKNOWN')
    15            READ (5,*) N, RY
    16            T=0.00
    17            X=0.00
    18  C         A=0.00
    19            XMAX=X
    20            DO 20 I=1,N
    21            READ (5,*) X1
    22               IF (ABS(X1). GT. XMAX) THEN
    23               XMAX=ABS(X1)
    24               ENDIF
    25            IF (X1*X. GE. 0) THEN
    26                     XM=(X1+X)/2
    27                     X=X1
    28                     T=T+0.02
    29  C                  A1=0.02*XM
    30  C                  A=A+A1
    31                     WRITE (14,100) X, T
    32  100                FORMAT (1X, F14.6, F14.6)
    33            ELSE
    34                     DELTAT=0.02*ABS(X)/(ABS(X1)+ABS(X))
    35                     T=T+DELTAT
    36  C                  DELTAA=0.5*ABS(X)*DELTAT
    37  C                  A=A+DELTAA
    38                     TD=T
    39                     ETA=RY/XMAX
    40                     X=0.00
    41                     WRITE (14,200) X, T, XMAX, TD, ETA
    42                     WRITE (13,200) X, T, XMAX, TD, ETA
    43  200                FORMAT (1X, 5F12.4)
    44                     XMAX = 0.0
    45                     A = 0.0
    46                     T = 0.0
    47             END IF
    48  20        CONTINUE
    49            STOP
    50            END
```

main Local Symbols

Name	Class	Type	Size	Offset
A	local	REAL*4	4	0002
X1.	local	REAL*4	4	0006

Microsoft FORTRAN Optimizing Compiler Version 5.00

main Local Symbols

Name	Class	Type	Size	Offset
I	local	INTEGER*4	4	000a
N	local	INTEGER*4	4	000e
T	local	REAL*4	4	0012
TD.	local	REAL*4	4	0016
X	local	REAL*4	4	001a
ETA	local	REAL*4	4	001e
XM.	local	REAL*4	4	0022
RY.	local	REAL*4	4	0026
DELTAT.	local	REAL*4	4	002a
XMAX.	local	REAL*4	4	002e

Global Symbols

Name	Class	Type	Size	Offset
main.	FSUBRT	***	***	0000

Code size = 028b (651)
Data size = 0093 (147)
Bss size = 0032 (50)

No errors detected
No errors detected

Program to calculate the raw predicted normalized hysteretic energy for sine pulses method

Line# Source Line Microsoft FORTRAN Optimizing Compiler Version 5.00

```
 1
 2            PROGRAM AUTOREAD
 3            DIMENSION DATA (43,15), PUT (375,2), sineETA(12)
 4
 5  C       DATA:    AXUM DATA
 6  C       PUT:     INPUT TD AND ETA FROM TDAREA'S RESULT 'PULSES'
 7  C       ETA:     STRENGTH RATIO
 8  C       PERIOD:  PERIOD OF STRUCTURE
 9  C       NTD:     NUMBER OF TD
10  C       RY:      YIELD SHEAR OF STRUCTURE
11  C       TDT:     READIN TD/T
12  C       DETA:    14 ETA VALUES IN DATA
13
14            OPEN (UNIT=11, FILE='sineETA', STATUS='OLD')
15            OPEN (UNIT=8, FILE='DATASIN', STATUS='UNKNOWN')
16            OPEN (UNIT=9, FILE='NEHSIN', STATUS='UNKNOWN')
17            OPEN (UNIT=10, FILE='PUT',STATUS='UNKNOWN')
18
19            DO 1 II=1,41
20           READ(8,*) (DATA(II,JJ),JJ=1,13)
21     1      CONTINUE
22
23            SUM = 0
24            READ (5,*) PERIOD, NTD, RY
25            DO 15 I = 1, NTD
26            READ (10,*) PUT(I,1),PUT(I,2)
27    30                ETA = PUT(I,2)
28               IF ((ETA .LT. 0.4) .OR. (ETA .GT. 2.0)) GOTO 15
29    40                TDT = PERIOD / (PUT(I,1)*2)
30               IF ((TDT .LT. 0.5) .OR. (TDT .GT. 1.5)) GOTO 15
31    55        CONTINUE
32  C
33            IFOUND = 0
34    75        DO 25 M = 1,41
35              IF (IFOUND.EQ.0.AND.DATA(M,1).GT.TDT) THEN
36                          MA = M - 1
37                          MB = M
38                          IF(MA.EQ.0) MA=1
39                          XLARG = DATA(MB,1)
40                          SMAL = DATA(MA,1)
41                          IFOUND=1
42               ENDIF
43    25         CONTINUE
44
45            IFOUND=0
46    85         DO 35 L = 1,12
47              N = L + 1
48              K = L - 1
49              READ (11,*) sineETA(L)
50              IF (IFOUND.EQ.0.AND. ETA .GT. sineETA(L)) THEN
51                   XA = DATA(MA,L)
52                   XB = DATA(MB,L)
53                   XC = DATA(MA,N)
54                   XD = DATA(MB,N)
55                   XAB = - ((XLARG - TDT)/(XLARG - SMAL)) * (XB - XA) + XB
56                   XCD = - ((XLARG - TDT)/(XLARG - SMAL)) * (XD - XC) + XD
57                   YL = sineETA(K)
58                   YS = sineETA(L)
```

Line# Source Line Microsoft FORTRAN Optimizing Compiler Version 5.00

```
                X=-((YL - ETA)/(YL - YS)) * (XAB - XCD)+XAB
                      WRITE (9,150) PUT(I,1), PUT(I,2),X
150                    FORMAT (1X, 3F14.6)
          SUM = SUM + X
          IFOUND=1
          ENDIF
35        CONTINUE
         REWIND(11)
15        CONTINUE
         WRITE (9,160) SUM
160       FORMAT (1X, 'SUM OF NHE IS', F20.6)
         STOP
         END
```

main Local Symbols

Name	Class	Type	Size	Offset
PERIOD.	local	REAL*4	4	0002
IFOUND.	local	INTEGER*4	4	0006
I	local	INTEGER*4	4	000a
SINEETA	local	REAL*4	48	000e
K	local	INTEGER*4	4	003e
L	local	INTEGER*4	4	0042
M	local	INTEGER*4	4	0046
N	local	INTEGER*4	4	004a
MA.	local	INTEGER*4	4	004e
MB.	local	INTEGER*4	4	0052
II.	local	INTEGER*4	4	0056
JJ.	local	INTEGER*4	4	005a
X	local	REAL*4	4	005e
XA.	local	REAL*4	4	0062
XB.	local	REAL*4	4	0066
ETA	local	REAL*4	4	006a
DATA.	local	REAL*4	2580	006e
XAB	local	REAL*4	4	0a82
XC.	local	REAL*4	4	0a86
XD.	local	REAL*4	4	0a8a
XCD	local	REAL*4	4	0a8e
YL.	local	REAL*4	4	0a92
NTD	local	INTEGER*4	4	0a96
RY.	local	REAL*4	4	0a9a
YS.	local	REAL*4	4	0a9e
TDT	local	REAL*4	4	0aa2
SMAL.	local	REAL*4	4	0aa6
SUM	local	REAL*4	4	0aaa
PUT	local	REAL*4	3000	0aae
XLARG	local	REAL*4	4	1666

Global Symbols

Name	Class	Type	Size	Offset
main.	FSUBRT	***	***	0000

Code size = 0607 (1543)

Microsoft FORTRAN Optimizing Compiler Version 5.00

```
Data size = 0091 (145)
Bss size  = 166a (5738)

No errors detected
```

Program for fast Fourier transform

Line# Source Line Microsoft FORTRAN Optimizing Compiler Version 5.00

```
 1  c
 2  c.... FFT and IFT program developed by J.M. Ricles
 3  c.... June 1986
 4  c
 5        program ftrec
 6        character*3 itype,ft,ift,ftc,iftc
 7        character*13 filein,fileout
 8        dimension a(16384,2),x(10)
 9        data ft,ift/'fft','ift'/,ftc,iftc/'FFT','IFT'/
10        nsize=16384
11        mmax=14
12        pi2=8.0*atan(1.0)
13        write(6,100)
14   100  format(5x,'Fast Fourier Transform Program, version 1.3',/,
15       $     5x,'    Developed by Jim Ricles ',//,
16       $       5x,'      Enter Input file name >',$)
17        read(5,200) filein
18   200  format(a13)
19        write(6,300)
20   300  format(5x,'      Enter Output file name >',$)
21        read(5,200) fileout
22        open(1,file=filein,status='old')
23        open(2,file=fileout,status='new')
24        rewind 1
25        rewind 2
26  c.... Initialization
27        write(6,400)
28   400  format(5x,'Which type of Transformation to be performed?',/,
29       $       5x,'   (FFT - Direct FFT)',/,
30       $       5x,'   (IFT - Inverse FFT)',/,
31       $       5x,'Enter FFT or IFT > ',$)
32        read(5,500) itype
33   500  format(a3)
34        if(itype.eq.ft.or.itype.eq.ftc) then
35        sign=-1.0
36        write(6,610)
37   610  format(5x,'Enter value of m, dt ',/,
38      &       5x,'(note: # points in record = 2**m)     >',$)
39        read(5,620) npts,dt
40        write(6,650)
41   650  format(5x,'Specify:# col of data, col # for t',
42      $          ' col # for data >',$)
43        read(5,*) ncol,inum1,inum2
44        else
45        sign=1.0
46        write(6,630)
47   630  format(5x,'Enter value of m, df ',/,
48      &       5x,'(note: # points in record = 2**m)    >',$)
49        read(5,620) npts,dt
50  c        dt=pi2*dt
51        write(6,660)
52   660  format(5x,'Specify:# col of data, col # for f,',
53      $ ' col # for data( Fourier Amp.),col # for data (Phase ang.) >',$)
54        read(5,*) ncol,inum1,inum2,inum3
55        endif
56   620  format(i5,f10.0)
57  c
58  c.... determine size for transformation
```

Line# Source Line Microsoft FORTRAN Optimizing Compiler Version 5.00

```
    c       n=(te-ts)/dt +1
    c       m=alog(float(n))/alog(2.0) + 1
    c       ndim = 2**m
            m=npts
            ndim=2**npts
    c.... assign end time in record as ndim points ahead of start time
           ts=0.0
           te=ts + dt*float(ndim)
           write(6,800)
     800   format(5x,'-- Summary of Analysis being Performed --',/)
           if(sign.lt.0.0) then
           write(6,810) itype,ts,te,dt,ndim
     810   format(5x,'Type of Analysis ..................... ',a3,/,
          $       5x,'Start Time in Record, t0 ............ ',f8.3,/,
          $       5x,'End Time in Record, (t0 + ndim)...... ',f8.3,/,
          $       5x,'Time interval in Record, dt ......... ',f8.3,/,
          $       5x,'Number of points in trans., (ndim)... ',i6,//)
           else
           write(6,820) itype,ts,te,dt,ndim
     820   format(5x,'Type of Analysis ..................... ',a3,/,
          $       5x,'Start Freq in Record, f0 ............ ',f8.3,/,
          $       5x,'End Freq in Record, (f0 + ndim) ..... ',f8.3,/,
          $       5x,'Freq interval in Record, df.......... ',f8.3,/,
          $       5x,'Number of points in trans., (ndim)... ',i6,//)
           endif
           if(m.gt.mmax) then
           write(6,900) m,mmax
     900   format(5x,'m =',i5,'  exceeds mmax =',i5,/,
          $       5x,'** Storage Capacity Exceeded !')
           stop
           endif
    c.... read array to be transformed
    c.... note that end of record for FFT may be padded with zeros
    c.... if record is not sufficient in length of ndim + t0 beyond
    c.... pointer
           do 10 i=1,ndim
           a(i,1)=0.0
           a(i,2)=0.0
       10  continue
    c
    c.... read data
           ic=0
        1  continue
           read(1,*,end=1000) (x(i),i=1,ncol)
           t=x(inum1)
    c        if(t.ge.ts.and.t.le.te) then
           ic=ic+1
           a(ic,1)=x(inum2)
           a(ic,2)=0.0
           if(sign.gt.0.0) a(ic,2)=x(inum3)
    c       endif
           go to 1
     1000  continue
    c
    c.... do transformation
    c
           write(6,950)
      950  format(5x,'Performing Transformation, note that if the',
```

Line# Source Line Microsoft FORTRAN Optimizing Compiler Version 5.00

```
  117        $       'original record',/,
  118        $       5x,'does not have ndim points beyond the start time',
  119        $          ' (freq),',/,
  120        $  5x,'then it will be assumed that unassigned points are equal',
  121        $     ' to zero.')
  122         call fft(a,m,nsize,sign,dt)
  123   c
  124   c.... output of results
  125         delt=1.0/(dt*float(ndim))
  126         do 20 i=1,ndim
  127         xk=float(i) - 1.0
  128         if(sign.lt.0.0) then
  129   c      fk=xk/(dt*ndim)
  130         fk=xk*delt
  131         else
  132         fk=xk*delt
  133         endif
  134         write(2,975) fk,a(i,1),a(i,2)
  135    20   continue
  136    975  format(3(2x,f11.4))
  137         stop
  138         end
***** fft.for(138) : warning F4999: IFT : variable declared but not used
***** fft.for(138) : warning F4999: IFTC : variable declared but not used
```

main Local Symbols

Name	Class	Type	Size	Offset
FT.	local	CHAR*3	3	0000
A	local	REAL*4	131072	0000
IFT	local	CHAR*3	3	0004
FTC	local	CHAR*3	3	0008
NPTS.	local	INTEGER*4	4	000a
IFTC.	local	CHAR*3	3	000c
I	local	INTEGER*4	4	000e
NSIZE	local	INTEGER*4	4	0012
PI2	local	REAL*4	4	0016
ITYPE	local	CHAR*3	3	001a
IC.	local	INTEGER*4	4	001e
M	local	INTEGER*4	4	0022
FK.	local	REAL*4	4	0026
T	local	REAL*4	4	002a
DT.	local	REAL*4	4	002e
X	local	REAL*4	40	0032
FILEOUT	local	CHAR*13	13	005a
TE.	local	REAL*4	4	0068
XI.	local	REAL*4	4	006c
TS.	local	REAL*4	4	0070
NDIM.	local	INTEGER*4	4	0074
DELT.	local	REAL*4	4	0078
INUM1	local	INTEGER*4	4	007c
INUM2	local	INTEGER*4	4	0080
INUM3	local	INTEGER*4	4	0084
NCOL.	local	INTEGER*4	4	0088

Microsoft FORTRAN Optimizing Compiler Version 5.00

main Local Symbols

Name	Class	Type	Size	Offset
SIGN.	local	REAL*4	4	008c
MMAX.	local	INTEGER*4	4	0090
FILEIN.	local	CHAR*13	13	0094

```
    c.....................................................
    c
    c       subroutine fft
    c
    c       a subroutine based on the fast fourier transform
    c       method to perform a discrete fourier transform.
    c
    c.....................................................
          subroutine fft(a,m,ndim,sign,di)
          dimension a(ndim,2),u(1,2),w(1,2)
          fr(b,c,d,e)=b*d-c*e
          fi(b,c,d,e)=b*e+c*d
          pi=4.0*atan(1.0)
          n=2**m
          amp=2.0/float(n)
          nv2=n/2
          nm1=n-1
          j=1
    c
    c.... Inverse FFT
          if(sign.gt.0.0) then
          do 100 i=1,n
          theta=a(i,2)
          xreal=a(i,1)*cos(theta)*0.50
          ximag=a(i,1)*sin(theta)*0.50
          a(i,1)=xreal
          a(i,2)=ximag
      100 continue
          endif
    c
          do 7 i=1,nm1
          if(i.ge.j) go to 5
          tr=a(j,1)
          ti=a(j,2)
          a(j,1)=a(i,1)
          a(j,2)=a(i,2)
          a(i,1)=tr
          a(i,2)=ti
      5   k=nv2
      6   if(k.ge.j) go to 7
          j=j-k
          k=k/2
          go to 6
      7   j=j+k
          do 20 l=1,m
          le=2**l
          le1=le/2
          u(1,1)=1.0
          u(1,2)=0.0
```

Line# Source Line Microsoft FORTRAN Optimizing Compiler Version 5.00

```
  188          ang=pi/float(le1)
  189          w(1,1)=cos(ang)
  190          w(1,2)=sign*sin(ang)
  191          do 20 j=1,le1
  192          do 10 i=j,n,le
  193          ip=i+le1
  194    c      tr=a(ip,1)*u(1,1)-a(ip,2)*u(1,2)
  195          tr=fr(a(ip,1),a(ip,2),u(1,1),u(1,2))
  196    c      ti=a(ip,1)*u(1,2) + a(ip,2)*u(1,1)
  197          ti=fi(a(ip,1),a(ip,2),u(1,1),u(1,2))
  198          a(ip,1)=a(i,1)-tr
  199          a(ip,2)=a(i,2)-ti
  200          a(i,1)=a(i,1) + tr
  201       10 a(i,2)=a(i,2) +ti
  202    c      tr=u(1,1)*w(1,1) - u(1,2)*w(1,2)
  203          tr=fr(u(1,1),u(1,2),w(1,1),w(1,2))
  204    c      ti=u(1,1)*w(1,2) + u(1,2)*w(1,1)
  205          ti=fi(u(1,1),u(1,2),w(1,1),w(1,2))
  206          u(1,1)=tr
  207       20 u(1,2)=ti
  208    c.... Direct FFT
  209          if(sign.lt.0.0) then
  210          do 200 i=1,n
  211          xc=a(i,1)
  212          xs=a(i,2)
  213          xamp=sqrt(xc*xc + xs*xs)
  214          xtheta=atan2(xs,xc)
  215          a(i,1)=xamp*amp
  216          a(i,2)=xtheta
  217      200 continue
  218          endif
  219    c
  220          return
  221          end
***** fft.for(221) : warning F4202: FFT : formal argument DI : never used
```

FFT Local Symbols

Name	Class	Type	Size	Offset
DI.	param			0006
SIGN.	param			000a
NDIM.	param			000e
M	param			0012
A	param			0016
__V156.	param			fffa
__V157.	param			fffc
__V158.	param			fffe
LE1	local	INTEGER*4	4	00a2
B	local	REAL*4	4	00a6
C	local	REAL*4	4	00aa
D	local	REAL*4	4	00ae
E	local	REAL*4	4	00b2
I	local	INTEGER*4	4	00b6
J	local	INTEGER*4	4	00ba
K	local	INTEGER*4	4	00be

Microsoft FORTRAN Optimizing Compiler Version 5.00

FFT Local Symbols

Name	Class	Type	Size	Offset
L	local	INTEGER*4	4	00c2
NM1	local	INTEGER*4	4	00c6
XTHETA	local	REAL*4	4	00ca
N	local	INTEGER*4	4	00ce
LE	local	INTEGER*4	4	00d2
U	local	REAL*4	8	00d6
ANG	local	REAL*4	4	00de
NV2	local	INTEGER*4	4	00e2
W	local	REAL*4	8	00e6
IP	local	INTEGER*4	4	00ee
PI	local	REAL*4	4	00f2
XC	local	REAL*4	4	00f6
TI	local	REAL*4	4	00fa
AMP	local	REAL*4	4	00fe
TR	local	REAL*4	4	0102
XS	local	REAL*4	4	0106
XAMP	local	REAL*4	4	010a
XIMAG	local	REAL*4	4	010e
THETA	local	REAL*4	4	0112
XREAL	local	REAL*4	4	0116

Global Symbols

Name	Class	Type	Size	Offset
FFT	FSUBRT	***	***	0641
main	FSUBRT	***	***	0000

Code size = 0fad (4013)
Data size = 0175 (373)
Bss size = 011a (282)

No errors detected
No errors detected

Appendix B

Base Correction of Sine Excitation

It has been discussed in the context that base correction may not be a big issue for simple pattern ground excitation as hysteretic energy will remain the same value. However base correction of sine-wave excitation has been studied and the findings are presented in this Appendix.

For a given ground acceleration of sine excitation, the directly integrated velocity and displacement time histories can be described in Figure B-1. Since the ground velocity is always non-negative, the ground displacement tends to increase until the end of the excitation. Using base correction the ground velocity time history can be made fluctuating about the zero axis, and the ground displacement reasonably deviating from its original position (Figure B-2).

Such base correction is efficient in terms of eliminating the "train effect" resulted from relative displacement response diagram of structure with very low strength ratio. Figure B-3 is an example to show the situation, where the structural relative displacement keeps increasing in one direction along with time history. While using the base corrected ground acceleration as shown in Figure B-2, the "train effect" disappears from the resultant relative displacement as can be seen in Figure B-4.

As the ground displacement, structural relative displacement and absolute displacement are all different after base correction, the resultant input, kinetic and strain energies will accordingly change except the hysteretic energy after first several cycles of excitation since the difference between maximum structural displacement and minimum one remains the same for each cycle of the excitation. Therefore, base correction of simple pattern ground excitations does not give much influence on hysteretic energy which is the major concern in this research.

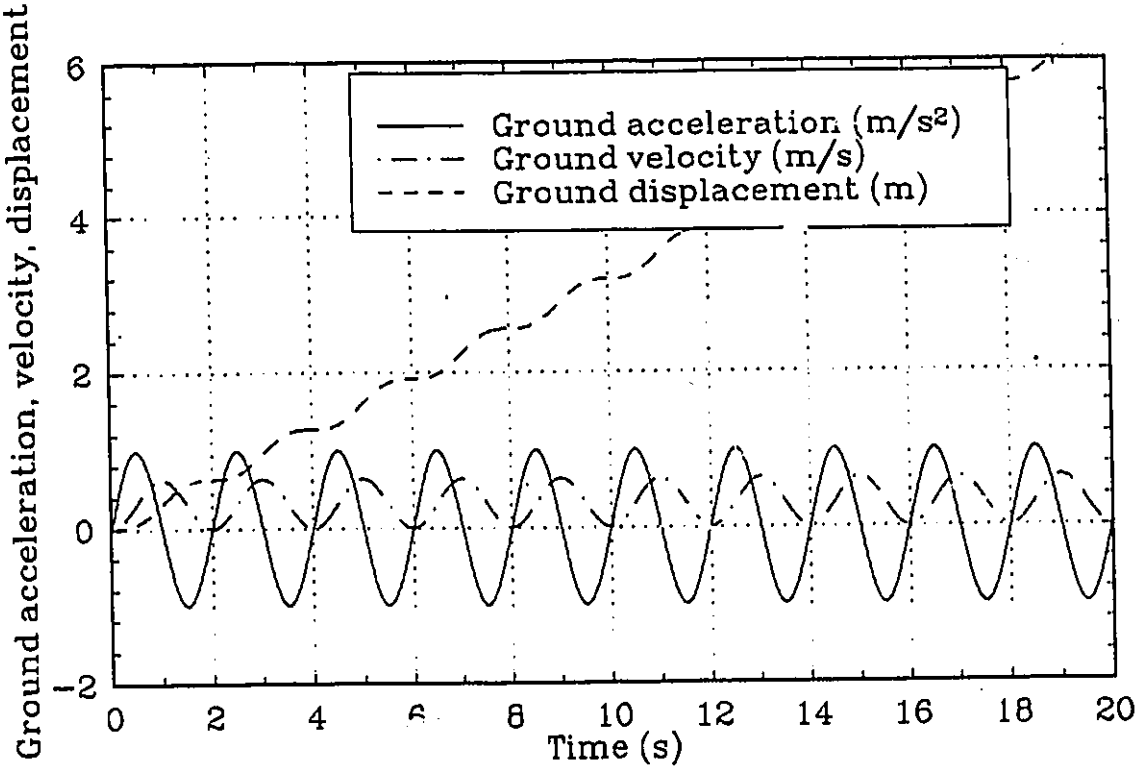

Figure B-1 Non-base-corrected sine excitation time histories

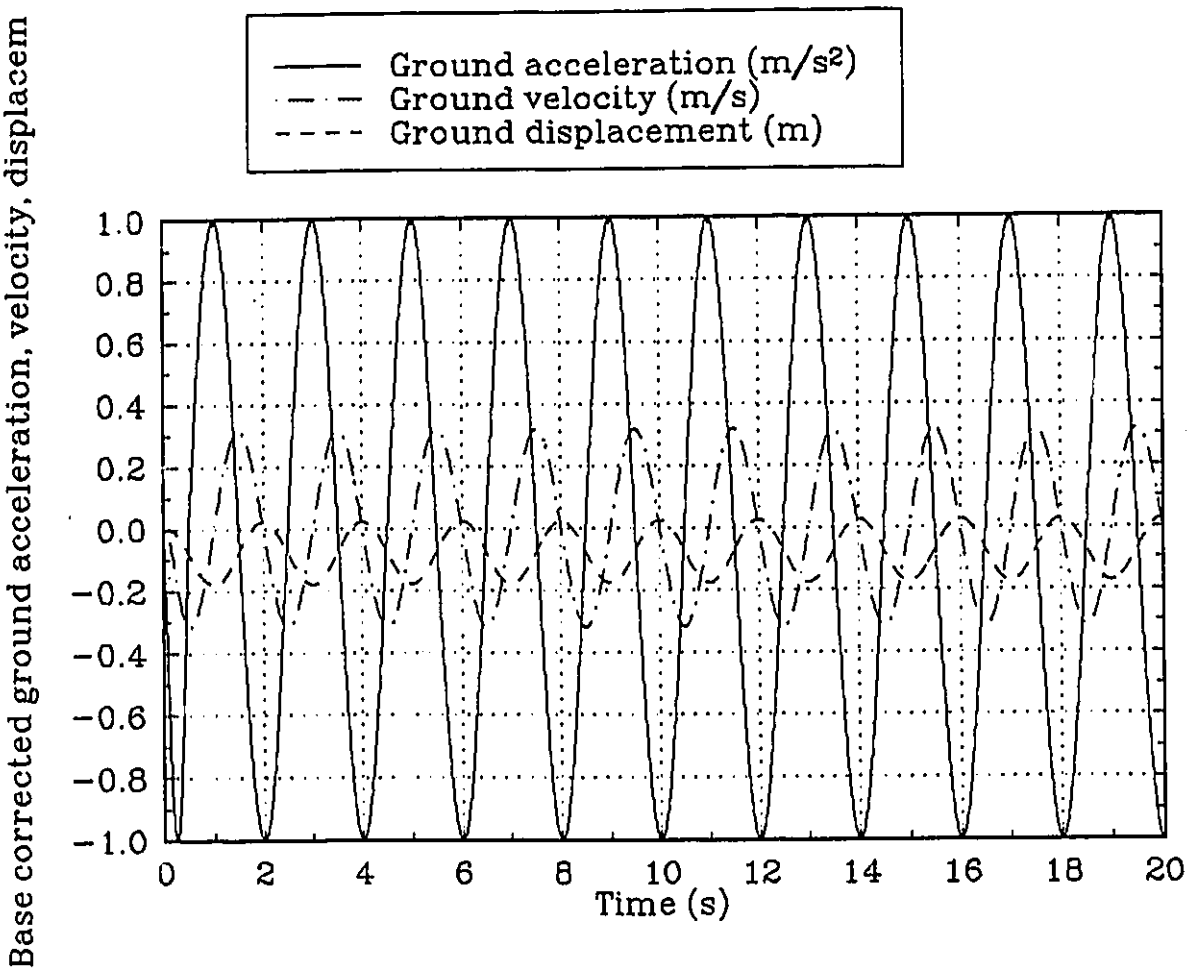

Figure B-2 Base corrected sine excitation time histories

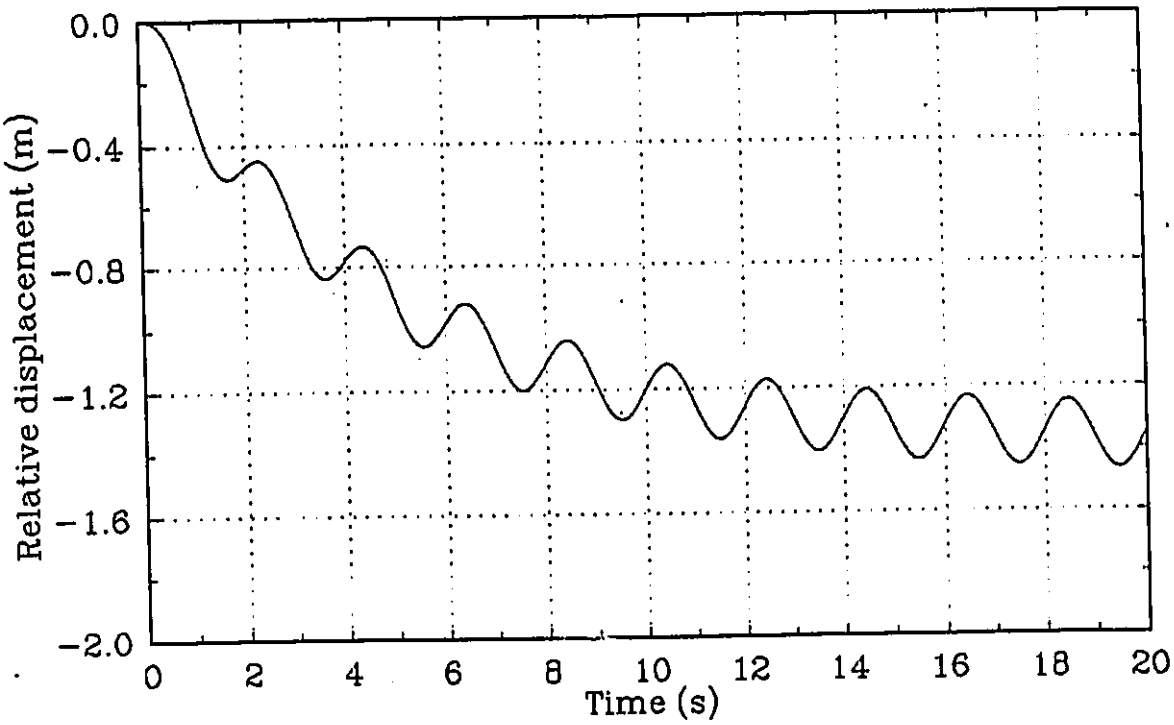

Figure B-3 Structural relative displacement time history under a non-base corrected sine excitation ($\beta = 1$, T = 2.0s, $\eta = 0.1$, $\xi = 0\%$)

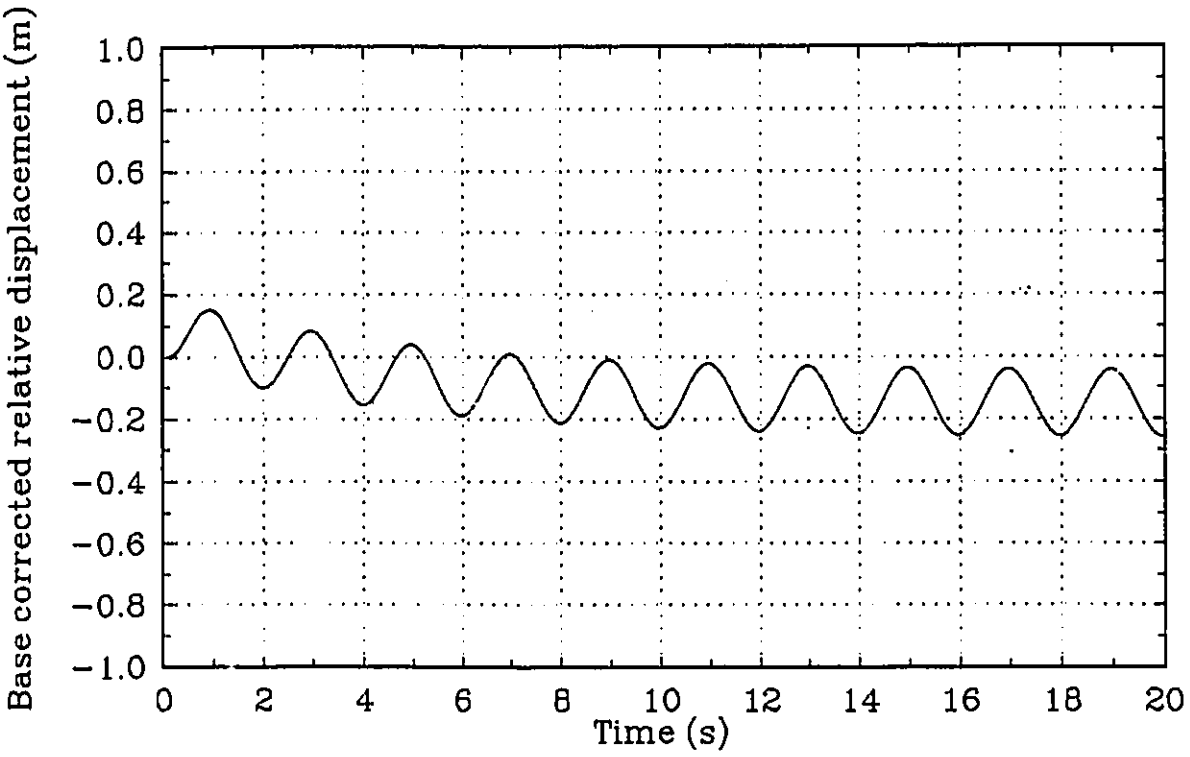

Figure B-4 Structural relative displacement time history under a base-corrected sine excitation (β = 1, T = 2.0s, η = 0.1, ξ = 0%)

Appendix C
Comparison of Different Normalized Pulse Spectra with Sine Spectra

In the normalized hysteretic energy spectra for sine-wave excitation, it is believed that structures with smaller β values behave as if they are subjected to pulse excitation. In order to compare the results from sine excitation with those from a real one-cycle sine pulse excitation and two continuous reverse-sign rectangular pulses excitation, Figure C-1 is constructed. $(E_h/NR_y\Delta_y)\eta$ is used for vertical axis to show that for larger β values there is almost linear relationship among normalized hysteretic energy responses for various η under one location of β.

In Figure C-1, it can be seen that the two continuous reverse-sign rectangular pulses result in the biggest energy demand. It can be also comprehended that one-cycle sine pulse is not equivalent to continuous sine excitation, therefore there must exist some error in later part of the research due to using sine excitation spectra in converted sine pulse method to predict energy demand for real earthquakes.

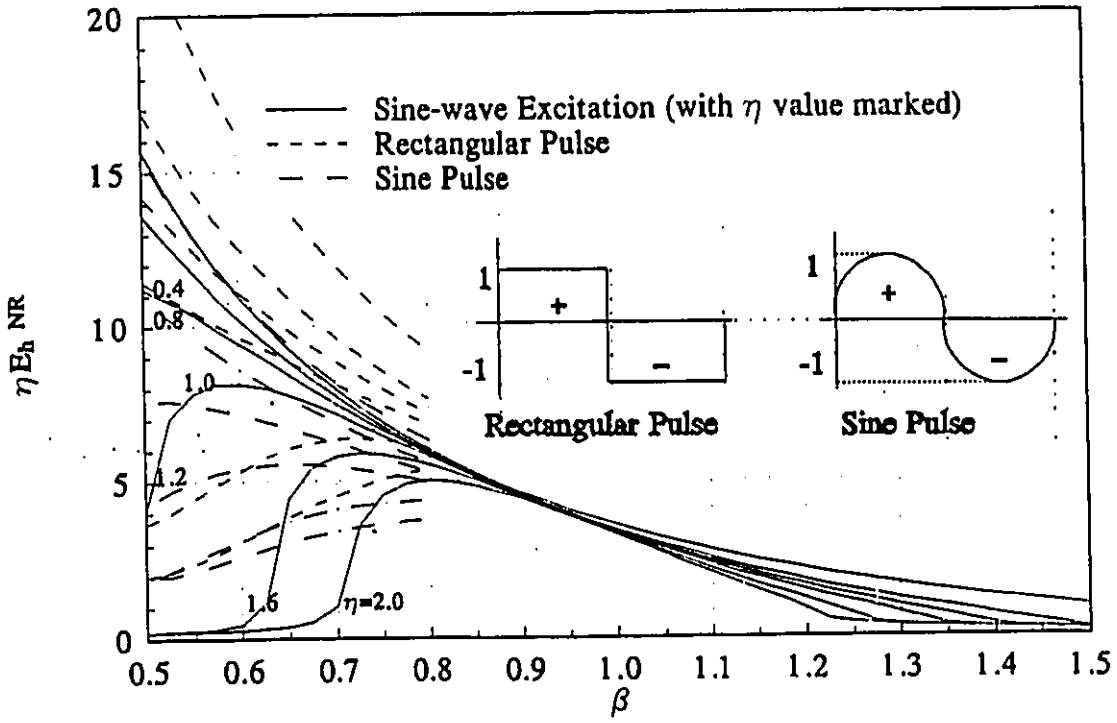

Figure C-1 Comparison of normalized hysteretic energy spectra under sine-wave, reverse-sign rectangular and sine pulse excitations (ξ = 0%)